Viscous flow of magmas from Unzen volcano, Japan – implication for magma mixing and ascent

Viskositäten von Magmen des Unzen Vulkans, Japan – Bedeutung für Magmenmischung und -aufstieg

Von der Naturwissenschaftlichen Fakultät der Universität Hannover

zur Erlangung des Grades

Doktor der Naturwissenschaften

Dr. rer. nat.

genehmigte Dissertation

von

Dipl. Geol. Francesco P.Vetere

Geboren am 30.05.1975 in Cosenza (Italien)

2006

Prüfungsvorsitz: Prof. Dr. Jürgen Böttcher

Referent: Dr. PD Harald Behrens

Korreferenten: Prof. Robert L. Linnen

Mitglieder der Prüfungskommission: PD Dr. Harald Behrens
Prof. Dr. François Holtz
Prof. Dr. Joachim Deubener (TU Clausthal)

Tag der Promotion: 24.01.2006

Acknowledgements

Thanks to *Harald Behrens and François Holtz*, for all your help, for introducing me in this fantastic experimental petrology world, ignored before coming to Hannover.

Thanks *Harald* especially for the help in the lab, for proposing this subject and for helping me along the way. I appreciated a lot your time devoted to me and all knowledge I learned from your experience.

Thanks to *Jan Schüßler* and *Piero Del Gaudio* for all your help. Thanks Jan, for the help, especially in the chemical lab.

Thanks to*, Matthias Hann, Kevin Klimm and Antje*, *Dominich Schreen Kai Spickenbom, Sandrin Feig Holger Strauß, Roman Botcharnikov*, *Shigeru Yamashita, Renat Almeev, Magnus Johansson, Jan Stelling, Elke Schlechter, Oliver Beermann, Fred Blaine, Veerle Vanacker, Regina Kappes, Sara Fanara, Paola Donato, Valeria Misiti*

Thanks to *Marcus Nowak*, *Jürgen Köpcke Friedhelm von Blanckenburg, ,Ronny Schönberg.* All of your suggestions were appreciated.

Thanks to *Willy*, *Otto* and *Bettina* and all other guys working there. How many ovens I destroyed?

Antje Wittemberg, Eule You were great during this time.

I appreciated a lot the help given to me by *Miriam Haack, Hella Wittmann* and Kevin Norton in correcting this thesis in good English.

Thanks to *Pascal Richet* and *Daniel Neuville* that gave me the possibility to work in their lab in Paris.

Thanks to *Hiroaky Sato* for his jewels suggestions

Grazie a *Guido Ventura* e *Rosanna De Rosa* per avermi dato la possibilitá di lavorare qui ad Hannover.

A special thanks to all the people I want to thanks but I forget right now. I apologize for that. Thanks!

Un grazie alla mia famiglia per il supporto datomi durante questi anni. Grazie a mia mamma *Lina*, al mio papà *Silvio* alla mia sorellina *Annarita* e a mio fratello *Marcello*.

Un sentito grazie a *Licia, Enrico, Pier, Francesca* e *David* per aver "sopportato" la mia mogliettina durante la mia assenza.

Infine, ma non per ultima, voglio ringraziare mia moglie ***Stephanie*** per la pazienza e per tutto lo stress sopportato a causa della mia assenza. Spero di poter rimediare e magari recuperare tutto il tempo perduto. Se sono riuscito in questa non facile impresa è sopratutto grazie a te. Grazie di cuore per essermi stata sempre vicina.

Zusammenfassung

Das Ziel dieser Arbeit ist die Untersuchung der Viskosität andesitischer Schmelzen und Magmen. Insbesondere richtet sich die Aufmerksamkeit auf Magmenzusammensetzungen des Vulkans Unzen (Japan), um magmatische Prozesse während der letzten Eruption 1991-1995 besser zu verstehen. Diese Eruption wurde wahrscheinlich durch Mischung eines felsischen und eines andesitischen Magmas ausgelöst.

Im Gegensatz zu bereits detaillierter untersuchten felsischen (rhyolitischen) Magmen gibt es bisher für mafische, wasserhaltige Schmelzen mit andesitischer oder basaltischer Zusammensetzung noch keine umfassenden Modelle zur Vorhersage deren Viskositäten. Diese Arbeit ist Teil eines Forschungsprojekts zur Untersuchung der präeruptiven Bedingungen und der Ursachen der Eruption von 1991-1995 des Vulkans Unzen.

Der erste Teil dieser Arbeit konzentriert sich auf experimentelle Untersuchungen an einer Fe-freien synthetischen Schmelzzusammensetzung, die der des Unzen Andesits entspricht, wobei jedoch das in der natürlichen Zusammensetzung enthaltene Eisen im synthetischen Analogon durch entsprechende Anteile an Al, Ca und Mg ersetzt wurden. Die Verwendung Fe-freier Schmelzen vereinfacht experimentelle Untersuchungen, u.a. weil dadurch eine Kristallisation von Fe-Ti-Oxiden vermieden wird. Die Viskositäten Fe-freier andesitischer Schmelzen wurde im Bereich hoher Viskositäten (10^1-10^6 Pa·s) unter Verwendung der „falling sphere(s)"-Methode bestimmt und im Bereich niedriger Viskositäten (10^8-10^{13} Pa·s) mittels eines „parallel-plate"- Viskosimeters gemessen. Bei der „falling sphere(s)"-Methode wird der Zusammenhang zwischen der Absinkgeschwindigkeit von Platin-, Palladium- oder Korund-Kugeln in Schmelzen und

deren Viskosität zur Bestimmung von Schmelz-Viskositäten genutzt. Aus den gewonnen Daten wurde ein Modell zur Vorhersage der Viskosität in Abhängigkeit von Wassergehalt und Temperatur entwickelt.

Im zweiten Teil der Arbeit wurden Viskositäten einer Fe-haltigen Schmelze mit einer Zusammensetzung ähnlich der eines Unzen Andesits mit den gleichen experimentellen Methoden bestimmt, mit denen auch die Fe-freien Andesite untersucht wurden. Insbesondere wurde der Einfluss des Redoxzustands von Eisen in der Schmelze auf die Viskosität untersucht. Anhand der gewonnen Erkenntnisse über den Einfluss von Wasser und Temperatur auf die Viskosität Fe-freier Schmelzen und den Einfluss des Eisen-Redoxzustandes, wurde ein neues Modell zur Beschreibung der Viskosität (η in Pa·s) in Abhängigkeit von Temperatur T (in K), Wassergehalt w (in Gew%) und Eisen-Redoxverhältnis Fe^{2+}/Fe_{tot} entwickelt:

$$\log\eta = -5.72 + \frac{8530.8}{(T-59.8)} + \frac{1845.1}{(T-650.6)} * \exp\left[\frac{196.1}{\left(\frac{Fe^{2+}}{Fe_{tot}} * T\right)}\right] * \exp\left(-452.5 * \frac{w}{T}\right)$$

Die Anwendung der gewonnen Viskositätsdaten auf das vulkanische System des Unzen zeigt, dass die Viskositäten der rhyolitischen und andesitischen Schmelzen vor und während der Mischung nahezu identisch sind. Dies ermöglicht eine effiziente Magmenmischung und könnte die beobachtete homogene Zusammensetzung der Grundmasse der vulkanischen Gesteine des Unzen erklären.

Der letzte Teil dieser Arbeit behandelt die Viskosität Kristall-führender andesitischer Magmen, die im Bereich hoher Viskositäten ($10^{9.5}$-10^{12} Pa·s) und niedriger Viskositäten (10^{3}-$10^{3.5}$ Pa·s) untersucht wurden. Im Bereich hoher Viskositäten wurde eine „creep“-Apparatur für die Messungen unter Atmosphärendruck im Temperaturbereich zwischen 779 -1028 K verwendet. Ausgangsmaterialien für diese

Messungen waren wasserhaltige Proben (0.8 und 3.8 Gew% H_2O), die unter Hochdruckbedingungen vorbehandelt wurden, was zur Teilkristallisation führte (21 bis 38 Vol% Kristalle). „Falling sphere“-Experimente wurden in einer intern beheizten Gasdruckanlage (IHPV) bei einem Druck von 300 MPa und Temperaturen zwischen 1373 und 1523 K an Proben mit Wassergehalten von 0.52, 2.98 und 4.02 Gew% H_2O durchgeführt. In diesen Experimenten wurden den Proben Zirkon-Kristalle zugegeben, welche nur eine sehr geringe Löslichkeit in der andesitischen Schmelze bei hoher Temperatur besitzen. So bleibt das gewählte Kristall/Schmelze-Verhältnis in der Probe während der Messungen konstant. Die Ergebnisse zeigen, dass sowohl im Bereich niedriger als auch im Bereich hoher Viskositäten, die gemessenen Viskositäten höher sind als von der Einstein-Roscoe-Gleichung vorhergesagt wird, die häufig zur Berechnung von Magmenviskositäten verwendet wird. Die Viskosität eines Magmas mit 20 Vol% Kristallanteil und 4.02 Gew% H_2O in der Schmelze kann bis zu einer log-Einheit höher sein als von der Einstein-Roscoe-Gleichung vorhergesagt wird.

Schlagworte: Viskosität, Magma, Unzen

Abstract

The objective of this is work the study of the viscosity of andesitic melts and magmas. Particular attention is given to compositions from Unzen volcano (Japan) to understand magmatic processes occurring during the last eruption in 1991-1995. This eruption was probably caused by mixing between a felsic and an andesitic magma. In contrast to widely studied felsic melts (rhyolite), there is no comprehensive model to predict the viscosity of mafic hydrous melts such as andesite or basalts. This study is part of a general project aimed at understanding the pre-eruptive conditions and the causes of the 1991-1995 eruption at Unzen.

The first part of this thesis focuses on the investigation of a synthetic andesite analog in which iron was replaced by appropriate proportions of Al, Ca and Mg. The study of the viscosity of Fe-free melts simplifies the experimental procedures (e.g. no crystallization due to Fe-Ti oxides). The viscosity of a Fe-free andesite was measured in the low viscosity range (10^1 – 10^6 Pa·s) using the falling sphere(s) method and in the high viscosity range (10^8 – 10^{13} Pa·s) using parallel-plate viscometry. The sinking velocity of Pt and Pd spheres, and in one case of a corundum sphere, was used to measure the melt viscosity. Using this procedure, a model was created for the prediction of viscosity as a function of water content and temperature.

In a second step, the viscosity of an iron-bearing melt with composition similar to Unzen andesite was determined experimentally with the same techniques and devices as used for the Fe-free andesite. Particular attention was given to the influence of oxidation state of iron in the melts on the viscosity. Based on our knowledge of the effect of water and temperature on viscosity of Fe-free melts and on the effects of the

redox state of iron, a new model was derived to describe the viscosity η (in Pa·s) as a function of temperature T (in K) and water content w (in wt%) and Fe^{2+}/Fe_{tot} ratio:

$$\log\eta = -5.72 + \frac{8530.8}{(T-59.8)} + \frac{1845.1}{(T-650.6)} * \exp\left[\frac{196.1}{\left(\frac{Fe^{2+}}{Fe_{tot}} * T\right)}\right] * \exp\left(-452.5 * \frac{w}{T}\right)$$

The application of the viscosity data to Unzen volcanic system shows that the viscosities of the rhyolite and andesite melts from the two end-member magmas are nearly identical prior and during mixing. This enables an efficient magma mixing and may explain the homogeneous composition of the groundmass observed in Unzen volcanic rocks.

The last part of this work focuses on the viscosity of crystal-bearing andesite. The viscosity was studied in the high ($10^{9.5}$-10^{12} Pa·s) and low viscosity range (10^{3}-$10^{3.5}$ Pa·s). Creep data were carried out at room pressure and in the temperature range 779 - 1028 K using hydrous sample containing between 0.8 and 3.8 wt% $H_2O_{tot.}$ The samples were treated at high pressure (crystallization experiments) and contained approximately 21 – 38 vol% crystals. Falling sphere experiments were performed in IHPV at 300 MPa and temperature between 1373 and 1523 K in samples containing 0.52, 2.98 and 4.02 wt% $H_2O_{tot.}$ Zircon crystals, which are only sparingly soluble in andesitic melt at high temperature, were added to fix the desired crystals/melt ratio. The results show that, in both the high- and low-viscosity ranges, viscosity is higher than predicted by the Einstein-Roscoe equation, which is commonly used to predict the viscosity of magmas. The viscosity can be up to one log unit higher than that predicted by the Einstein-

Roscoe equation for mixtures composed of 20 vol% crystals and melts containing 4.02 wt% H_2O.

Keywords: viscosity, magma, Unzen

Content

1 Introduction

It has been suggested that the injection of a nearly aphyric andesitic magma into a highly crystalline magma chamber with rhyolitic melts initiated the 1991-95 eruption (e.g., *Nakada and Motomura, 1999; Venezky and Rutherford 1999; Holtz et al., 2005*). To understand and to model these processes detailed knowledge of the rheological behaviour of the involved magmas is required.

The main parameters which govern the viscosity of magmas are bulk composition of the melt (in particular the water content) and temperature (*Bottinga and Weill, 1972; Shaw, 1972; Persikov, 1991; Giordano and Dingwell, 2003b*), but also pressure (*Kushiro et al., 1976; Scarfe et al., 1987; Behrens and Schulze, 2003*), dispersed crystals (*Lejeune and Richet, 1995; Bouhifd et al, 2004; Sato H., 2005*) and bubbles (*Lejeune et al., 1999*) may have an important influence. For volcanism related to subduction zones, melts of rhyolitic to andestic compositions are of particular interest. An extensive amount of work has been devoted to silicic systems in the last decade (see *Giordano et al., 2004* and references therein). However, few studies on the viscosity of andesitic melts are available.

During the last decade, an extensive experimental effort has been devoted to the effect of water on the viscosity of silicate melts (*Hess and Dingwell, 1996; Richet et al., 1996; Scaillet et al., 1996; Schulze et al., 1996, 1999; Romano et al., 2001, 2003; Whittington et al., 2000, 2001; Liebske et al., 2003; Zhang et al., 2003; Giordano et al., 2004*). Techniques applied in the high viscosity range (10^8 to 10^{13} Pa·s) include micro-penetration (e.g., *Hess and Dingwell, 1996*), parallel plate viscosimetry (e.g., *Richet et al., 1996; Whittington et al., 2000*) and the evaluation of kinetics of interconversion of hydrous species (*Zhang et al., 2003*). In the low viscosity range (0.1-10^6 Pa·s) the falling sphere technique is the only established method for viscosity determinations at elevated pressures (e.g., *Shaw, 1963*). Indirect constraints on viscosity may be feasible from diffusivity of network former using the Eyring relationship (*Chakraborty, 1995*).

Among the parameters controlling viscosity, especially the influence of dissolved volatiles, redox state of iron and crystal fraction are poorly understood and have not yet been quantified. Dissolved water depolymerizes the silicate network and simultaneously, strongly reduces melt viscosity. On adding, for instance, 1 wt% water to a dry rhyoltic melt at 1000°C, the viscosity decreases by more than four orders of magnitude (*Schulze et al., 1996, Hess and Dingwell, 1996*).

Iron is present in silicate melts at state conditions, e.g. P, T, fo_2, similar to the Earth's crust in both divalent and trivalent state. Fe^{2+} and Fe^{3+} have different structural influences on silicate melts. Fe^{3+} behaves more like a network former and Fe^{2+} more like a network modifier. Therefore, changing the Fe^{2+}/Fe^{3+} ratio in a melt (e.g., by changing the imposed oxygen fugacity) will affect the polymerization of the melt and thus the melt viscosity. Thus, an iron-bearing melt become less viscous when the Fe^{2+}/Fe^{3+} ratio increases. Dissolved water influences the prevailing oxygen fugacity by the reaction $H_2 + ½\ O_2 = H_2O$. This allows, iron species to be selectively stabilized in complexes with hydrous species (H_2O molecules and OH groups). Changes in coordination of cations by hydration of melts are well known for transition metals such as Ni (*Nowak and Keppler, 1998; Farges et al. 2001*).

To avoid complications due to heterovalent iron, iron-free analogue compositions are commonly used in experimental studies (*Richet et al. 1996*). However, the direct application of these results to natural melts is often questionable due to:

a) different structural bonding of the substituting cations (Mg^{2+}, Ca^{2+}, Al^{3+}) compared to Fe^{2+} and Fe^{3+} and

b) the variation of redox state of iron due to dissolved water (*Baker and Rutherford, 1996; Botcharnikov et al., 2005*).

Viscosities of hydrous rhyolitic melts have been intensively studied in the past ten years (see review of *Dingwell, 1999*). Based on experimental data, an empirical model was developed by *Hess und Dingwell (1996)*, which enables the calculation of viscosity of rhyolitic melts as a function of water content and temperature in a large temperature range. The effect of pressure on viscosity was found to be negligible at 900°C in the range of 3 – 10 kbar for a melt containing 6 wt% H_2O (*Schulze et al., 1996*). The pressure dependence at lower temperatures and lower water contents is unknown for rhyolitic melts. A negative pressure dependence, increasing with decreasing temperature, is expected from results for another polymerized composition, Albite (*Schulze 1999; Behrens and Schulze, 2003*).

Much less is known on viscosity of rhyodacitic to andesitic melts. Viscosity changes by varying SiO_2 and alkali contents might be estimated from studies of *Holtz et al. (1999), Romano et al. (2001) and Whittington et al. (2001)*. This study is focused on the andesite system.

Viscosity measurements are only possible using stable melts (for which η is typically $<10^6$ Pas) or supercooled melts with $\eta > 10^8$ Pa·s. In the intermediate viscosity range samples rapidly crystallize during experiment. Therefore, experimental data have to be interpolated between the high and the low viscosity range. It has been established that most silicate melts do not show a simple *Arrhenius* temperature dependence (e.g., *Neuville et al. 1993, Hess and Dingwell 1996, Goto et al. 1997*). Thus, by measuring viscosity exclusively in the high or the low viscosity range and extrapolating the data to intermediate viscosity, the data possibly might have a large error.

Recently, *Dingwell* and coworker started a systematic investigation of the dependence of viscosity on melt composition (*Giordano and Dingwell, 2003*). Their investigation includes dacitic melts from the Unzen volcano. Their work is focused on the effect of water content on viscosity at ambient pressure near the glass transition. Effects of pressure, redox state of iron and suspended crystals are not investigated.

In the case of Unzen volcano in Japan (our main research subject) melt compositions vary from rhyolitic (residual melts after partial crystallization) to andesitic and basalt-andesitic (magma injection of the magma chamber below the volcano). Iron contents range from 1 wt% (rhyolite) to more than 8 wt% (andesite). Water contents of the melts in magma chambers below the Unzen volcano were estimated to be around 6 wt% (*Holtz et al., 2005*; *Sato et al. 2005*).

In this work I have investigated the viscosity behavior of melts with andesitic composition related to the last eruption at Unzen volcano in Japan. *Holtz et al., (2005)* suggested that mixing of an almost aphyric andesitic magma containing 4 ± 1 wt% H_2O with a crystal-rich low temperature magma containing ryholitic melt with up to 8 wt% H_2O initiated the 1991 eruption of the Unzen (Japan) volcano. By using new viscosity data for hydrous andesite in both, high and low viscosity ranges an attempt is made to get deep understanding of mixing processes initiated the 1991-1995 eruption at Unzen.

The first step of the experimental approach was to study the viscosity of an iron-free analogue andesite composition. This has a considerable technical advantage so that precise data can be obtained. Falling sphere experiments were performed to constrain the variation

of viscosity with a range of water content from nominally dry to 5.6 wt%, temperatures in the range of 1323 to 1573 K in the pressure range from ambient to 500MPa. These experiments were carried out in an internally heated pressure vessel (IHPV). Additional experiments with parallel plate viscosimetry allow the data set to be extended to the low viscosity range. By combining the experimental viscosity data with those from *Richet et al., (1996)* and *Liebske et al., (2003)*, an empirical equation has been developed to predict the viscosity of andesitic melts over a wide range of temperature and water content.

In a successive step, a natural andesite was investigated with the same techniques and in the same range of temperature. In this case the maximum water content investigated was 6.2 wt%, the pressure range varied from 200 to 2000 MPa. Additionally, the Fe^{2+}/Fe^{3+} ratio was investigated with a modified *Wilson* method to investigate the dependence of the viscosity on the redox state of iron.
Using viscosity models elaborated for hydrous rhyolitic melts *(Hess and Dingwell, 1996)* and for Fe-bearing andesitic melt (this study) the melt viscosities prior to eruption, the evolution of viscosities of mixed silicate melts and the efficiency of magma mixing will be discussed.

Consecutively the viscosity behavior in a partially crystallized andesite was investigated and compared to the predictions of previous models like *Einstein-Roscoe* model (*McBirney and Murase, 1984*) or *Sato (2005).*

2. Unzen volcano.

2.1. Location

The Unzen volcano has an elevation of 1.359 m and is situated in a depression known as the Unzen graben, Japan, at 32.75 N, and 130.30 E (Fig. 2.1, 2.2 and 2.4).

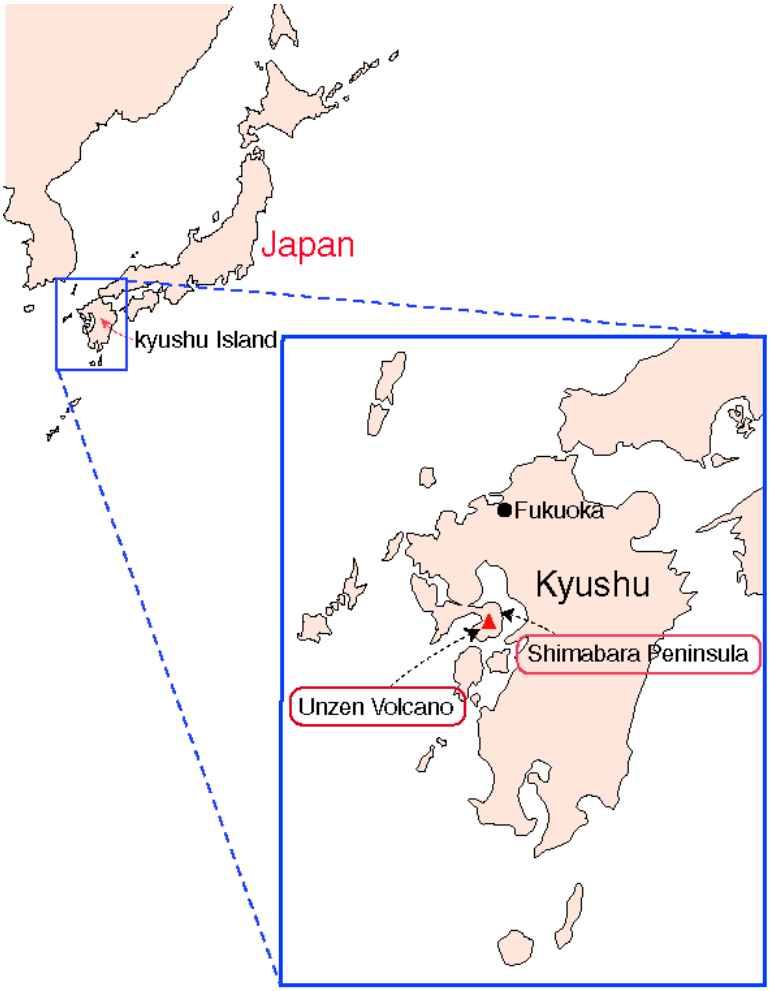

Fig. 2.1. Location of Unzen volcano (http://133.5.170.64/Museum/Museum-e/Part2-e/Part2-e.htm)

The Unzen graben (Fig. 2.2 and 2.5) has a west to east extension of 30-40 km. Repeated geodetic measurements (around the Shimabara peninsula) in the past 100 years suggest ongoing subsidence of the Graben *(Tada, 1985; Hoshizumi et al., 1999)*. Unzen is a composite volcano with a volume of at least 35 km^3 and consists of multiple volcanic

cones *(Watanabe et al., 1995; Hoshizumi et al., 1999)*. As indicated in Figure 2.3, the volcano is located in the western part (~70km) of the "volcanic front of SW Japan".

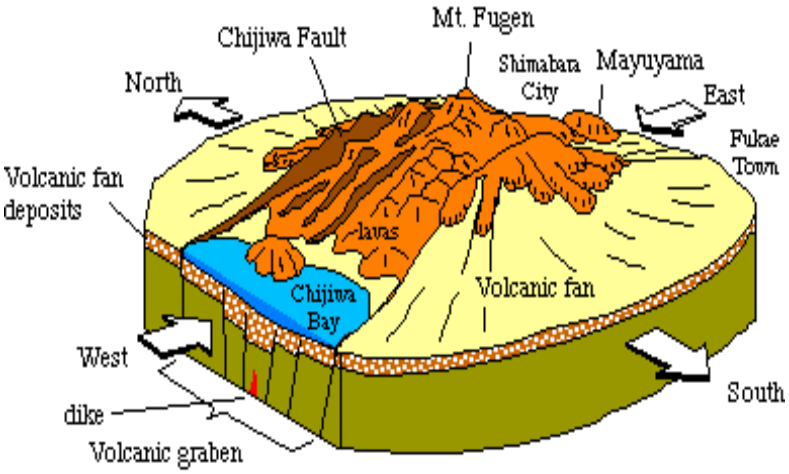

Fig. 2.2. Unzen Graben in the shimabara peninsula.(http://hakone.eri.u-tokyo.ac.jp/unzen/index.html)

This front is an imaginary line situated at the rim of the Philippine Sea plate (named "PHS", see Fig. 2.3) which subducts beneath SW Japan causing numerous volcanoes. In spite of not being located directly at the volcanic front, Unzen exists as one of several "intra-arc to back-arc rifts" (*Hoshizumi et al., 1999*). The back-arc rifts are formed by frictional drag from the subducting slab, which pulls the adjacent mantle down. The subducted material has to be compensated for, leading to zones of extension.

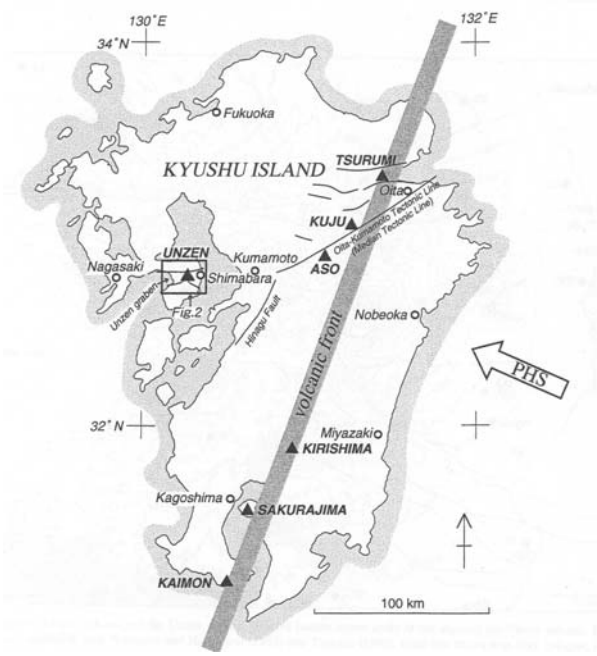

Fig 2.3. Location of Unzen volcano with respect to the Japan's volcanic front.
Map of Kyushu Island. Solid triangles are active volcanoes, arrow points direction of Phillippine Sea plate after *Seno, (1977)*

2.2 Geology

The geologic history of the Unzen area can be separated into three periods: Pre-Unzen, Older Unzen, and Younger Unzen. The Pre-Unzen period dates back to 0.5 Ma, ending with the Tonosaka andesite. This formation possibly marks the first volcanic rocks erupted in the area, prior to the formation of the Unzen volcano. The Pre-Unzen rocks have a thickness of several hundred meters and overlay sedimentary rocks.

The Older Unzen is thought to be located in the same area as the current volcano, but this cannot be confirmed due to the existence of cross-cutting faults and heavy erosion. The estimated age for the Older Unzen volcano lies between 200 and 300 ka, the volume erupted during this period is in the order of 120 cubic kilometers. Since the formation of the Younger Unzen volcano (100 ka), which comprises Nodake volcano, Myokendake volcano, and Fugendake volcano, Unzen has subsided nearly 200 meters. Between the Older and Younger period, there was a long period of inactivity lasting 100.000 years *(Hoshizumi et al., 1999)*. The Younger Unzen period started at less than 100 ka, and ca. 8 cubic kilometers of volcanic material has been erupted. It includes the Nodake, Myokendake, Fugendake, and Mayuyama volcanoes (*Hoshizumi et al., 1999*; parts of these volcanoes can be seen in Fig. 2.2 and 2.4). The Fugendake volcano has erupted multiple times, e.g. in 1663 and 1792. The 1792 eruption was associated with of earthquakes and fumarolic activity leading to an eruption of dacite that flowed 2 km to the north. One month after the eruption, the Mayuyama dome collapsed, triggering a debris avalanche as well as tsunami, killing 15,000 people. Many islands offshore from Shimabara City are actually blocks which were transported by the debris flow (Fig. 2.4). The eruption in 1792 was one of the most catastrophic ones in Japan's history.

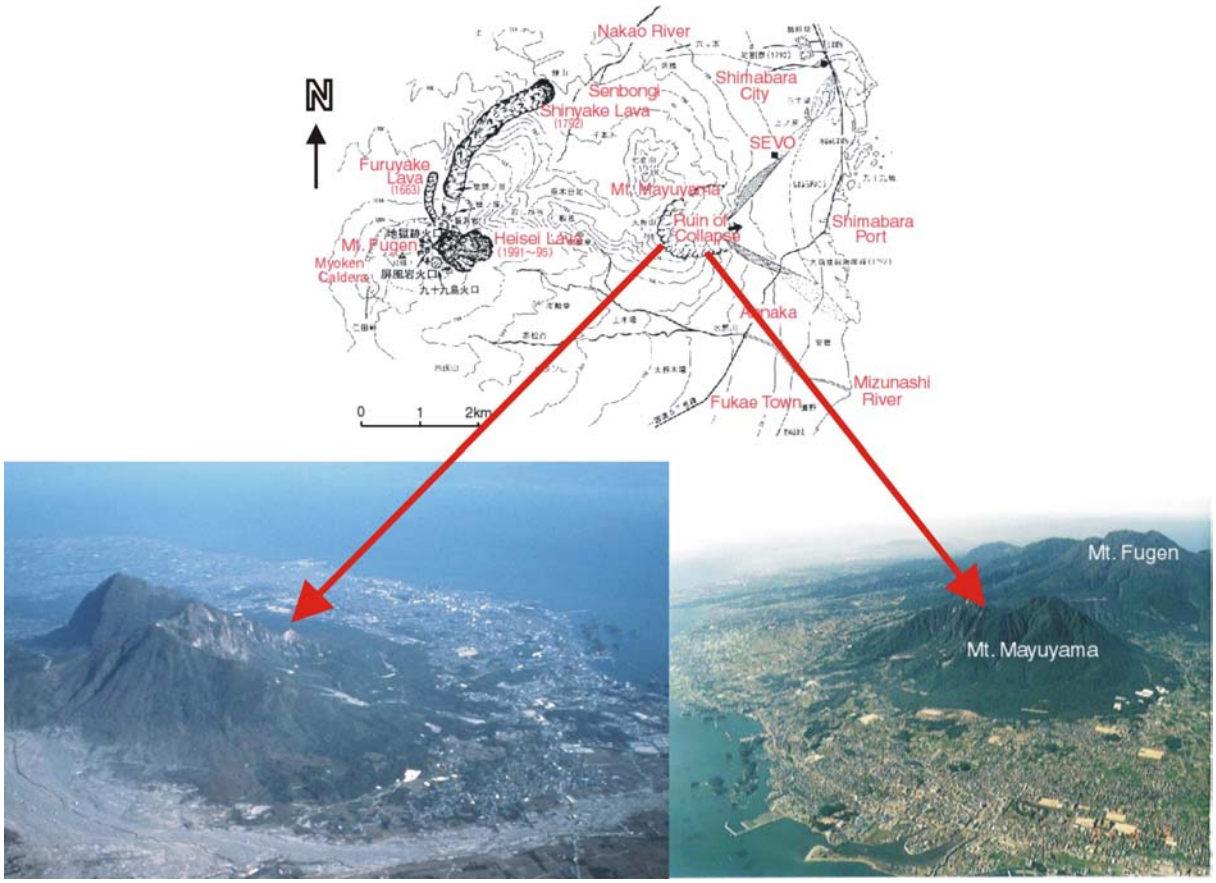

Fig. 2.4. Mount Mayuyama: dome collaps caused by the 1972 eruption. http ://133.5.170.64/ Museum / Museum-e/Part2-e/taihen-e/taihen-e.htm

2.3. The 1991-1995 eruption.

The Fugendake volcano was also responsible for the eruptions of 1990-1995. Upwelling of mantle in the back-arc region might have been responsible for magma genesis in the Unzen area (*Hoshizumi et al., 1999*). The eruption that started in 1991 and continued until 1995 was the first eruption at Unzen in 198 years. Altogether, 43 persons were killed during a pyroclastic flow on June 3rd, 1991 *(Hoshizumi et al., 1999)* including the volcanologists Harry Glicken, Maurice Krafft, Katia Krafft and 40 Japanese journalists. Another person was killed in a pyroclastic flow on June 23, 1993 (*Nakada et al., 1999*). The eruptions were characterized by the growth of lava domes and followed by pyroclastic flows, which were triggered by dome collapse *(Miyabuchi, 1999)*. From a seismic point of view, the events that occurred at Unzen from 1989 to 1996 are classified as:

(I) volcano-tectonic (VT) earthquakes, probably indicating fracture of the basement rock triggered by build-up of excess pressure in the deeper magma reservoir; (II) high-frequency (HF) earthquakes at the emergency of the dome; (III) low-frequency (LF) earthquakes during magma discharge, volcanic tremor and seismic waves excited by rockfall or pyroclastic-flow events (see Fig 2.8 for a schematic view of seismic events). The most significant precursor to the first eruption was an isolated tremor followed by continuous tremors *(Nakada et al., 1999)*. The hypocenter approached the surface at an ascent rate of 10-50m/day, probably reflecting the ascent of the magma. Taking this ascent rate into account, one can conclude that magma upwelling from a chamber located in 7 to 13 km depth needs about 2 years to ascend to the surface. Repeated leveling and GPS surveys during the volcanic activity showed continuous subsidence in the western flank of the volcano *(Ishihara, 1993; Nishi et al 1999)*. The main source of the ground subsidence was estimated to be located about 7-13 km below the surface and about 4 km west of the summit. Based on the distribution of the VT earthquakes, *Umakoshi et al. (1994)* proposed a magma ascent path at 13 km depth beneath the western shore of the Shimabara Peninsula, that rise to the east at an angle of 40-50°.

The total volume of magma erupted was 2.1×10^8 m^3 (dense rock equivalent). During all of the eruption time and dome growth, about 9400 pyroclastic flow events were counted seismologically by Japan Metereological Agency (JMA).

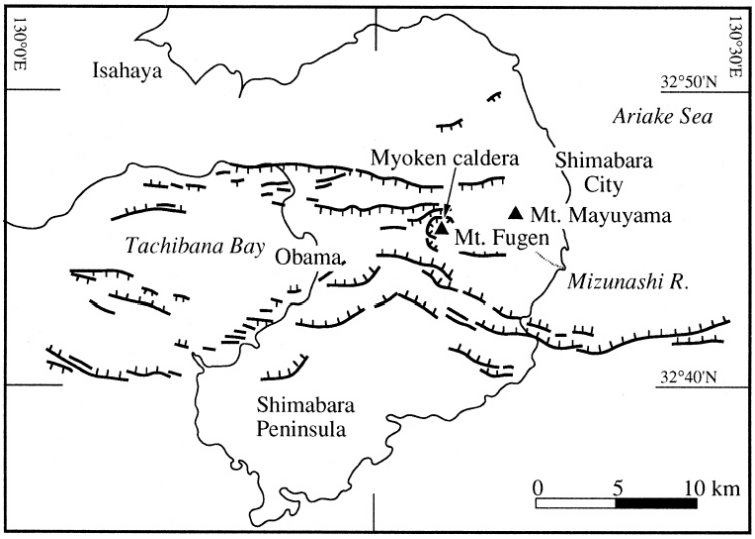

Fig. 2.5. Map showing Shimabara Peninsula on which Unzen Volcano is located. Unzen developed within the active volcanic graben. The highest peak before the 1991–95 eruption was Mt. Fugen (1359 m) within the Myoken caldera *(Nakada et al.,1999* modified from *Tsukuda 1993)*.

More than 99% of these pyroclastic flows were Merapi-type (dome collapse type), only one flow was accompanied by explosion (Pelee-type). All these pyroclastic flows covered the eastern part of Mt. Fugen (Mizunashi river Fig. 2.5) due to the dome's growth to the east *(Nakada et al. 1999).*

2.4 Petrology of 1991-1995 eruption and mixing models.

The 1991-1995 eruption of Unzen volcano generally was effusive, with about 2.1×10^8 m^3 of viscous magma having been extruded. The effusion rate was highest in the beginning (1991), with ≈ 4.6 m^3/s, and decreased with time to almost zero before the second pulse, which had a low effusion rate and occurred in 1993 *(Nakada et al., 1999)*. The products of the eruption have a dacitic bulk-rock composition with SiO_2 content varying between 64.5 and 66 wt%. The phenocryst abundance increases with increasing mafic compositions of the whole rock (total phenocryst contents from 20 to 30 vol. %; *Holtz et al., (2005); Sato et al. (2005); Nakada & Motomura, (1999)*). Enclaves found in the erupted material are basalt to andesite in composition and plot around the mafic end of the products (Fig.2.6).

The Unzen 1991-1995 lava is porphyritic and contains phenocrysts of plagioclase, hornblende, biotite, quartz, apatite, magnetite, ilmenite as well as trace amounts of augite and orthopyroxene.

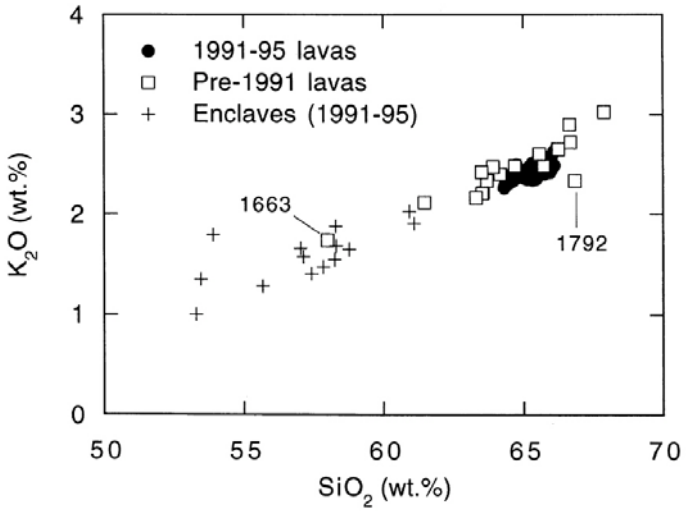

Fig. 2.6. SiO_2 vs K_2O diagram of the Unzen volcanic rocks. Historical lava are labeled as 1792 and 1663. (From *Nakada and Motomura 1999*)

The presence of hornblende as phenocrysts in a rhyolitic to rhyodacitic ground mass implies nearly H_2O saturated conditions at depth. One of the following conclusions is that Unzen magma is interpreted to have degassed almost completely during ascent in the magmatic conduit *(Nakada & Motomura 1999)*. The glass content in the groundmass varies from 50 to 80 vol. %.

For the erupted dacite the amount of water found was measured by Karl-Fische titration and ranges between 0.4 wt% and 0.1 wt% for the September 1991 and for the spine samples, respectively.

Phenocrysts commonly show compositional zoning. Reverse zoning at the rims of plagioclase, hornblende and magnetite has been interpreted as evidence for magma mixing, which took place just before and during the eruption. *(Nakamura, 1995; Nakada & Motomura, 1999; Venezky& Rutherford, 1999; Holtz et al., 2005; Sato et al., 2005)*.

It is assumed that the dacite was formed by mixing of high and low temperature (*T*) magmas (Fig. 2.7). The magnetite phenocrysts derived from the low-*T* magma are reversely zoned in Ulvospinel due to the mixing with high-*T* magma (the ulvospinel content in magnetite microphenocrysts increases from 17 to 35 mol% from the core to the rim of the phenocryst).

A diffusion calculation for reequilibration of the reverse zonings gives the time interval from magma mixing to quenching *(Nakamura, 1995)*. For the mixed dacite erupted from May 1991 to May 1993, the typical diffusion time was estimated to be a few months regardless of the effused sequence of 2 years. This indicates that the mixing process was continuous during effusion; otherwise, an increase in the diffusion time should be noted if the mixing processes occurred in one single event. The invariability of the other mixing signatures, such as the thickness of reaction rims around biotite phenocrysts, also support a continuous mixing model. The low-T end-member magma was estimated by mass-balance calculation to be a crystal-rich mush of dacitic composition. These observations led to a new model (see Fig. 2.7) wherein the highly crystallized remnant magma of the preceding activity mixes with the newly injected hot magma of similar bulk composition just prior to the effusion. The proposed mechanism implies that this type of magma mixing is an inevitable process in periodically erupting polygenetic volcanoes.

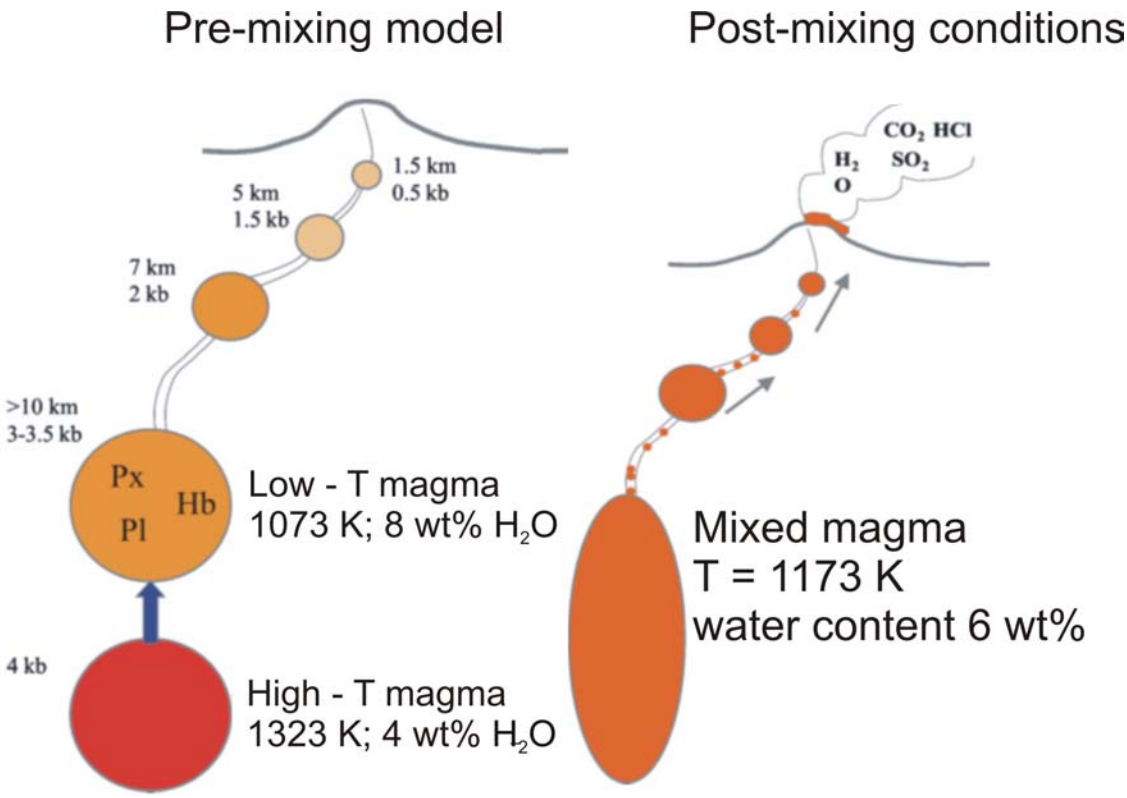

Fig. 2.7. Unzen: mixed processes model (*Holtz et al*., *2005* Unzen workshop).

The melt composition of the low temperature magma was estimated from the composition of glass inclusions in the plagioclase phenocrysts, which give a SiO_2 content of 76-77 wt% (anhydrous basis). The SiO_2 content of the high temperature magma was extrapolated from an interpolation between the melt inclusions in phenocryst and the groundmass (for the mixing line see *Holtz et al., 2005*).

The mixing model is illustrated in Fig. 2.7. In the case that this model is accepted for the generation of the Unzen magmas, it has to be noted that then, the two end-member magmas have to have the same viscosity.

Recently, *Browne et al. (2005),* suggest a different source for the dacite magma erupted at Unzen from 1991 to1995. The model (Fig 2.8) is based on magma mingling processes and was modelled by studying the two different types of enclaves found in the Unzen products. These enclaves are:

Porphyric, produced when intruding basaltic magma engulfed melt and phenocrysts of the resident silicic magma;

Equigranular, produced by prolonged mixing and granular crystallization with a slow cooling rate within the interior of the mafic intrusion.

The two different types of enclaves are interpreted to have been derived from different, but not independent mode of formation. The mechanism is shown in Fig. 2.8 (a,b,c,d) as described by *Browne et al., (2005)*:

a)The first step is the intrusion of high-alumina olivine-bearing basalt magma into the base of the silicic magma chamber. The mafic input starts to engulf and dissolve host phenocrysts, thereby assimilating the host magma.

b) The intruded magma is now an andesite hybrid which rapidly crystallizes. The successive second boiling in response to the heat loss to the silicic host magma generates the porphyric enclaves (P-type).

c) As consequence, the temperature of the host magma is increased by conduction and by incorporation of P-type enclaves. Thus, the mafic inclusions slowly crystallized as a framework of equigranular crystals.

d) Equigranular enclaves (E-type) are stripped off the cooling inclusions by convective stirring or are possibly disrupted by a new injection of magma and dispersed into the host magma.

Following this model, the eruption was initiated by an input of basaltic magma into the silicic magma reservoir.

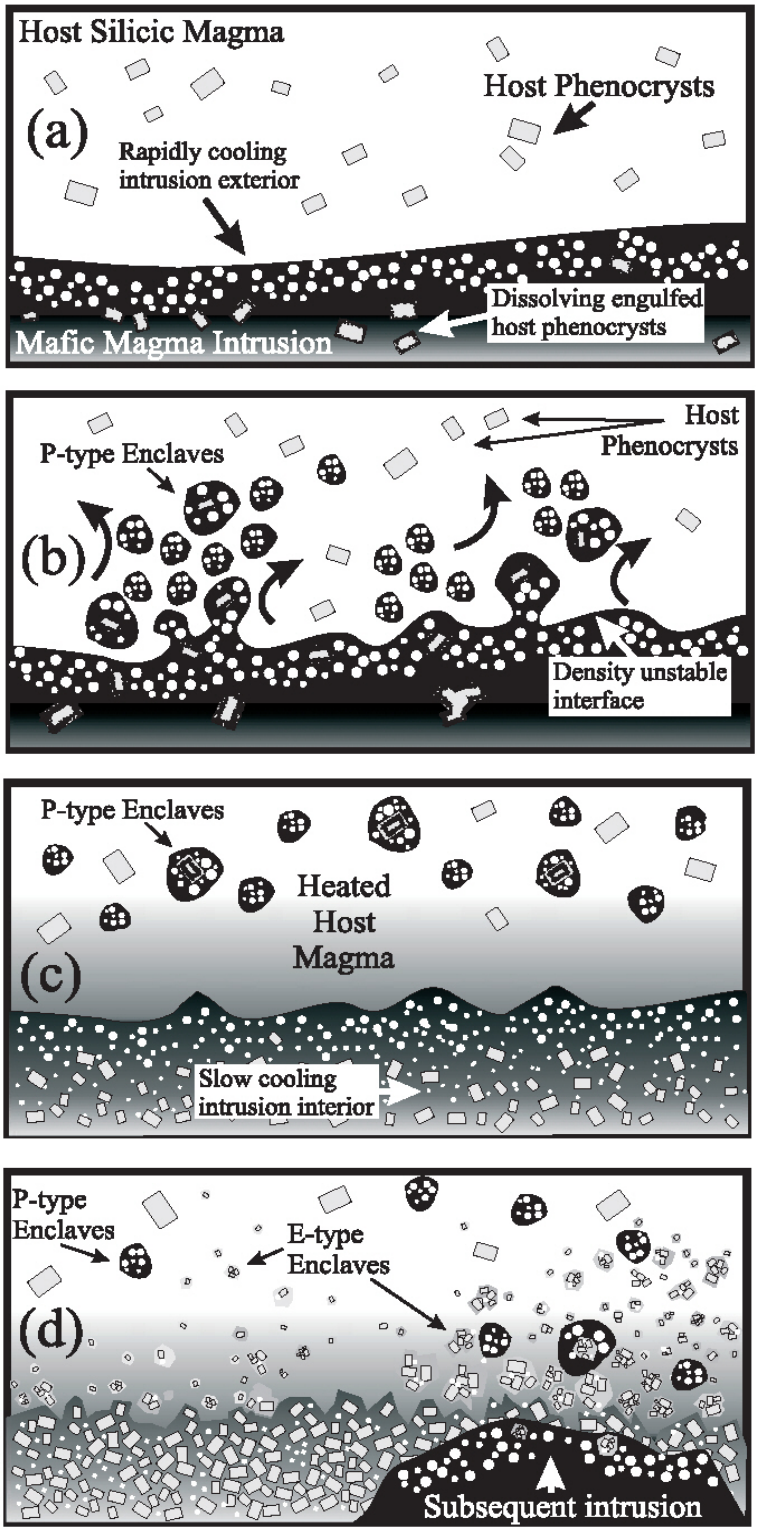

Fig. 2.8. model for the formation of Porphiric and Equigranular enclaves in the Unzen magma chamber. (see text for explanation) *(*from *Browne et al., 2005).*

2.5. The Unzen scientific drilling project (USDP).

In May 1997, about 75 scientists from Japan, USA, Germany, UK, Belgium, France, and Israel met in Shimabara to consider what had been learned during the Unzen episode. During this meeting the idea of the Unzen Scientific Drilling Project (USDP) was born.

The goal of this meeting was to provide a new level of understanding of this type of volcanism, which has been dominated by effusive eruption of crystal rich magma for the past 500 kyr. The Unzen scientific drilling project, a six year project divided in two phases, started in April 1999. It is cosponsored by the Japanese Government (MEXT) and International Continental Drilling Program (ICDP).

In the first phase of the project, two holes were drilled into the volcano's flank (USDP 1 and 2; Fig.2.9). In the second phase, the magma conduit of the 1991-1995 eruption was intersected by the drill hole (USDP 3and 4; Fig.2.9). The project was successfully ended in February 2005 with Unzen workshop 2005 at Shimabara city.
The last step (USDP4) of the project, in which core samples and drilling mud recovered were investigated, resulted in the following conclusions *(Nakada et al., 2005)*:

1) Physical measurements and analysis of spot cores indicate that the conduit was successfully penetrated by the USDP-4.
2) The conduit zone of Unzen volcano consists of multiple parallel dikes and veins of different ages and is about 500 m wide in north-south direction. The conduit zone dikes are up to 40 m thick.
3) The feeder dike of the last eruption has cooled from 850 °C to less than 200 °C in nine years by effective hydrothermal circulation. The dike lava is devitrified and hydrothermally altered.
4) Degassing of ascending magma at the drilled depth probably occurred along the cracks propagated by magma gas pressure.
5) Microlites of the conduit lava are smaller in size but similar in number density to those in the dome lava. This suggests that magma ascended slower as it reached

shallower depths and/or that microlite growth occurred during the second half of dewatering.

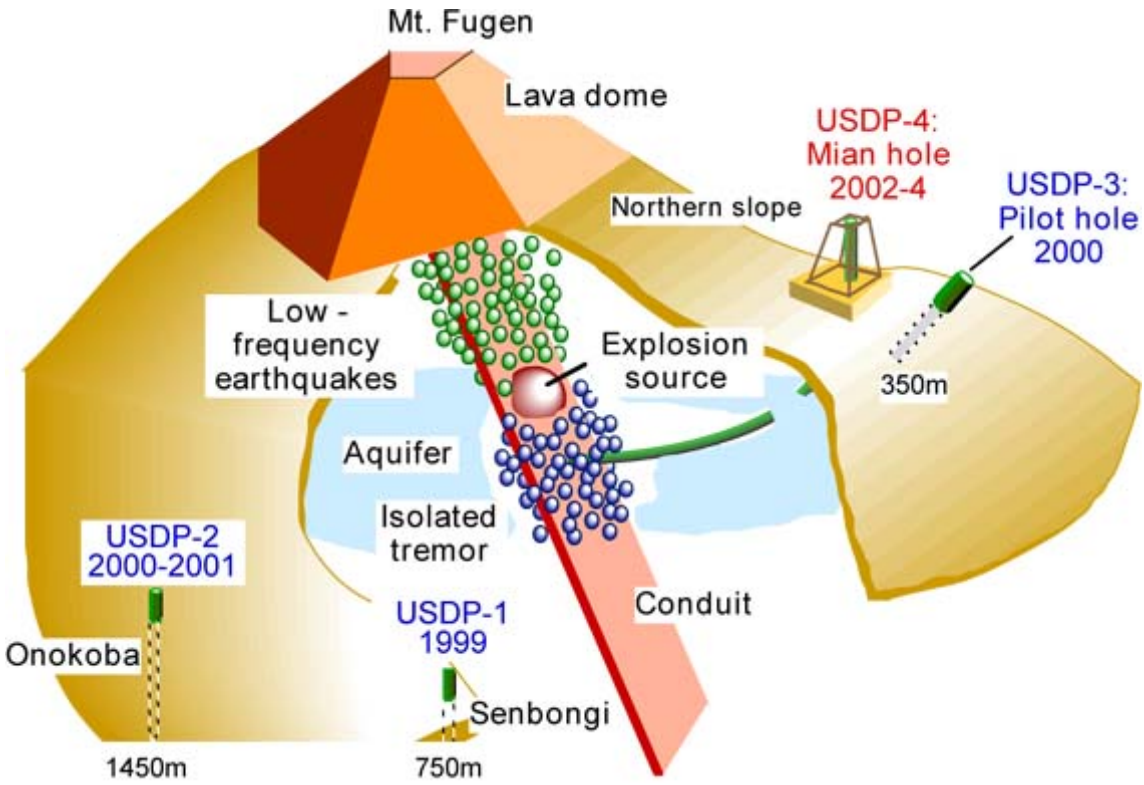

Fig. 2.9. schematic view of USDP in the different stage. The project was successfully ended in February 2005 with a final workshop at Shimabara city. (Picture from the site: http://hakone.eri.u-tokyo.ac.jp/vrc/usdp/index.html.)

3. Properties of silicate melts.

3.1 Basic knowledge.

In order to well understand processes introduced in the previous chapter, concerning eruptions stiles occurred at Unzen volcano, it is helpful to have a brief introduction on the chemical properties of melts. SiO_4^{4-} tetrahedra are major constituent of silicate melts. Si^{4+} is four-fold coordinated. Each SiO_4^{4-} (in polymerized melts) is connected to similar tetrahedra by Si-O-Si linkages. In the case that one oxygen connects two SiO_4^{4-} tetrahedra, this oxygen is defined as bridging oxygen (BO). On the other hand, if the oxygen is connected with a cation, which is not tetrahedrally coordinated, it is called non-bridging oxygen (NBO). Cations acting as network formers are, e.g., Si^{4+}, Al^{3+}, Fe^{3+}, B^{3+}, and Ge^{3+}; all these cations are usually tetrahedrally coordinated and are able to form structural units linked together by bridging oxygen atoms. In silicate melts, the bond between network-forming cations and oxygen is very strong. This is illustrated in table 3.1, which shows the characteristic force γ of cations that are usually present in silicate melts (*Kuryaeva, 2004*). From table 3.1, is possible to note that the degree of ionicity of the bond with oxygen increases in the order: $Si^{4+} < Al^{3+} < Ti^{4+} < Fe^{3+}$. The coordination of Ti^{4+} was studied by *Mysen et al. (1980)* and *Wood et al. (1980)*. These authors found a tetrahedral coordination for Ti^{4+}, meaning that titanium cations are network former and can be presented in forms of clusters in silicate melts and glasses (*Virgo et al., 1982*). *Rao (1963)* and *Cormier et al. (1998)* described Ti as playing dual role in glasses as a former and modifier. This is usually associated with the presence of $^{[4]}Ti$ (network-former) or $^{[6]}Ti$ (network modifier). However, x-ray absorption

measurements show that Ti-containing silicate glass can be considered as a composition-dependent mixture of 4-, 5-, and 6-coordinated Ti (*Farge et al., 1996; Ponader et al., 1996*). *Farge et al. (1997)* observed that the coordination chemistry of Ti in glasses and melts is controlled mostly by the NBO/T ratio and the type of network modifier around Ti.

Dingwell and Virgo (1988) have shown that the stability of tetrahedrally coordinated Fe^{3+} decreases in the order of K > Na > Ba > Sr > Ca > Mg when these elements are used to compensate the charge in iron-oxygen structural units.

Li^+, K^+, Na^+, Ca^{2+}, Mg^{2+}, and Fe^{2+} are network modifiers. The coordination number in silicate glass and melts is 4 for Li-O bonds, while for K-O bonds, the coordination number varies from ~ 7 to 10.4. Na-O coordination number can vary between 5 and 8. Ca-O and Mg-O bonds can vary from 4 to 8 (for more details see *Brown et al., 1995*). Some of them act as charge balancing ions for either Al^{3+}, Fe^{3+}, or B^{3+}. These cations can also acts as network modifiers if their concentration exceeds the amount of charge balancing cations. Then Al^{3+}, Fe^{3+}, and B^{3+} are octahedrally coordinated *(Mysen, 1988)*, but there is alsoevidence by NMR (Nuclear Magnetic Resonance) for 5 coordinated Al.

Table 3.1 Characteristic force γ of the cations (after *Godovikov 1979*).

Cation	γ	Cation	γ	Cation	γ
Si^{4+}	225.6	Mg^{2+}	61.1	Na^+	18.5
Al^{3+}	128.7	Fe^{2+}	44.4	Sr^{2+}	16.4
Ti^{4+}	94.8	Li^+	28.5	Ba^{2+}	11.5
Fe^{3+}	86.3	Ca^{2+}	22.1	K^+	7.3

Note: γ is the ratio between the ionization potential of the n*th* electron and the orbital radius of an ion with a charge n^+: $\gamma = \mathrm{I}_n / r_{orb}^{n^+}$.

Al^{3+} plays a special role since it is able to replace Si^{4+} cations. The substitution of Al^{3+} for Si^{4+} is more favoured in the presence of large-sized monovalent (such as K^{+}) than in the presence of small-sized divalent cations (Mg^{2+}) (*Kuryaeva, 2004*).

In dependence of the chemical composition, the degree of polymerization in glass can vary (polymerization is a chemical reaction in which one or more small molecules combine to form larger molecules). The number of non-bridging oxygens per tetrahedrally coordinated cation (NBO/T) is a way to quantify the degree of polymerization in a melt. If NBO/T=0, the melt is fully polymerised. According to *Mysen et al. (1985)* the NBO/T can be calculated:

$$\frac{NBO}{T} = \frac{1}{T} \cdot \sum_{i=1}^{i} n \cdot M_i^{n+} \qquad 3.1$$

where T is the total atomic abundance of tetrahedrally coordinated cations, M_i^{n+} is the proportion of network modifying cations, "*i*", with electrical charge n^{+} after subtraction of the portion required for charge-balancing trivalent cations on tetravalent sites (*Mysen, 1988*).

Melts have a structure which is very sensitive to composition and temperature. When a small compositional change (for example replacing network forming cations by modifying cations) takes place, this will be reflected in a change in the strength of Si-O-Si bonds and in the properties of the melt such as activation energy of diffusion, viscous flow and conductivity (*Mysen, 1988*).

3.2 Rheology and Viscosity: a bit of history.

Rheology is defined as the science of deformation and flow of matter. The term itself originates from the greek term “rheos” meaning “to flow”. Rheology is applicable to all types of materials, from gases to solids. The science of rheology is young, only about 70 years of age, but its history can be traced in the Old Testament. There, one can find the term “rheology” which translates into *“everything flows if you just wait long enough”*. It was also described by the Greek philosopher *Heraclitus* as “panta rei” : everything flows. *Reiner*, together with *E. Bingham*, was the founder of the science of rheology in the mid–20s. One of the main issues of rheology is its definition and the classification of materials. Glass, for instance, is usually defined as a solid material, but, for eyample, if the thickness of an old church window is measured from the top to the bottom a difference will be noted. Glass does in fact flow like a liquid, albeit very slowly. An air bubble captured in a glass object will rise, surely but slowly, due to the difference in density between air and glass. The process may, however, take centuries to be observed and is of course not evident to human beings, as the time of observation is too short. One way of characterizing a material is by its relaxation time, i.e. the time required to reduce a stress in the material by flow. Typical magnitudes of relaxation times for materials are:

Table 3.1. Relaxation time of matter. (New Food Volume 3 Issue 2, 2000)

Matter state	Time (seconds)
Gases	$< 10^{-6}$
Liquids	10^{-6} - 10^{2}
Solids	$> 10^{2}$

The Deborah number, *D*, named after the prophetess *Deborah*, is a way to characterize the flow behavior of a material. The Deborah number is the ratio between the time of relaxation and the time of observation. Consequently, the Deborah number is large for materials of high viscosity and low for material of low viscosity. Another way to define material rheologically is by the terms viscous, elastic or viscoelastic. By definition an ideal viscous fluid is unable to store any deformation energy. Hence, it is irreversibly deformed when subjected to stress. It flows and the deformation energy is dissipated as heat, resulting in an increase of temperature. A viscous fluid can therefore be described as a fluid, which resists to the act of deformation rather than the state of deformation, whereas an elastic material resists the act as well as the state of deformation. A number of materials feature both behaviors, storing some of the deformation energy in their structure as well as losing some by flow. These materials are called viscoelastic. In section 3.2.3 I will focus on different rheological models but prior to this, I will go into detail viscosity and its relationship to volcanology.

3.2.1 What is viscosity and why is it so important, especially in volcanology?

This question is best answered by an example. Imagine a styrofoam cup with a hole in the bottom. If you pour honey into the cup you will find that the cup drains very slowly. That is because the honey's viscosity is large compared to other liquids viscosities. If you fill the same cup with water, for example, the cup will drain much quick. In other words, viscosity is a measure of a fluid's resistance to flow. It describes the internal friction of a moving fluid. A fluid with a high viscosity resists to motion because its molecular makeup provides high internal friction. A fluid with a low viscosity flows

easily because its molecular makeup results in very little friction once it is in motion. Gases also have a viscosity, although it is a little more difficult to notice under ordinary circumstances. Viscosity is an important subject in volcanology. The less viscous a magma is, the more likely it is to erupt. On the other hand, when lavas featuring higher viscosities erupt, they usually do so explosively. Viscosity also affects the shapes of lava flows and of the mountains they erupt from. The more viscous the magma, the thicker the lava flow. A volcano erupting a very viscous magma usually forms steep slopes. Thus, shield volcanoes like on the Hawaiian islands have gentle slopes (less than 10 degrees), whereas the slopes of stratovolcanoes like the Cascades in the northwestern mainland or Unzen in Japan are much steeper (roughly 25 degrees). As expected, Hawaiian volcanoes erupt more fluid lavas (basalt) than the Cascade or the Unzen volcanoes do, which erupt andesitic or dacitic lavas.

Viscosity in magma is a result of a number of factors. Viscosity is mainly dependent upon the degree of polymerization within the melt, this gives rise to the melt having a structure. The higher the degree of polymerization, the higher the viscosity and vice versa. Polymerization is controlled by the following factors: SiO_2 content, temperature, volatile content, and content of other elements. It increases with increasing SiO_2 content, accompanied by a temperature decrease and where there are low volatile contents. The presence of Al also increases polymerization. However, the presence of Na, Ca, Mg and Fe decreases polymerization. It can therefore be seen that in basic igneous lavas (basalts, table 3.2), the viscosity is low and therefore when erupted, lava flows quite easily. In acid igneous magmas (rhyolites), the viscosity is very high, leading to explosive eruptions as the lava resist to motion. Table 3.2 shown a list of materials and their viscosity.

Tabble 3.2. List of materials and their viscosity

Material	Viscosity (Pa s)
water	0.1
Engine Oil	1
Plasticine	100
Asphalt	1000
Basalt lava	10-100
Granites (magma)	10^5-10^{11}

From http://www.brookes.ac.uk/geology/sedstruc/viscosit/vis.htm.

Therefore, the prediction of viscosity is an important tool to interpret the nature of volcanic eruptions. The explosiveness of a volcano is also determined by viscosity, because with decreasing viscosity, the ability of the magma to release volatiles also decreases, resulting in a higher explosive potential. A magma with a high viscosity produces violent explosive eruptions, whereas magmas with low viscosities produce lava flows. Viscosity can, by all means, be used as a classification tool as it may save lives if and when an eruption occurs.

3.2.2. Newtonian behavior.

We note viscosity as the measure of the internal friction of a fluid. This friction becomes apparent when a layer of fluid is forced to move in relation to another layer. The greater the friction, the greater the amount of force required to cause this movement, which is called "shear." Shearing occurs whenever the fluid is physically moved or distributed, as in pouring, spreading, spraying, mixing, etc. Therefore, highly viscous fluids require more force to be moved than less viscous materials.

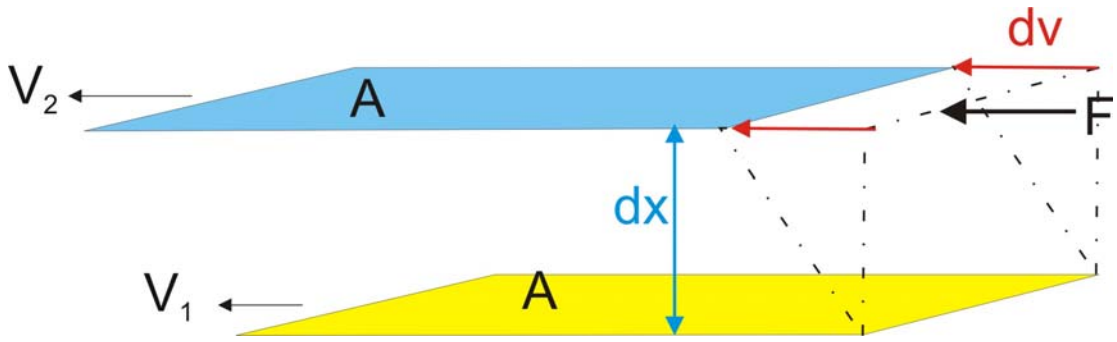

Fig. 3.1. Schematic sketch showing two parallel planes of fluid moving in the same direction but with different velocities.

Isaac Newton defined viscosity by considering the model represented in the figure 3.1. Two parallel planes of fluids with an equal area "A" are separated by a distance "dx" and are moving in the same direction but at different velocities "V_1" and "V_2". Newton assumed that the force required to maintain this difference in speed was proportional to the velocity gradient (dv/dx). A mathematic expression for this scenario is:

$$\frac{F}{A} = \eta \cdot \frac{dV}{dx} \qquad (3.2.1)$$

The term F/A indicates the force per unit area required to produce the shearing action. It is referred to as "shear stress" and will be symbolized by "σ" [units: N/m^2 =Pa or

historically dine/cm^2]. When the force is distributed normally upon a surface, it is called normal stress; when it is distributed parallel upon a surface, it is called shear stress. The viscosity is obtained as the ratio of shear stress and shear rate (ε):

$$\eta = \frac{\sigma}{\varepsilon} \tag{3.2.2}$$

Newtonian viscosity means that shear stress is linearly proportional to the velocity gradient in the direction perpendicular to the plane of shear or that shear stress is proportional to shear rate (Fig. 3.2). If a fluid does not obey this relation, it is termed a non-Newtonian fluid.

3.2.3 Non-Newtonian behavior.

A non-Newtonian fluid is a fluid in which the viscosity changes with the applied shear force. As a result, a non-Newtonian fluid does not have a well defined viscosity. To give an example, think of corn starch added to a cup of water. If you start to stir slowly you reach a point (named “shear thickening”) where the non-Newtonian behavior of the matter becomes apparent. The application of force by the finger, spoon etc. causes the fluid to behave like a solid. If the force is released, the matter will recover its liquid behavior. In the industry, fluids of this sort are for instance being used for bullet resistant body armor, useful for their ability to absorb the energy of high velocity projectile impact, but remaining soft and flexible when struck at low velocity. Another example of non-Newtonian fluid is quicksand. If one accidentally falls into quicksand, it

is better to move slowly and stay calm so one can move freely and the quicksand will act like a liquid and allowing to get out. Thrashing around too quickly will make the quicksand act like a solid and one can get stuck or even sink in much quicker.

To have an idea about the behavior of matter in a general view, it's helpful to consider the most general classification models of Newtonian and non-Newtonian fluids (Fig. 3.2).

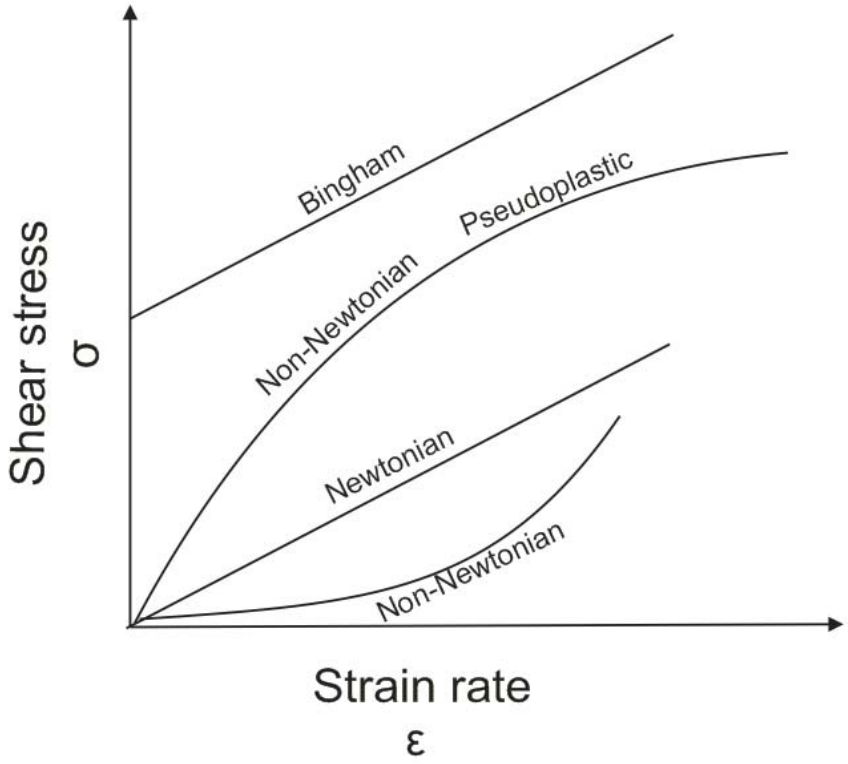

Fig. 3.2. Shear stress versus rate of shear strain for Newtonian and non-Newtonian liquids. The slope of these lines gives the viscosity of the liquid, which for a Newtonian one remains constant regardless of shear stress. The viscosity of non-Newtonian liquids varies with the applied shear stress. (from *Philpotts 1990*).

An interesting type of non-Newtonian fluid is called time-dependent viscosity. It can be divided into:

a) *Rheopectic* in which apparent viscosity increases with duration of stress (i.e. some lubricants); the longer the fluid is subject to shear, the higher its viscosity. (Fig. 3.3a)

b) *Thixotropic* in which apparent viscosity decreases with duration of stress (i.e. non-drip paints and tomato ketchup). It is a property of some non-Newtonian pseudoplastic fluids to show a time-dependent change in viscosity; the longer the fluid is subject to shear, the lower its viscosity (Fig. 3.3b)

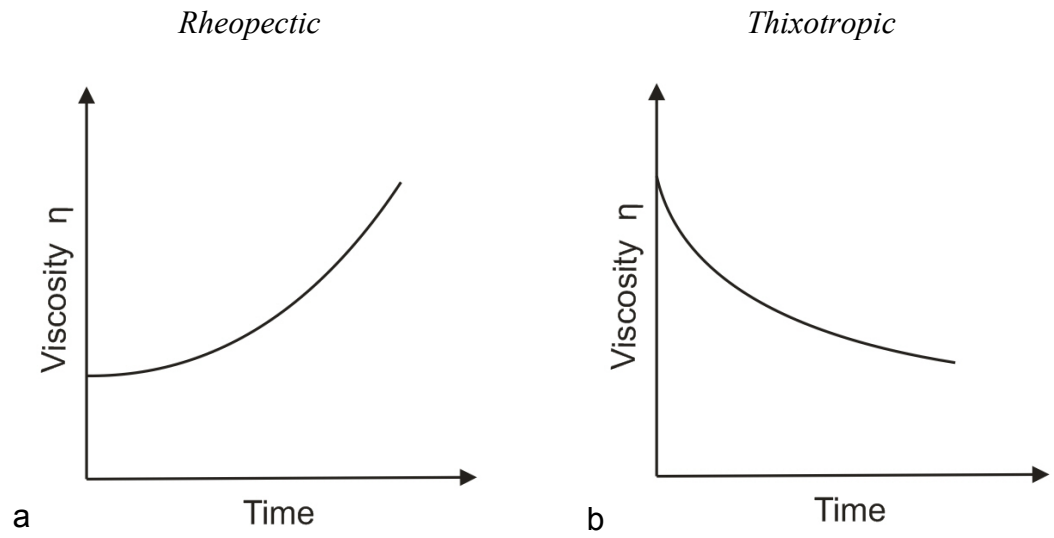

Fig.3.3. Two examples for non-Newtonian behavior:
a) viscosity increases with time (*Rheopectic*) b) viscosity decreases with time (*Thixotropic*)

3.2.4 Describing and modelling viscosity.

Over the last few decades, many attempts have been made in order to predict viscosity as a function of composition, temperature, and dissolved volatile content. Starting from the *Adam and Gibbs (1965)* theory (including the non-Arrhenian behavior of silicate melts) or the model of *Bottinga and Weill (1972)* (first model to predict viscosity in the

low viscous range), a huge effort has been devoted to understand the mechanisms of viscous flow. Unfortunately, until now, there is no generally applicable model that can predict viscosity for all natural compositions. However, it is clear that the mechanisms are related to short and medium range rearrangements in the melt. According to *Stebbins (1995)*, the local structural rearrangements requiring *Si-O* breaking execute primary control on viscosity. On the other hand, *Dingwell and Webb (1990)* state that the mechanism for viscous flow in silicate melts at the atomic scale is due to the relation of diffusion of *Si* cations and *O* anions in the strongly bonded network. If we consider the simplest form, the temperature viscosity relationship can be described by the *Arrhenius equation*:

$$\eta = A_e \exp(E_e / RT) \tag{3.3}$$

where η is the viscosity, A_e an adjustable pre-exponential factor, E_e is the activation energy, R the gas constant, and T the absolute temperature. The activation energy can be described as a potential energy barrier atoms have to overcome moving from one site to another in the melt (*Glasstone et al., 1941*). However, when plotting log η vs. 1/T, for most compositions the curvature of the viscosity data shows that the activation energy is not constant but decreases with temperature (*Richet and Bottinga, 1995)*.

Using the Arrhenius law, *Shaw (1972)* derived a simple empirical model to describe the viscosity of a Newtonian fluid as the sum of the contributions due to the single oxides constituting a silicate melt:

$$\ln \eta(T) = \Sigma_i x_i \ln_i = \Sigma_i x_i \left(A_i + \frac{B_i}{T} \right) \tag{3.4}$$

where x_i is the molar fraction of oxide component *i*, *Ai* and *Bi* are constant and *T* is the temperature (*K*).

Richet (1984), Richet and Bottinga (1995), Baker (1996), Hess and Dingwell (1996), and *Toplis et al. (1997)* have shown that the Arrhenius relation (Eq. 3.3), and the conclusion derived from it (e.g. *Shaw, 1972*), are largely insufficient to describe the viscosity of melts over the entire temperature interval that are now accessible using new techniques. Many studies have demonstrate the failure of this model (e.g. *Neuville et al., 1993*).

An empirical equation that fits viscosity vs. temperature (above the Tg; see section 3.3) very well is the *Vogel-Fulcher-Tamman (VFT)* equation*:*

$$\eta = A \exp [B /(T-T_0)] \qquad (3.5)$$

where A, B and T_0 are adjustable empirical parameters. One can write this equation as:

$$Log\ \eta = A + [B /(T-T_o)] \qquad (3.6)$$

where *A*, *B* and T_o are adjustable empirical parameters. The first term (*A)* can be seen as the viscosity value for infinite temperature ($T \rightarrow \infty$); *B* is a constant representing the pseudo activation energy associated with viscous flow; T_o is the value at which the viscosity approaches on infinite high value ($\eta \rightarrow \infty$). T_0 is always found to be lower than Tg (see section 3.3). All these parameters are needed for fitting viscosity-temperature data. Equation (3.6) has no physical meaning for $T<T_0$.

The *Adam & Gibbs (1965)* theory uses a thermodynamic approach to describe kinetic properties. This theory conveys the relation between structural relaxation properties of glass forming melts and properties like *Tg* and heat capacity (C_p). This theory suggests that viscous flow in liquids occurs through the interaction of molecular groups in the liquids, with an average probability *w(T)* that is inversely proportional to the structural relaxation time τ:

$$w(T) = \bar{A}exp[-B_e/(T \cdot S_{conf})] = \tau^{-1} \quad (3.7)$$

where $\bar{A}$ and B_e are dependent on the composition with a negligible temperature dependence with respect to the product $T \cdot S_{conf}$ and:

$$S_{conf}(T) = K_B \ln\Omega = Configurational\ Entropy \quad (3.8)$$

Where k_B is the *Boltzmann* constant and Ω represent the number of all the possible configurations of the system. Since the structural relaxation time is inversely proportional to the average probability of structural rearrangement, we can write:

$$\tau = A_\tau exp\ (B_e/T \cdot S_{conf}) \quad (3.9)$$

And, because the viscosity is proportional to the structural relaxation time:

$$\eta = A_e\ exp\ (B_e/T \cdot S_{conf}) \quad (3.10)$$

Where A_e is a pre-exponential constant *(Richet & Bottinga, 1995)*.

One of the more recent equations to predict viscosity is the *Avramov (AV) equation.*

This equation is able to predict the change in viscosity as a function of temperature for a specific composition. The *Avramov* theory derives an equation describing the relationship of viscosity and temperature for a given composition and by fitting experimental data, parameters can be derived (*Avramov, 1998a*). The basic idea is that the structural units of the system jump with a frequency depending on the activation energy (*E*). The structural units have to overcome *E* in order to jump to a higher energetic state. The whole model is based on the probability distribution function describing the activation energy needed for this jump (*Avramov & Milchev, 1988; Avramov, 1994*). Passing through the degree of disorder, melt entropy, jump frequency, vibration frequency, entropy, and a parameter named dispersity of activation energy (characterising the probability), it is demonstrated that viscosity is inversely proportional to the average of jump frequency (*Avramov, 1998b*).

The main jump frequency (ν) depends on the entropy in relation to the dispersity (ψ) and is described as:

$$\nu = \nu_0 \exp\left\{-\frac{E_{\max}}{\psi_r}\left[-\frac{2(S-S_r)}{ZR}\right]\right\} \qquad (3.11.1)$$

where ν_0 is the vibration frequency, E_{max} is the maximum activation energy, ψ_r is the dispersity at a given reference state at which the entropy is S_r, R is the gas constant and Z the so called degeneracy or the numbers of channels along which the building unit can escape from the given position (*Avramov, 1998b*).

The viscosity is inversely proportional to the average jump frequency:

$$\eta = \eta_\infty \exp\left\{\frac{E_{\max}}{\psi_r}\exp\left[-\frac{2(S-S_r}{ZR}\right]\right\} \qquad (3.11.2)$$

where η_∞ is the viscosity at infinite temperature. It is possible determine how viscosity depends on any control parameter like temperature *T*, pressure *P* and composition *x* by solving the corresponding entropy dependence *S=S(T,P,x)*.

It is convenient to chose Tg(glass transition temperature, see section 3.3) as reference state, because above Tg, the entropy can be expressed via the heat capacity C_p as :

$$S = S_g + C_p \cdot \ln\left(\frac{T}{T_g}\right) \tag{3.11.3}$$

so that the temperature dependence of η becomes:

$$\eta = \eta_\infty \exp\left[\varepsilon\left(\frac{T_g}{T}\right)^{\alpha_{AV}}\right] \tag{3.11.4}$$

where $\varepsilon = E_{max}/\psi$; $\alpha_{AV}=2\Delta C_p/ZR$ (C_p is the heat capacity).

Avramov (1998a) proposed the parameter ε as a dimensionless activation energy at the glass transition temperature which can be calculated as:

$$\varepsilon = \log \eta\,(Tg) - \log \eta_\infty \tag{3.11.5}$$

α_{AV} is described as a fragility index (fragility see section 3.3). It can be calculated that $\log \eta_\infty = -1.5 \sim -1.7$ when $\log \eta\,(Tg) = 12$ *(Avramov, 1998b)*.

The error in viscosity calculation is mainly given from the composition. In figure 3.4 the drop in viscosity is given in dependence of composition at Tg of pure solvent. The curve is built for Z=10. For lower Z values the drop in viscosity can reach 7 orders of magnitude *(Avramov, 1998b)*.

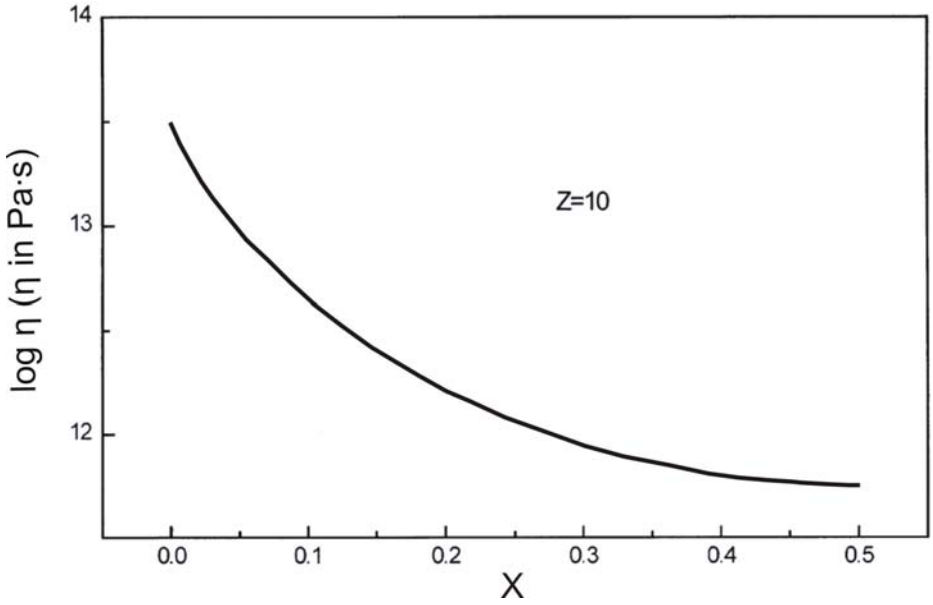

Fig. 3.4. Composition dependence of viscosity (from *Avramov 1998b*).

3.3. Glass transition temperature.

The glass transition (*Tg*) range is a kinetic barrier separating the glass state from the (super cooled) liquid state. *Tg* is a nonequilibrium phenomenon inherently dependent on the rate of temperature change (*Richet & Bottinga, 1995*). This range, in which transition occurs, varies with the cooling rate. Therefore, the properties of the glass are not only dependent on temperature but also on the thermal history. A slow cooling rate provides a lower *Tg* than a faster cooling rate. Generally, the temperature value at which log η = 12 (Pa·s) is named Tg. However, Tg is defined for a specific heating/cooling procedure to make values comparable. During cooling, when passing through the range of glass transition, a rate of 2K/min is used and during heating 5K/min *(Scholze, 1991).* Often, Tg values are derived from dilatometric or colorimetric measurements. When using this procedure the viscosity at Tg is equal to $10^{12.3}$ Pa·s.

3.4. Strong and fragile melts.

The reason why some melts show an Arrhenian and others non-Arrhenian viscosity temperature dependence over a long range in temperature and viscosity can be explained by using the *Adam-Gibbs* theory. The Adam-Gibbs approach for the shear viscosity (see *Richet and Bottinga, 1995*; *Moynihan, 1995*) of an equilibrated melt above Tg is given by:

$$\eta = \eta_0 \exp\left[\frac{B_\eta}{TS_C(T)}\right] \qquad 3.13$$

where η_0 and B_η are constants. The melt viscosity will be roughly Arrhenian and log η vs. 1/T will plot roughly linear if the temperature dependence of the configurational entropy $S_c(T)$ and hence the value of ΔC_p ($\Delta C_p = C_{p\text{-liquid}} - C_{p\text{-glass}}(Tg)$) are small. A highly temperature dependent $S_c(T)$ and a large value of ΔC_p will result in highly non-Arrhenian behavior.

Following the strong and fragile theory proposed by *Angell, (1985)* the VFT equation (3.5) can be written as:

$$\eta(T) = \eta_0 \exp\left(\frac{F_i T_0}{T - T_0}\right) \qquad 3.14$$

where η_0 is the pre-exponential term, F_i, is the fragility index and T_0 is the VTF temperature at which the viscosity diverges. *Angell (1985)* uses the F_i parameter to distinguish between two opposite manners of liquids: *strong* and *fragile*. Liquids that strongly diverge from Arrhenian behavior are called *fragile* and feature F_i value is low. High F_i values correspond to *strong* liquids and they show an Arrhenian behavior.

Hence, in Angell's terms, strong liquids have small ΔC_p values and fragile liquids have large ΔC_p values *(Angell, 1985)*. An example is given in fig 3.4.

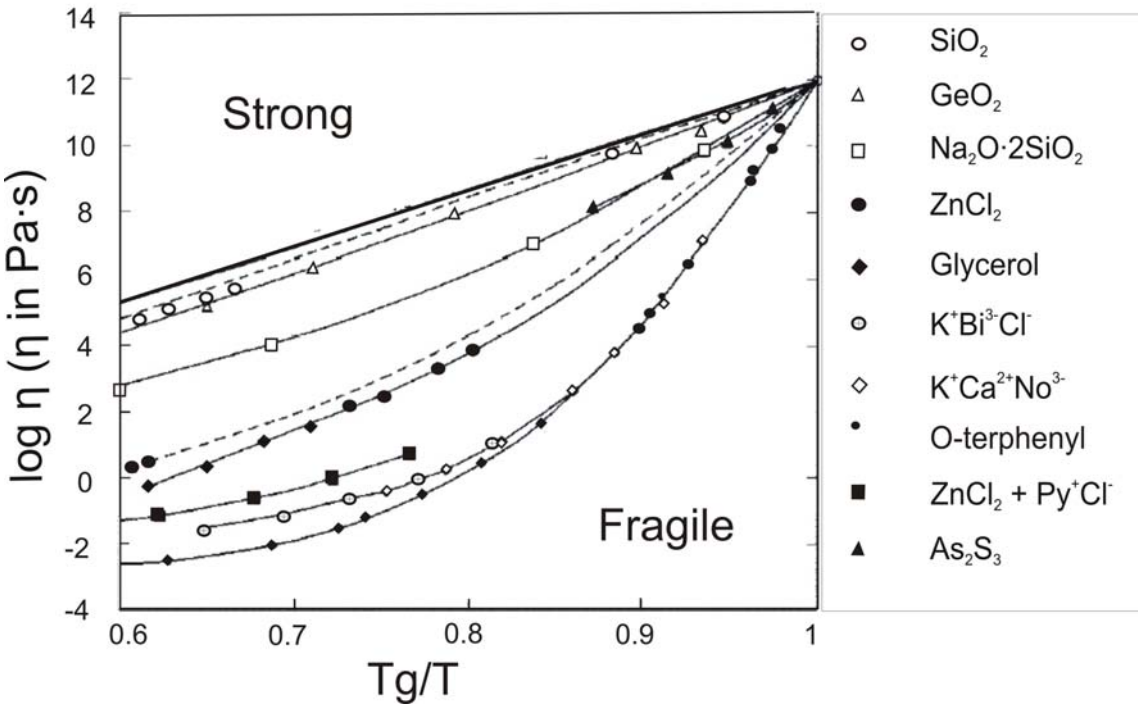

Fig. 3.4. Strong melts follow approximately Arrhenian behavior (linear relationship), while fragile melts have a curvature or non Arrhenian behavior (from *Huang and McKenna, 2001*).

In other words, a strong liquid with a small ΔC_p has a structure which maintains its "integrity" fairly well as the temperature increases above Tg, whereas a fragile liquid with a large ΔC_p has a structure which "falls apart" rapidly with increasing temperature. An important property that controls the fluid dynamic properties of magmatic systems is their ability to flow. A measure of the rapidity with which these properties change with temperature as they approach the glass transition temperature *Tg* is given by the fragility. Fragility can be defined thermodynamically (thermodynamic fragility see *Kauzmann, 1948*) or rheologically (kinetic fragility, see *Martinez and Angell, 2001; Giordano and Dingwell, 2003a).* It is also possible to estimate a deviation from the Arrhenian behavior using the ratio T_0/Tg (Kinetic fragility, *Giordano and Dingwell, 2003a*).

3.5 Pressure effects on viscosity

In the literature the degree of melt depolymerization *(NBO/T)* is commonly used as parameter to determine the dependence of viscosity on pressure (*Brearley et al., 1986; Scarfe et al., 1987; Bottinga and Richet, 1995; Scarfe et al., 1987*). These authors found that some silicate melts, like $CaMgSi_2O_6$ (with NBO/T>1), show a positive effect of pressure on viscosity (increasing pressure and increasing viscosity), whereas major silicate and aluminosilicate melts with NBO/T<1 (e.g. $NaAlSi_3O_8$, $NaAlSi_2O_6$, K_2O-MgO-$5SiO_2$, andesite, tholeitic basalt) display a decrease in viscosity when pressure increases (negative pressure effect). High temperature-high pressure viscosities in the system Ab-Di were measured using the falling sphere method (*Kushiro, 1978; Scarfe et al., 1979; Brearley et al., 1986; Brearley and Montana, 1989; Persikov and Bukhtiyarov, 1999; Mori et al., 2000; Suzuki et al., 2002*). In contrast to the Di melt, which shows a positive pressure dependence of viscosity, the Ab melt exhibits negative pressure dependence. *In situ* falling sphere experiments of *Suzuki et al. (2002)* indicate that the viscosity of Ab melts decrease with increasing pressure at least up to 5.3 GPa.

An “anomalous” negative pressure dependence was observed for highly polymerized silicate melts of various compositions (*Scarfe et al., 1987*). In the frame of *Adam-Gibbs* (AG) theory, *Gupta (1987)* postulated that the negative *P*-dependence originates from a larger coefficient of thermal expansion of the glass compared to the liquid. Another explanation can be found in a decreasing polymerization under applied pressurie due to larger partial molar volumes of bridging oxygens compared to non-bridging oxygens (*Bottinga and Richet, 1995*). Several authors have suggested that the anomalous viscosity behaviour is correlated to pressure-induced changes in coordination of Si, Al and oxygen or to distortions of T-O-T and O-T-O bond angles (T = tetrathedrally

coordinated cations such as Si and Al) in the silicate network (*Waff, 1975; Woodcock et al., 1976; Sharma et al., 1979; Bryce et al., 1999; Suzuki et al., 2002*). However, so far none of these explanations is generally accepted.

In more recent study, *Behrens and Schulze, (2003* chose X_{NBO} (equals to NBO/(NBO +BO) as the main compositional variable in graphical presentations. X_{NBO} is preferred over *NBO/T* (ratio of non-bridging oxygens to tetrahedral cations) because it is a valid thermodynamic compositional variable for a two oxygen mixing model, in contrast to *NBO/T* which has no ultimate thermodynamic justification. Furthermore, the degree of melt polymerization can be quantified in terms of X_{NBO} (X_{NBO} = 0 - completely polymerized melts; X_{NBO} = 1 - completely depolymerized melts). *Behrens and Schulze (2003)*, as observed in previous studies, reported that the dependence of melt viscosity on pressure changes from positive for Di-rich compositions to negative for Ab-rich compositions. In the high viscosity range they find a marked effect of pressure on viscosity when compared with the low viscosity range (e.g. the viscosity of pure Di melt increases by one order of magnitude at 1016 K but only by about 0.1 log units at temperature 1800-2100 K when the pressure rises from 0.1 to 400 MPa). Keeping these results in mind, it is possible to argue that polymerized melts (like anhydrous rhyolite) should become more viscous during isothermal ascent while depolymerised melts like basalt or hydrous rhyolite should become less viscous *(Behrens and Schulze, 2003)*.

Liebske et al. (2003) demonstrated a non-dependence of pressure on the viscosity of an anhydrous andesite. In the hydrous sample, a positive pressure effect was observed which maybe due to an increased depolymerization in the melt. In contrast to this, as I will show in chapter 4 and 5, the viscosity data for iron free and Fe-bearing andesite in the pressure range of ambient to 2000 MPa does not reveal any notable dependence on pressure.

3.6 Volatiles in magmatic system.

Volcanic gases mainly consist of elements like hydrogen, oxygen, carbon and sulphur, which form H_2O, CO_2, SO_2, H_2S, H_2, CO and O_2. Other minor constituents are HCl, HF, N_2, Ar, and B. Their abundance varies considerably from one volcano to another and even in the same volcano at different times (e.g. *Symonds et al., 1994*). Among all these gaseous phases, H_2O and CO_2 are the most abundant and play a fundamental role in the chemical-physical parameters governing melts and magmatic behaviors *(Bourgue, 2003)*.

The effects of water on rheological properties of materials are remarkable. Small concentrations of water in the range of 100 to 1000 ppm dramatically weaken strong crystalline silicates, making them prone to ductile flow at temperatures typical of the crust and mantle *(Spera, 1999)*.

Spectroscopic studies at ambient pressure and temperature have shown that water in quenched silicate melts (glasses) is dissolved in two different ways: as hydroxyl and as molecular water *(McMillan, 1994)*. Both species are dissolved in proportions depending on the total amount of water and temperature. Below 3 to 4 wt%, OH is the major species dissolved in the melt (*Nowak and Behrens, 2001; Romano et al., 1995; Shen and Keppler, 1995; Silver and Stolper 1989; Silver et al.,1990; Zhang et al., 1995*). With a total amount of water exceeding 4 wt%, H_2O_{mol} is predominant. It has been demonstrated that the solubility of water is greater in silica rich melts than in felsic melts (For rhyolite and haplogranite: *Holtz et al., 1992 and 1995; Behrens and Jantos 2001; Tamic et al., 2001*; *Stolper, 1989*. For basalt: *Berndt et al., 2002* and *Dixon et al., 1995*). Like H_2O, CO_2 is dissolved in the melts in two different species: as CO_3^{2-} and molecular CO_2. However, compared with the solubility of water in silicate melts, the solubility of CO_2 is of minor importance. At the same pressure (main parameter governing the solubility of gaseous phases) and temperature conditions, CO_2 is dissolved 50 to 100 times less than water (*Bourgue, 2003*). In contrast to water, the CO_2 speciation does not depend on the total amount of CO_2, but on the silicate melt composition (*Bourgue, 2003; Brooker et al., 2001a*). The CO_2 solubility increases with

decreasing silica content (*Mysen et al., 1975; Mysen, 1976*). In liquids like basalts, CO_2 is dissolved as CO_3^{2-}, whereas in silica-rich liquids the predominant species is $CO_{2\ mol}$. In intermediate glasses both species are present. It is possible to observe a positive correlation between the CO_{2tot} and NBO/T (*Brooker et al., 2001b*). The greater the NBO/T value, the greater is the CO_2 solubility. The solubility of water and carbon dioxide is increased by increasing pressure whereas the effect of temperature is less pronounced and depends on composition and pressure. An exception to this is the solubility of CO_2 in melts with a nepheline composition, in which an increasing solubility with increasing temperature is observed (*Brooker et al., 1999*). Concerning rheological properties of melts, water decreases viscosity drastically. For example, by adding about 2 wt% water to an andesitic melt with a temperature of 1273 K, the viscosity will decrease about 2 log units. On the other hand, adding 3.5 wt% of CO_2 to a potassium silicate liquid causes a reduction of the viscosity by about two orders of magnitude (*Bourgue and Richet, 2001*). The effect of CO_2 becomes less significant when temperature is increased. However, the "depressing influence of CO_2 is strongest at low contents before tending to level off at concentration of about 3 wt%." (*Bourgue and Richet, 2001*).

Like water and carbon dioxide, fluorine reduces the viscosity of melts. The behavior of F has a strong effect on magma chamber dynamics and eruptive style of rhyolites (*Lange, 1995*). Viscosity of F-bearing silicate melts have been studied both in the low and high pressure range (*Dingwell et al., 1985; Dingwell and Mysen, 1985; Dingwell, 1989*). As shown by *Aoki et al. (1981)*, lamprorite can contain up to 2 wt% of F; the measurements of *Dingwell, (1989)*, indicate that this amount of fluorine in lamproritic melts will reduce the viscosity by less than 0.2 log units. In contrast, at temperatures below 1100°C, the effect of 6 wt% F reduces albite melt viscosity by more than 3 log units.

Chlorine may occur in concentrations of several wt% in volcanic gases and the emission, together with F, may influence the climate, both being greenhouse gases also playing a part in the generation of acidic rain. In contrast to F, Cl favours aqueous fluids and consequently plays an important part in hydrothermal fluids, whereas, as shown above, F has a great effect on melt properties such as viscosity.

It is commonly accepted that sulfur is present as sulfide (S^{2-}) or/and sulfate (SO_4^{2-}) in earth mantle derived melts, before being released as SO_2 and/or H_2S in volcanic emissions. In studies of volcanic gases, sulphur dioxide abundances are generally only exceeded by H_2O and CO_2. However, sulphur has been considered to possibly cause climate change and also may be used as tool for prediction of eruptions (*Carrol and Webster, 1995*).

Little is known about the influence of sulphur and clorine on melt viscosity, but it is expected to be small because of the low concentrations of these volatiles in melts.

4. Experiments (part 1). Fe-free Andesite

4.1 Viscosity of analogue andesite

The viscosity of a synthetic andesite-like melt was measured in the low viscosity range (10^1 – 10^6 Pa·s) using the falling sphere(s) method and in the high viscosity range (10^8 – 10^{13} Pa·s) using parallel-plate viscometry. Falling sphere experiments with melts containing 2.3 and 5.6 wt% H_2O were carried out in an internally heated gas pressure vessel (IHPV) at 500 MPa confining pressure. The sinking velocity of Pt and Pd spheres and in one case of corundum sphere was used to measure the melt viscosity. In addition, a creep experiment was performed at ambient pressure using a glass containing 2.73 wt% H_2O. A more water-rich glass (5.6 wt% H_2O) was investigated with a high pressure parallel-plate viscometer at 400 MPa confining pressure in an IPHV. By combining the new data with previous results for a similar melt composition the following expression was derived to describe the viscosity η (in Pa·s) as a function of temperature T (in K) and water content w (in wt%)

$$\log \eta = -4.86 + \frac{8154.4}{(T - 530)} - \frac{6060}{(T - 573)} \cdot \frac{w}{(w^{1.1584} - 2.4455 + 0.0052 \cdot T)}$$

This expression reproduces the experimental data (191 in total) in the viscosity range from 10^1 to 10^{13} Pa·s with a standard error of 0.15 log units.

4.2. Experimental and Analytical Methods

4.2.1 Starting materials

The starting composition is based on an andesite from Unzen Volcano (Pre Unzen 500 kyr; *Chen et al., 1993*). In order to avoid complications due to crystallization of iron-oxides (*Neuville and Richet, 1991; Liebske et al., 2003*) an iron-free analogue of the natural andesite was used. Ferrous iron in the natural composition was substituted by Ca and Mg preserving the same Mg/Ca ratio as in the natural andesite and ferric iron was replaced by Al. The anhydrous glass was synthesized by melting a mixture of oxides and carbonates at 1873 K for 4 h in a Pt crucibles in air. The glass was quenched by pouring the melt on a brass plate (Fig.4.1). More details of synthesis conditions are given in *Liebske et al. (2003)*. To synthesize hydrous glass, distilled water was added stepwise to a dry glass powder into Pt capsules varying in inner diameter from 4 to 8 mm and in length from 30 to 45 mm. A 1:1 mixture of grain size fractions < 200 μm and 200 - 500 μm was used to minimize the pore volume. For further compaction the charge was compressed with a steal piston after each addition of powder. After welding shut the capsule was tested for leakage by annealing at 383 K for at least one hour. The synthesis was performed in an internally heated gas pressure vessel (IHPV) at 500 MPa and 1523 K for 24 h. Quenching was initiated by switching off the heating power of the furnace in the IHPV (initial quench rates of 200 K/min). The resulting glasses were inspected for bubbles and crystals using an optical microscope. Only crystal-free and bubble-free samples were used for viscosity experiments. The homogeneity of the chemical composition of the glasses was confirmed by electron microprobe (Cameca SX100).

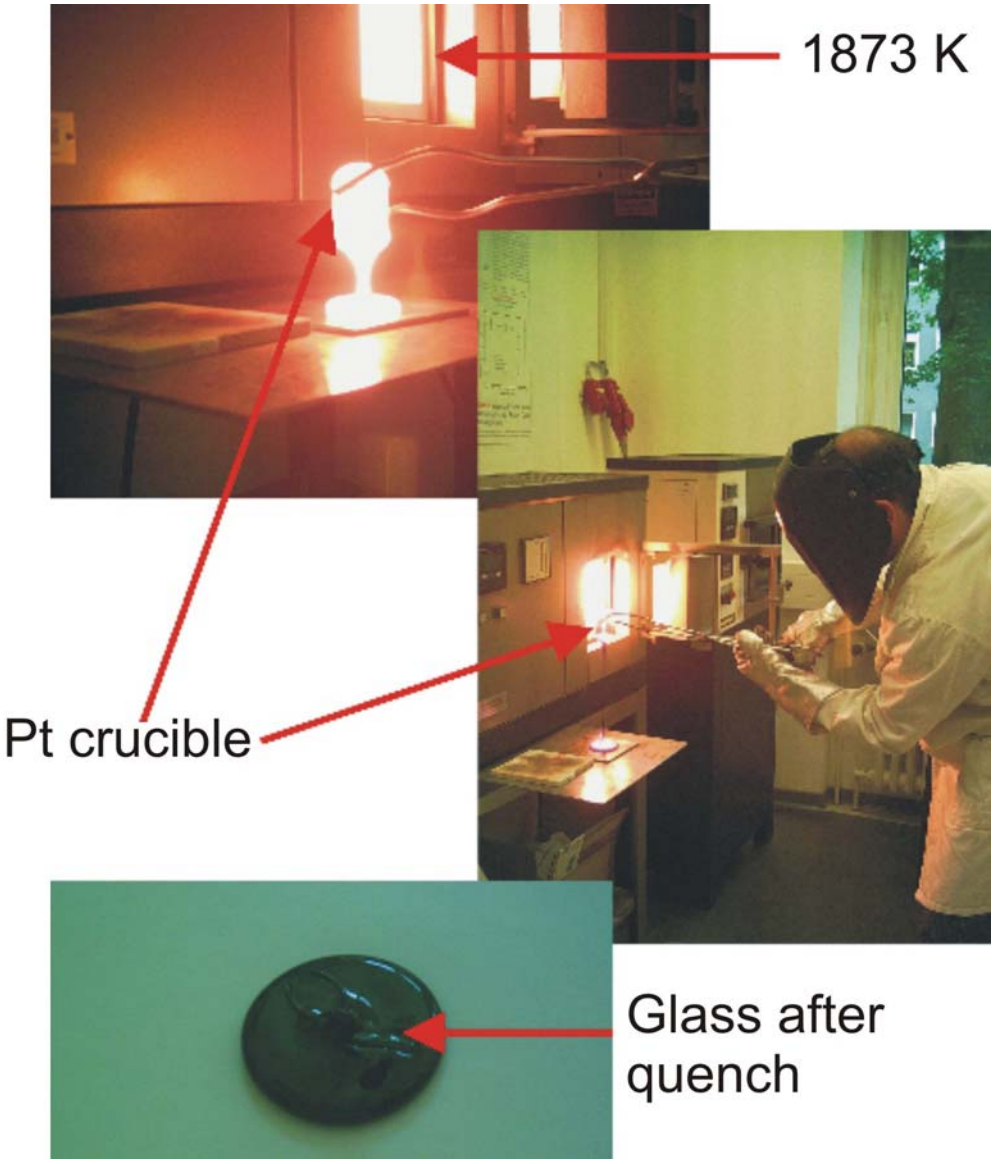

Fig.4.1. Details in making glass: 1 atm.- 1873 K.

The composition of the anhydrous glass is close to that used in viscosity experiments of *Liebske et al. (2003)* but is slightly more basic than that used in the study of *Richet et al., (1996)* (see Table 4.1), in particular MgO and K_2O are higher (by 2.3 wt% and 0.9 wt%, respectively). As shown for sample MD10 in Table 4.1, the dry and hydrous compositions are nearly identical (except for H_2O) after the high temperature viscosity experiments.

4.2.2 Water determination

The H_2O contents of the glasses were determined by Karl-Fischer titration (KFT) and infrared spectroscopy. To correct for unextracted water after KFT, a quantity of 0.13 wt% was added to the measured values (*Behrens and Stuke, 2003*). The accuracy of the KFT analysis is estimated to be 0.10 wt% including the uncertainty in the amount of unextracted water and the error in the titration rate (for details of the analytical technique and error estimation see *Behrens and Stuke, 2003*). To test the homogeneity of H_2O in selected samples, wafers from both ends were analyzed by KFT. Results of both analyses agree within 8 % relative (Table 4.2).

The peak heights of the near-infrared (NIR) absorption bands at 4500 cm^{-1} (combination mode of OH groups) and 5200 cm^{-1} (combination mode of H_2O molecules) were used to analyze the water content of hydrous glasses after experiments, i.e., to identify gradients in water content near the surface of the sample. Absorption spectra of doubly polished glass slabs with thickness of 0.2-0.5 mm were recorded using an IR microscope Bruker IRscopeII connected to an FTIR spectrometer Bruker IFS88. A slit aperture between the objective and the detector was used to limit the analyzed sample volume. In the focus plane, the area selected by the slit was typically 20 - 30 μm wide and 100 – 150 μm long. Spectra were recorded in the near-infrared (NIR) using a tungsten light source, a CaF_2 beamsplitter and a narrow range MCT detector. Typically 50-100 scans were accumulated for each spectrum with a spectral resolution of 4 cm^{-1}. Simple linear baselines were fitted to both NIR peaks (TT baseline according to *Ohlhorst et al., 2001*). This baseline correction is reliable to quantify H_2O_t (sum of H_2O molecules and water dissolved as OH) but may have systematic errors in the determination of hydrous species concentrations (cf *Ohlhorst et al., 2001*).

The water content of the nominally dry starting glass was determined by measuring the peak height of the mid-infrared (MIR) absorption band at 3550 cm^{-1} after subtracting a linear baseline. A bulk spectrum was collected in the main chamber of the FTIR spectrometer while fixing a polished glass wafer on a hole aperture 2 mm in diameter. Measurement conditions were: globar light source, KBr beam splitter, DTGS detector, 2 cm^{-1} spectral resolution, 100 accumulated scans. The same procedure was applied to measure the water content of the dry glass used by *Liebske et al. (2003).*

Concentrations of hydrous species and total water were calculated from peak height of absorption bands using the Lambert-Beer law (e.g., *Stolper, 1982*). In the calculation the density-water content relationship and the molar absorption coefficients of the absorption bands are needed beside the sample thickness which was determined for each section with a precision of ± 2 μm using a Mitutoyo micrometer. Densities of 12 synthesized glasses with water contents of 1-8 wt% were measured by weighing single glass pieces in air and in water. Combining the density data with those from *Richet et al. (1996)* the following equation was obtained for the density ρ (in g/L) of hydrous andesitic glasses as a function of water content C_{H2Ot} (in wt%)

$$\rho = 2535\,(\pm 7) - 17.1\,(\pm 1.6)\cdot C_{H_2O_t} \qquad (4.1)$$

This equation which reproduces the experimental data within ± 1% was used in the IR evaluation for the viscosity samples.

Examples of near-infrared spectra recorded after viscosity experiments are shown in Fig. 4.2.

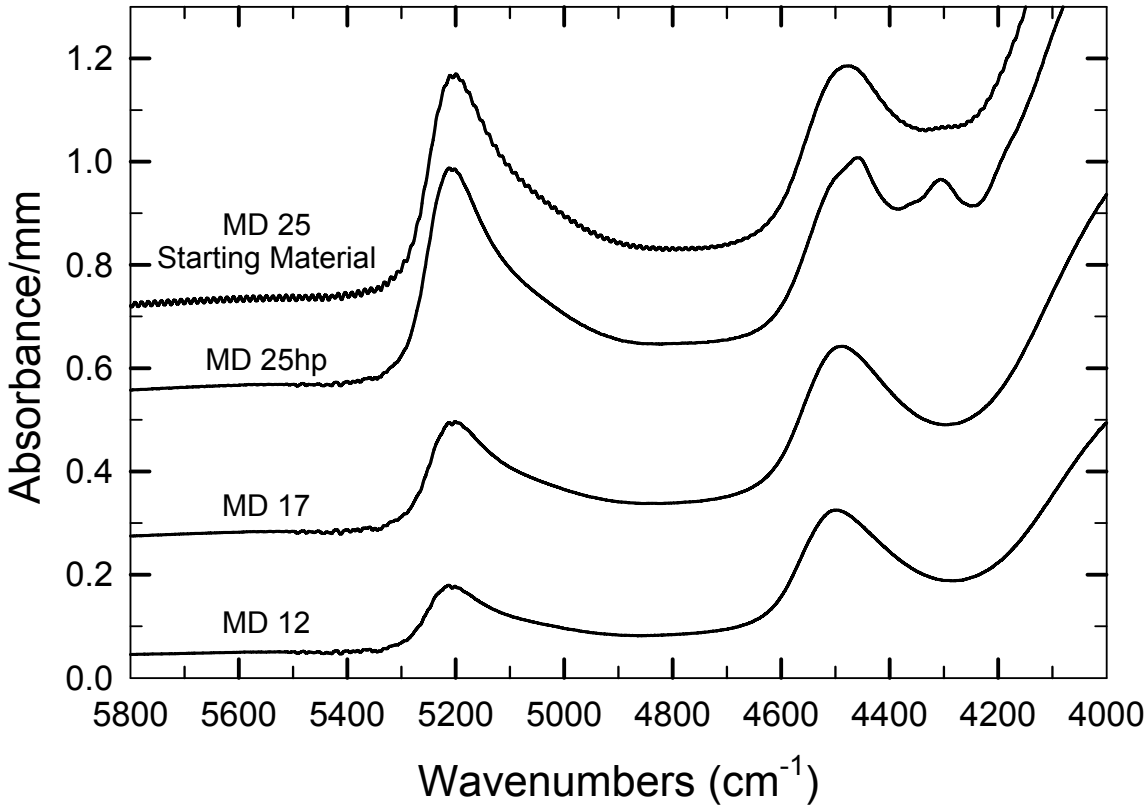

Fig.4.2. Near-infrared absorption spectra of hydrous andesitic glasses. Bands near 4500 cm^{-1} and 5200 cm^{-1} are due to combination vibrations of OH groups and H_2O molecules, respectively. Note the splitting of 4500 cm^{-1} band in the sample MD25hp after the creep experiment.

When applying the absorption coefficients from *Mandeville et al. (2002)*, the water content was systematically underestimated by NIR spectroscopy compared to KFT measurements. The deviation is especially pronounced at high water content, e.g., in sample MD10 4.90 wt% H_2O were detected by KFT, but NIR spectroscopy on a wafer cut directly beside that used for KFT yield only a value of 3.95 wt% H_2O. One possible reason for the discrepancy is the difference in composition of the glasses used in the viscosity experiments to those used for calibrating the near-infrared bands (see Table 4.1). As shown by several authors, the NIR absorption coefficients are very sensitive to the glass composition (*Silver et al., 1990; Ohlhorst et al., 2001*). A linear relationship between the cation proportion of Si^{4+}+Al^{3+} and the absorption coefficients for the NIR

combination bands was proposed by *Dixon et al. (1995)*. However, the difference in cation proportion of Si^{4+}+Al^{3+} of this Fe-free andesite to that used by *Mandeville et al. (2002)* is too small to account for the observed discrepancies in water content. With a set of 16 hydrous glasses including four samples used in viscosity experiments (MD10, MD12, MD13, MD17) a new calibration of the NIR absorption coefficients as described in *Ohlhorst et al. (2001)* was carried out. For the 4500 cm^{-1} band an absorption coefficient of 0.92 ± 0.03 $L \cdot mol^{-1} \cdot cm^{-1}$ was determined, similar to the value of 0.89 $L \cdot mol^{-1} \cdot cm^{-1}$reported by *Mandeville et al. (2002)*. The value of 1.04 ± 0.04 $L \cdot mol^{-1} \cdot cm^{-1}$ derived for the combination band at 5200 cm^{-1}, however, is 30% lower than the published value in Mandeville et al. (2002). All water contents based on NIR spectroscopy refer to the newly determined absorption coefficients.

Table 4.1. Electron microprobe analysis and water content of the starting material (wt%).

	MD (dry)	MD10 After exp.	Richet et al.(1996)	Liebske et al. (2003)	Mandeville et al. (2002)
SiO_2	59.19 (0.54)	57.95 (0.80)	62.40	58.69	62.93
TiO_2	0.02 (0.01)	0.02 (0.01)	0.55	0.01	1.13
Al_2O_3	21.57 (0.28)	19.82 (0.38)	20.01	21.57	16.73
FeO [a)]	0.06 (0.05)	0.09 (0.05)	0.03	0.02	0.00
MnO	0.06 (0.05)	0.05 (0.04)	0.02	0.02	0.00
MgO	5.50 (0.15)	5.11 (0.18)	3.22	5.38	3.26
CaO	9.49 (0.26)	9.15 (0.25)	9.08	9.49	7.49
Na_2O	3.40 (0.21)	3.25 (0.22)	3.52	3.30	3.47
K_2O	1.79(0.08)	1.58 (0.07)	0.93	1.57	1.52
P_2O_5	-	-	0.12	-	0.00
H_2O (IR)	0.009	4.60		0.016	
Total	101.15 (0.81)	101.6 (1.10)	99.88	100.21	100
NBO/T [b)]	0.21	0.21	0.15	0.20	0.17
Cation fraction Si^{4+} + Al^{3+} [c)]	0.75	0.61	0.78	0.76	0.79

Measurement conditions for MD and MD 10 were: defocused beam of 15 µm diameter, accelerating voltage of 15 kV and a beam current of 4 nA. Analysis for Fe-free andesites studied by *Richet et al. (1996), Liebske et al. (2003) and Mandeville et al. (2002)* are shown for comparison. Analyses reported by *Mandeville et al. (2002)* were averaged and normalized to 100wt%. H_2O contents of starting glasses were derived from the peak height of the IR absorption band at 3550 cm^{-1} using the calibration of Mandeville et al. (2002) for the Fe-free andesite included in the last column. The water content of the viscosity sample MD10 was calculated from the absorbances of the near-infrared combination bands at 4500 and 5200 cm^{-1} using the new absorption coefficients determined in this paper.

[a)] Total iron is given as FeO.

[b)] NBO/T is calculated on a H_2O-free basis.

[c)] The cation fraction of Si^{4+}+Al^{3+} equals to atomic ratio (Si+Al)/(P+Si+Ti+Al+Fe+Mn+Mg+Ca+Na+K).

[d)] Numbers in parenthesis correspond to 1 σ standard deviation

4.3 Viscosity experiments

4.3.1 Falling sphere experiments.

Viscosity measurements by the falling sphere method require the determination of the exact position of the sphere in the glass cylinder before and after experiment. The viscosity assemblage was prepared in the following way: A cylinder (diameter 4 to 6 mm) was cored after fixing the sample with dental cement. The cylinder was cut into two pieces, a smaller one (1-2 mm in length) and a longer one (10 to 15 mm in length). The rest of the glass was crushed to grain size <200 μm. A platinum tube was welded at one end with a Pt-cup to obtain a container with cylindrical shape. Then a small amount of crushed powder was filled in and the small cylinder was placed above. Before inserting the large cylinder, some Pt powder (grain size ~1 μm) was strewn on the first cylinder to serve as reference for measurement of the position of the spheres. Next, glass powder was filled on top and 2 - 3 Pt spheres were placed near the cylindrical axis, covered by additional glass powder. Using more then one sphere allows multiple determination of viscosity in a single experiment. (Fig.4.3). Not only the change in position of each sphere can be evaluated but also the vertical distance between the spheres which grows with increasing difference in radius and increasing difference in sphere density. Experiments were performed using Pt, Pd and corundum spheres.

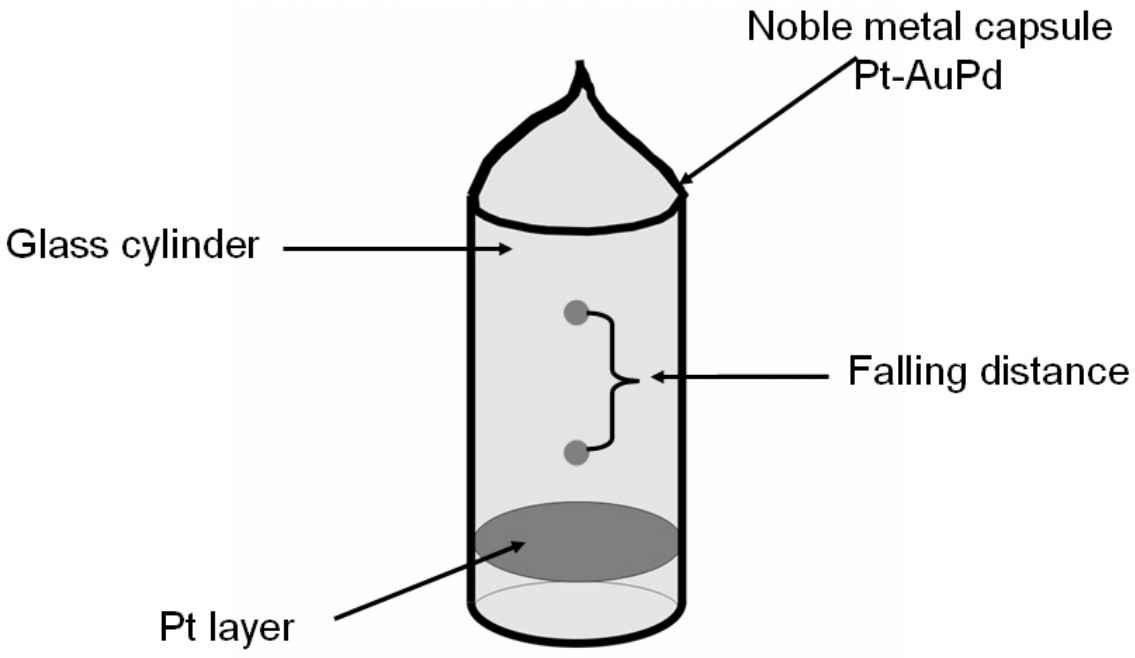

Fig. 4.3. Falling sphere(s) in a cylinder glass.

To produce Pt and Pd spheres with small radius (<50 μm) a 0.025 mm thick wire was twisted four times and melted by sudden d.c. current. Melt droplets were quenched in water to preserve spherical shape. Radius of hand-picked spheres was measured using a microscope calibrated with a micrometer section. Corundum spheres with 500 ± 10 μm diameter were purchased from the company *GROH & RIPP Idar-Oberstein, Germany*. After welding shut the capsule, a pre-experiment was performed in an IHPV at 1523 K and 500 MPa for a few minutes to establish well-defined starting positions of the spheres. After cooling and removal of the capsule walls, the positions of the spheres in the sample were measured with an optical microscope equipped with an x-y stage. An immersion oil with similar refraction index as the glass (1.622) was used to improve the visibility of the spheres. After cleaning with acetone and drying at room temperature, the viscosity sample was sealed again in a platinum capsule. In the viscosity experiment the sample was heated in an IHPV at 500 MPa with a ramp of 30 K/min to 1023 K and

then with a rate of 100 K/min to the final temperature. Quenching with an initial rate of ~200 K/min was achieved by switching off the heating power. Usually a series of viscosity experiments was performed with the same sample. The order of the runs is labelled by the sequence a,b,c…in Table 4.2.

From the settling distance d and the run time t the viscosity η is calculated by Stokes law:

$$\eta = \frac{2 \cdot t \cdot g \cdot \Delta\rho \cdot r^2 \cdot C_F}{9 \cdot d} \qquad (4.2)$$

where $\Delta\rho$ is the density difference between the sphere and the melt, g is the acceleration due to gravity (9.81 m/s^2), r is the radius sphere and C_F is the Faxen correction to account for the effect of viscous drag by the capsule wall on the settling sphere. Room temperature densities of Pt, Pd and corundum are 21.45, 12.02 and 3.98 g/cm^3, respectively. No correction was made for differential compression and thermal expansion of the solid materials because this would contribute less than 1% to the viscosity. Melt density at experimental conditions was calculated according to Lange (1994) using the partial molar volume of H_2O from *Ochs and Lange (1999)*.

Table 4.2. Experimental conditions and results of viscosity experiments with iron-free andesite (MD samples) using the falling sphere method. All experiments were performed at 500 MPa.

No.	H_2O_t initial (wt%)	H_2O_t final (wt%)	T (K)	Sphere radius (µm)	C_F	Dwell time (s)	Corrected time (s)	Falling distance (cm)	η (Pa s)
MD25a	$5.60^{t}/5.02^{t\text{-}IR}$		1473	47.5 ± 1 (Pt)	0.96	240	286	0.318	8.3 ± 1.8
	5.53^{b}			57.5 ± 1 (Pt)				0.572	6.8 ± 1.4
MD25b			1423	47.5 ± 1 (Pt)		600	643	0.579	10.3 ± 1.3
MD25c		5.37^{t}	1373	47.5 ± 1 (Pt)		900	940	0.709	12.3 ± 1.4
MD10a	$4.86^{t}/4.82^{t}$		1473	62 ± 2.5 (Pd)	0.98	720	766	0.438	13.6 ± 1.7
	4.87^{2}			57 ± 1 (Pt)				0.822	12.4 ± 1.6
	4.60^{IR}			250 ± 5 (co)	0.90			1.006	14.3 ± 1.9
MD10b			1373	62 ± 2.5 (Pd)	0.98	2160	2200	0.341	50.1± 5.6
				57 ± 1 (Pt)				0.824	35.7± 3.9
				250 ± 5 (co)	0.90			0.757	56.2 ± 6.3
MD10c		4.63^{t}	1523	62 ± 2.5 (Pd)	0.98	420	469	0.350	10.4± 1.6
MD10d		4.71^{b}	1423	62 ± 2.5 (Pd)		1440	1483	0.314	36.7 ± 4.2
MD10e *		$3.83^{s\text{-}IR}$	1323	62 ± 2.5(Pd)	0.90	2190	2227	0.064	270 ± 30
MD17a	$3.33^{t}/3.28^{b}$		1523	77.5±2.5 (Pt)	0.93	399	448	0.584	17.6 ± 3.1
	$3.02^{t\text{-}IR}$			67.5 ± 2.5(Pt)	0.86			0.456	20.8 ± 2.6
MD17b			1473	77.5±2.5 (Pt)	0.93	900	946	0.743	29.3 ± 3.3
				67.5 ± 2.5(Pt)	0.86			0.575	26.5 ± 3.2
MD17c		3.49^{b}	1423	77.5±2.5 (Pt)	0.93	1500	1543	-	-
		$3.21^{s\text{-}IR}$		67.5 ± 2.5(Pt)	0.86			0.738	33.7 ± 3.8
MD12a	$2.85^{t}/2.74^{t}$		1523	66 ± 2.5 (Pd)	0.98	1200	1249	0.314	35.0 ± 4.1
	2.55^{b}			51 ± 1 (Pt)	0.97			0.330	39.3 ± 4.6
MD12b	$2.60^{b\text{-}IR}$		1473	66 ± 2.5 (Pd)	0.98	2220	2266	0.416	47.9 ± 5.3
		2.66^{t}		51± 1 (Pt)	0.97			0.445	52.9 ± 5.8
MD12c		2.63^{b}	1573	66 ± 2.5 (Pd)	0.98	480	531	0.204	22.9 ± 3.5
MD13a	$2.42^{t}/2.10^{t\text{-}IR}$		1523	54 ± 1 (Pt)	0.85	399	448	0.107	42.7 ± 7.1
MD13b	2.24^{b}	2.23^{t}	1523			581	630	0.153	42.0± 5.8
MD13c		$1.84^{s\text{-}IR}$	1523			1800	1849	0.490	38.5 ± 3.7

Tab. 4.2. Experiments using same sample are presented in the order in which they were performed. Sphere radii were determined before incorporation in the glass. C_F refers to the Faxen correction. Supscripts t and b at water contents refer to measurements of slabs from the top and the bottom of the cylinder, respectively. An additional supscript IR is used to distinguish from KFT analyses. Supscripts s-IR refer to the average water content along the axis of the cylinder after experiments measued by IR.
After experiment MD10e, the sample was partially crystallized explaining the higher viscosity compared to the prediction of the model.

At experimental conditions the density of the melt is up to 10% lower than the glass density at room temperature, e.g. the melt MD25 containing 5.5 wt% H_2O (average of KFT) has a density of 2263 g/L at 1473 K, 500 MPa whereas the calculated glass density by Eqn. 4.1 is 2441 g/L. As a consequence, for the given example the settling distance would be underestimated by 2.6 % when using the room temperature density. To account for the density change from glass to melt, a correction factor was calculated for the distance as

$$d_{corr} = d_{r.t.} \cdot \sqrt[3]{\frac{\rho_{melt}(T,P)}{\rho_{glass,r.t.}}} \quad . \tag{4.3}$$

Based on theoretical considerations*, Faxen (1923)* derived the following relationship for the correction factor C_F

$$C_F = 1 - 2.104\left(\frac{r}{R}\right) + 2.09\left(\frac{r}{R}\right)^3 - 0.95\left(\frac{r}{R}\right)^5 \tag{4.4}$$

where R is the inner radius of the capsule. Although there might be some uncertainty in the validity of the Faxen correction (*Kahle et al., 2003*), Eqn. 4.4 was applied to all experiments for internal consistency and for consistency with previous studies. In most of experiments the ratio r/R is < 0.05 and C_F has only minor influence on the derived viscosity. The possible error related to this correction is estimated to be less than 5%.

Major sources of error in the falling sphere experiments are related to measurement of sphere radius, settling distance, run duration and sample temperature. Small deviation from spherical shape and uncertainty of microscopic measurement of the size of the sphere result in a possible error in sphere radius of 1 - 5 μm (see Table 4.2). The falling distance was measured with a resolution of ± 10 μm using a micrometer. The uncertainty in run duration when using the correction for heating and cooling outlined below is estimated to be ± 30 sec. Precision of temperature is ± 10 K including temperature gradients along the sample and fluctuation of temperature during the experiment. The overall error in the viscosity determination is estimated to be about 10%.

4.3.2 Creep measurements

At temperatures near those of the glass transition, creep experiments were performed to measure melt viscosity. To allow direct comparison to the high temperature data, large cylinders of hydrous andesite glasses (MD12 + MD25) about 30 mm in length were synthesized and cut into two parts. One part was used for falling sphere experiments. The second one was studied by parallel plate viscometry.

An experiment with sample MD12 containing 2.73 wt% H_2O was carried out at ambient pressure in Paris using the creep apparatus described by *Neuville and Richet (1991)*. In a second low temperature experiment, a water-rich andesitic glass (MD25, 5.6 wt% H_2O) was studied in Hannover at a pressure of 400 MPa using the parallel plate viscometer described by *Schulze et al. (1999)*. Experimental procedures are described by Richet et al. (1996) and *Schulze et al. (1999)*, respectively. In both types of experiments the rate

of deformation of cylindrical samples is measured when applying a constant uniaxial stress (*Neuville and Richet, 1991*). The viscosity is calculated as

$$\eta = \frac{\sigma}{3 \cdot \frac{d \ln l}{dt}} \tag{4.5}$$

where σ is the applied stress and l is the length of the cylinder. After the experiments two sections were cut along and perpendicular to the cylindrical axis and polished on both sides for IR investigation.

Based on measurements on NBS717 glass, the accuracy of the viscosity determination with the creep apparatus in Paris is better than 0.04 log unit (*Neuville and Richet 1991*). With the parallel-plate viscometer of *Schulze et al. (1999)* the viscosity of the DGG1 standard glass could be reproduced at ambient pressure within ± 0.08 log unit. At elevated pressure the reproducibility of viscosity data is within ± 0.15 log unit (*Schulze et al., 1999*).

4.4. Results

4.4.1. Falling sphere experiments

Results of falling sphere experiments with andesitic melts are summarized in Table 4.2 and Fig. 4.4. The minimum viscosity accessible with the used experimental technique is about 0.2 Pa·s when using a Pd sphere with a radius of 50 µm, a falling distance of 10 mm and run duration of 5 min. In short term experiments, the sinking of the sphere before reaching the final experimental temperature (during heating and cooling) may significantly contribute to the overall falling distance measured on quenched glasses. To

account for movement of spheres at temperatures below the target temperature T_{target}, the effective run duration $t_{effective}$ for each experiment was calculated, in a similar way as for diffusion experiments (*Koepke and Behrens, 2001*)

$$t_{effective} = \int \exp\left[\frac{-E_a}{R}\left(\frac{1}{T(t)} - \frac{1}{T_{target}}\right)\cdot\right] dt \qquad (4.5)$$

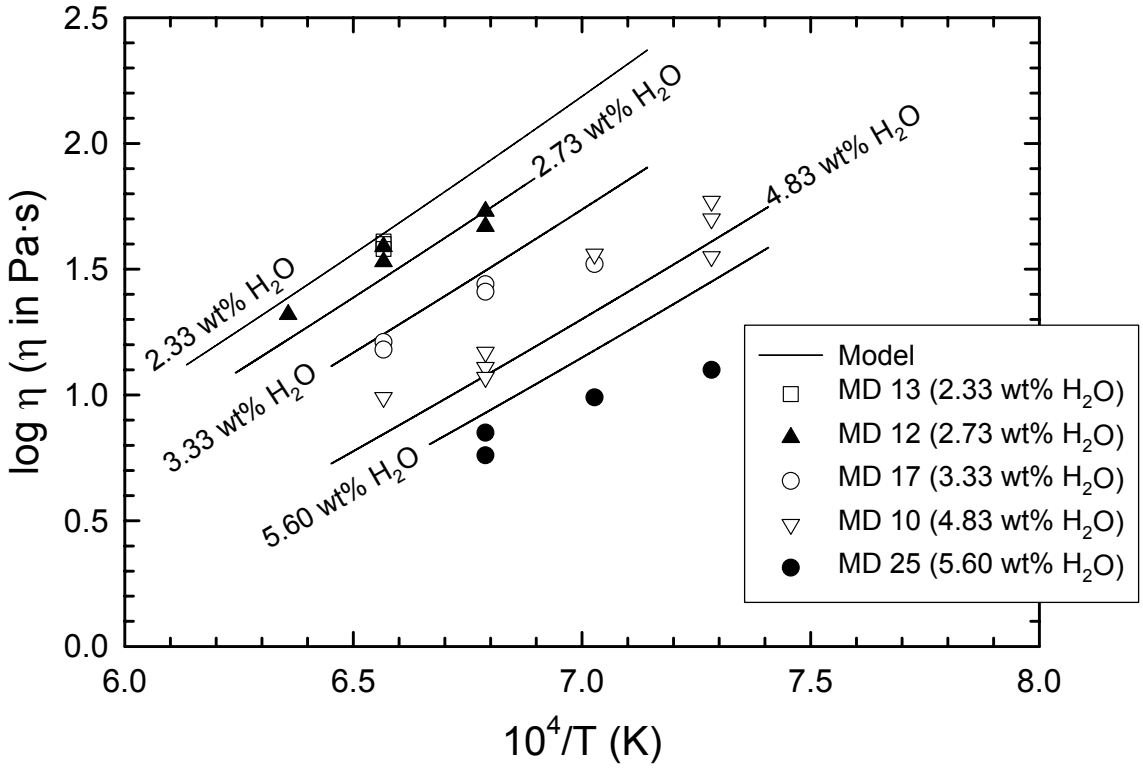

Fig. 4.4. Results of viscosity experiments using the falling sphere method in comparison with predictions by the model for different water contents.

where E_a is the activation energy for viscous flow and R is the universal gas constant. Although the viscosity is obviously non-Arrhenian over a wide temperature range, assumption of a linear variation of log viscosity with reciprocal temperatures appears to be a good approximation for temperatures above 1273 K (see Fig. 4.4). In a preliminary time correction the average activation energy for the dry melt in the high temperature range 1500 – 2000 K (133 kJ/mol, data from *Richet et al., 1996*) was used for all

compositions. Based on the so obtained viscosities the activation energy was determined for each water content to be used in a subsequent improved time correction. The maximum contribution of heating and cooling period to the effective duration was 20% in run MD25a.

To verify the reliability of the falling sphere(s) method, I performed three experiments with sample MD 13 containing 2.33 wt% at 1473 K with duration varying from 400 to 1800 s. The viscosities derived from these experiments agree within 10% relative (Table 4.2). This demonstrates that constant velocity is achieved for a Pt sphere with a radius of 54 μm, even for a settling distance of 1 mm. Acceleration and braking of spheres which was observed in the initial and in the final stage of in situ falling sphere experiments (*Kahle et al., 2003; Reid et al., 2003*) appears to have no significant effect in these experiments. The negligible contribution of non-stationary movement of spheres in these experiments is attributed to the pre-treatment of viscosity samples and to the large ratio of falling distance to sphere radius.

Spheres with different densities (Pt, 21.45 g/cm^3; Pd, 12.02 g/cm^3; corundum, 3.98 g/cm^3) gave identical viscosities at 1473 K for the melt containing 4.7 wt% H_2O. After the run at 1473 K, the corundum sphere showed no indication of dissolution. In a second experiment at lower temperature (1373 K) the corundum crystal was partially dissolved and surrounded by a rim of plagioclase (identified by backscattered electron images and electron microprobe analyses of a polished section) Fig. 4.5.

Nevertheless, the derived viscosity at 1373 K is close to that based on Pd and Pt spheres. The conclusion is that corundum spheres can be suitable for viscosity determination when the velocity of the sphere is fast compared to dissolution/crystallization of corundum. After the second experiment (MD10b), the part of the sample containing the corundum sphere was removed to avoid changes in melt

composition. Unfortunately, the Pt sphere was in the same volume so that only the Pd sphere was present in subsequent experiments. In one sample (MD17) two platinum spheres with different radius were incorporated.

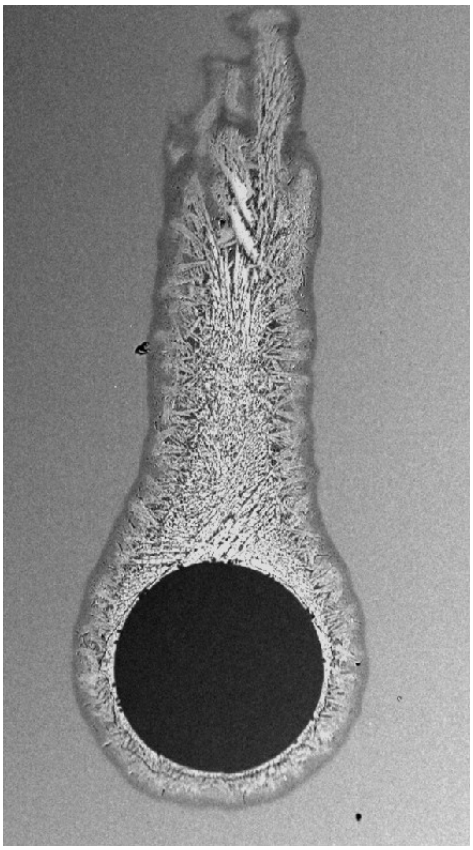

Fig. 4.5. Backscattered electron images of corundum sphere after falling sphere experiment at 1373 K, 500 MPa and dwell time of 2190 s.

In this case the viscosity might be determined also from the difference in the settling distance

$$\eta = \frac{2 \cdot t \cdot g \cdot \Delta\rho \cdot \left(r_1^2 \cdot C_{F1} - r_2^2 \cdot C_{F2}\right)}{9 \cdot \left(d_1 - d_2\right)} \tag{4.6}$$

where labels 1 and 2 refer to the two spheres. However, due to the relatively small difference in radius (less than 20%), the settling distance exceeds the distance between the spheres by more than a factor of three (Table 4.2). Hence, in this experiment the

precision was much lower for the two spheres method than for the single sphere method.

4.4.2. Parallel plate viscometry

Results of experiments in the high viscosity range are summarized in Table 4.3 and 4.4. In the creep experiment MD12 at ambient pressure the load on the sample was varied by a factor of three for each investigated temperature. For each temperature, the determined melt viscosity values agree within experimental error (Table 4.3). This indicates the Newtonian nature of viscous flow in andesitic melts under the experimental conditions. In the high pressure viscometer the stress is much lower (typical load of 0.2 to 1 kg compared to 0.4 – 30 kg in 1 atm creep experiments) so that Newtonian viscosity can be safely assumed for run MD25.

Table 4.3. Creep experiment at 1 atm with an iron-free andesite containing 2.73 % H_2O (MD12).

No.	T (K)	Stress (N/m^2)	log η (η in Pa·s)	No.	T (K)	Stress (N/m^2)	log η (η in Pa·s)
6.1	762	17593	12.34	2.1	801	1389	10.89
6.2	762	23380	12.43	2.2	801	3704	10.87
6.3	762	34954	12.39	2.3	801	6019	10.88
5.1	772	6019	12.02	3.1	812	1389	10.50
5.2	772	11806	11.99	3.2	812	2546	10.55
5.3	772	17593	11.95	3.3	812	3708	10.55
1.1	779	3703	11.70	7.1	823	1389	10.17
1.2	779	6018	11.65	7.2	823	2546	10.18
1.3	779	8333	11.58	7.3	823	3704	10.17
4.1	792	3704	11.21	8.1	834	463	9.91
4.2	792	6019	11.23	8.2	834	810	9.88
4.3	792	8334	11.24	8.3	834	1042	9.85

In both creep experiments the measurements started at a relatively low temperature (high viscosity). A repeated measurement at a similar temperature after a suite of viscosity determinations at higher temperature is consistent with the initial measurement (see Table 4.3 and 4.4) indicating that thermal history or possible loss of water during heating have minor influence on the rheological behaviour of the melt. NIR spectra of a polished slab of sample MD12 resemble spectra of andesitic glasses quenched from hyperliquidus conditions (Fig. 4.2) indicating that the local environment of hydrous species did not change noticeably during heating at temperature near the glass transition. On the other hand, the spectra of sample MD25hp containing initially 5.6 wt% H_2O show splitting of the OH combination band at 4500 cm^{-1} into a doublet. The sample was optically unchanged compared to the starting glass. No indication was found for crystalline phases by microscopic inspection. A possible explanation for the splitting of the 4500 cm^{-1} band is the formation of two different types of OH groups in the supercooled melt during annealing. KFT analysis of a part of the post-experimental glass yield a water content 0.35 wt% lower than that of the starting glass. IR microspectroscopy show uniform concentration of water in the whole sample except of a small layer (<50 μm) near the rim which was slightly depleted in H_2O. In isothermal plots the viscosity for sample MD25hp is consistent with data for melts with lower water content (Fig. 4.6). Therefore, we conclude that the change in water speciation has only a minor effect on the rheological properties of the melt.

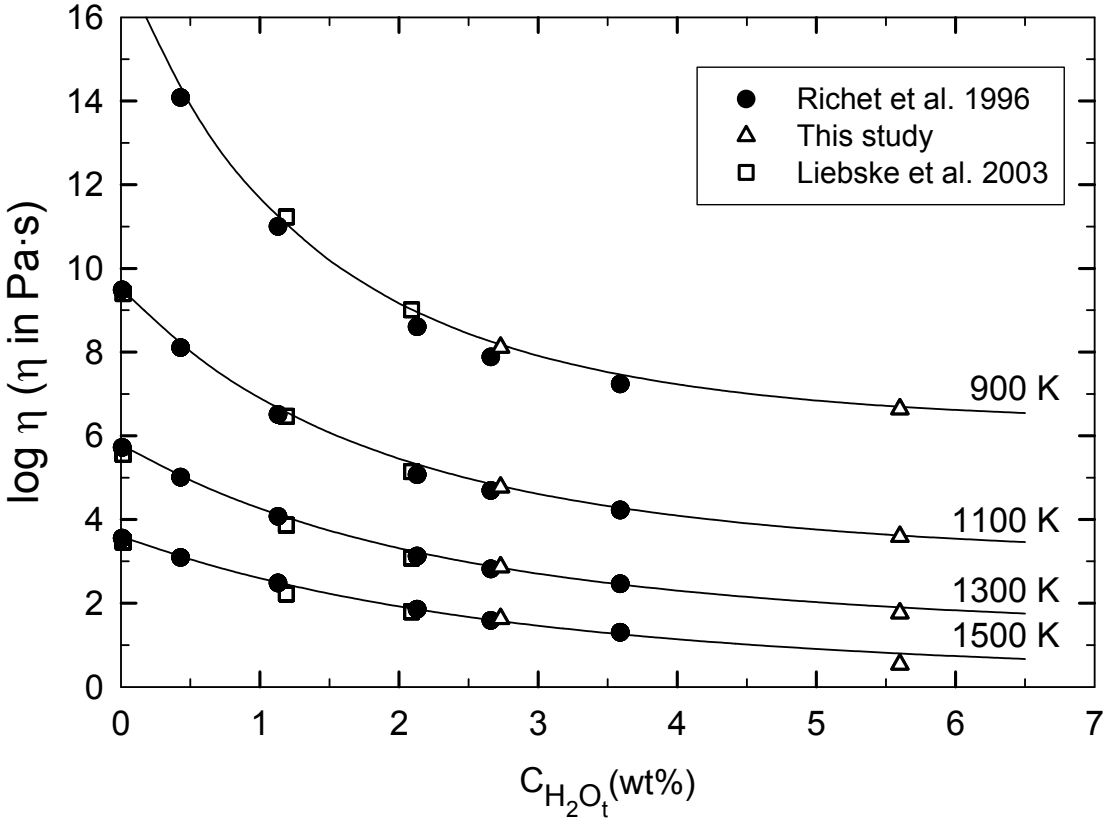

Fig. 4.6. Viscosity isotherms for andesitic melts.

The high viscosity data are compared with falling sphere data in Fig. 4.7. The deviation from Arrhenian behaviour is evident for both hydrous melts.

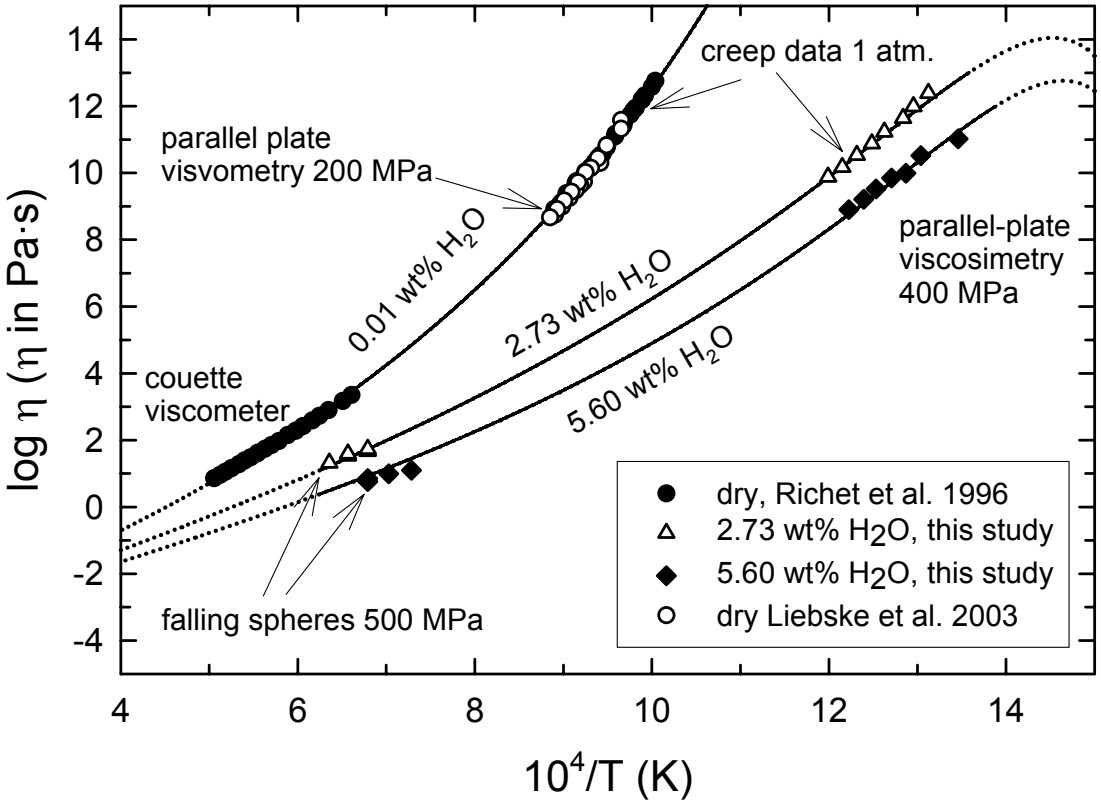

Fig. 4.7. Comparison of viscosity data for iron-free andesitic melts with predictions of the model. Note the gap in experimental data between the low and the high viscosity range. At these intermediate temperatures experiments fail because of rapid crystallization and models are required for interpolation of viscosity.

The curvature in plots of log viscosity versus reciprocal temperatures becomes more pronounced with increasing water content indicating that the fragility of the melt (Angell 1985) is enhanced by dissolved water.

Table 4.4. Viscosity of hydrous andesite (Sample MD25hp, 5.60 wt% $H_2O_{initial}$) at 400 MPa.

No.	T (K)	log η (η in Pa s)
1	743	11.02
2	767	10.52
7	777	9.99
3	787	9.85
4	798	9.52
5	807	9.21
6	818	8.90

4.5. Discussion

4.5.1. Comparison with previous studies

As shown by *Richet et al. (1996)* the effect of dissolved water on the viscosity of andesitic melts is especially pronounced at low water content. Hence, precise determination of the water content is required to set up a general model to describe the variation of viscosity with temperature, pressure and water content. Different analytical techniques were used in this study and in that of *Richet et al. (1996)* to measure the water content of the glasses (*Richet et al., 1996* derived the water content from the amount of H_2O loaded in the capsules for synthesis and from vacuum fusion analysis). In addition, the andesite analogue studied by *Richet et al. (1996)* is slightly more polymerized than the Fe-free composition used in this study as indicated by the lower NBO/T (Table 1). On the other hand, composition of the sample and analytical techniques in the work of *Liebske et al. (2003)* and this study are similar so that a direct comparison with these data is possible.

In order to compare the three data sets and to analyze the variation of viscosity with water content, viscosity isotherms were constructed. To interpolate and extrapolate experimental data, Vogel-Fulcher-Tamman (VFT) equations were calculated for each sample studied in the high viscosity range. For two hydrous samples falling sphere data were also available to constrain the VFT parameters. For other water contents, the viscosity at 1473 K estimated by interpolation of falling sphere results was included in fitting the VFT equation. Viscosity isotherms at 900, 1100, 1300 and 1500 K are shown in Fig. 4.6. The data from the three studies form a consistent trend with a steep decrease in viscosity at low water content turning over to a smooth variation at high water content. The viscosity trend is well described by the calculation model of *Richet et al.*

(1996) at low temperature for water contents below 4 wt%. In the high temperature range in which the model is poorly constrained (only one datum from *Kushiro, 1976* for a natural andesite was used to extrapolate the low-temperature data for hydrous melts towards higher temperature in *Richet et al. (1996)*, the experimental data are up to 0.3 log units higher than the predictions. It is noteworthy that results of creep experiment at 1 atm. (Table 4.4) agree well with the results of *Richet et al. (1996)* indicating that small compositional differences are of minor importance for the rheological properties of andesitic melts.

4.5.2. Towards an improved viscosity model

No *a priori* model is available from theory to describe the functional relationship between viscosity, temperature and melt composition. Several empirical approaches were used in the past to parameterize viscosity or fluidity for hydrous melts. The pioneering work of *Shaw (1972)* allows calculations for hydrous magmatic melts with different bulk compositions. However, due to a lack of experimental data for hydrous melts at that time, the model of *Shaw* has large uncertainty in predicting the effect of water on andesitic melt viscosity. Moreover, due to the use of an Arrhenian-type of equation an extrapolation to temperatures nearby the glass transition is not possible. Most of the viscosity models for specific compositions such as rhyolite (*Hess and Dingwell, 1996; Schulze et al., 1996; Giordano et al., in press*) and andesite (*Richet et al., 1996*) use extended versions of the VFT equation to account for non-Arrhenian temperature dependence of viscosity. Alternatively, in the case of rhyolite a power-law has been used to describe the temperature dependence of viscosity (*Zhang et al., 2003*). Each of the calculation models reproduces more or less well the experimental viscosity

data for a certain composition in a well-defined range of temperature and water content, but the same type of equation may fail for other melt compositions. Hence, setting up a viscosity model with a minimum number of parameters is still an attempt by trial and error.

Various types of equation were tested for viscosity as well as for fluidity using the combined data set for (iron-free) andesitic melts from *Richet et al. (1996)*, *Liebske et al. (2003)* and this study. Data were fitted using a non-linear regression. Best results were obtained with the following equation

$$\log \eta = -4.85 + \frac{8154.4}{(T - 529.9)} - \frac{5863.7}{(T - 576.9)} \cdot \frac{w}{(w^{1.15484} - 2.4455 + 0.0052 \cdot T)} \qquad (4.7)$$

where η is the viscosity in Pa·s, the T is temperature in K, and w is the water content in wt%. Eqn. 4.7 reproduces all experimental viscosity data (40 from this study, 93 from *Richet et al., 1996* and 58 from *Liebske et al. (2003)* with a standard error (1 σ) of 0.15 log units (Fig. 4.8). Pressure has only minor influence on viscosity of hydrous andesitic melts (*Liebske et al., 2003; Behrens and Schulze, 2003*) and, hence, the equation can be applied without significant error in the P-range 0.1 to 500 MPa. It is interesting to note that the viscosity at infinite temperature based on the model for andesite (log η = - 4.85, independent on water content) is close to the value of log η = - 4.31 ± 0.74 proposed by *Russell et al. (2003)* to be the viscosity limit for silicate melts in general.

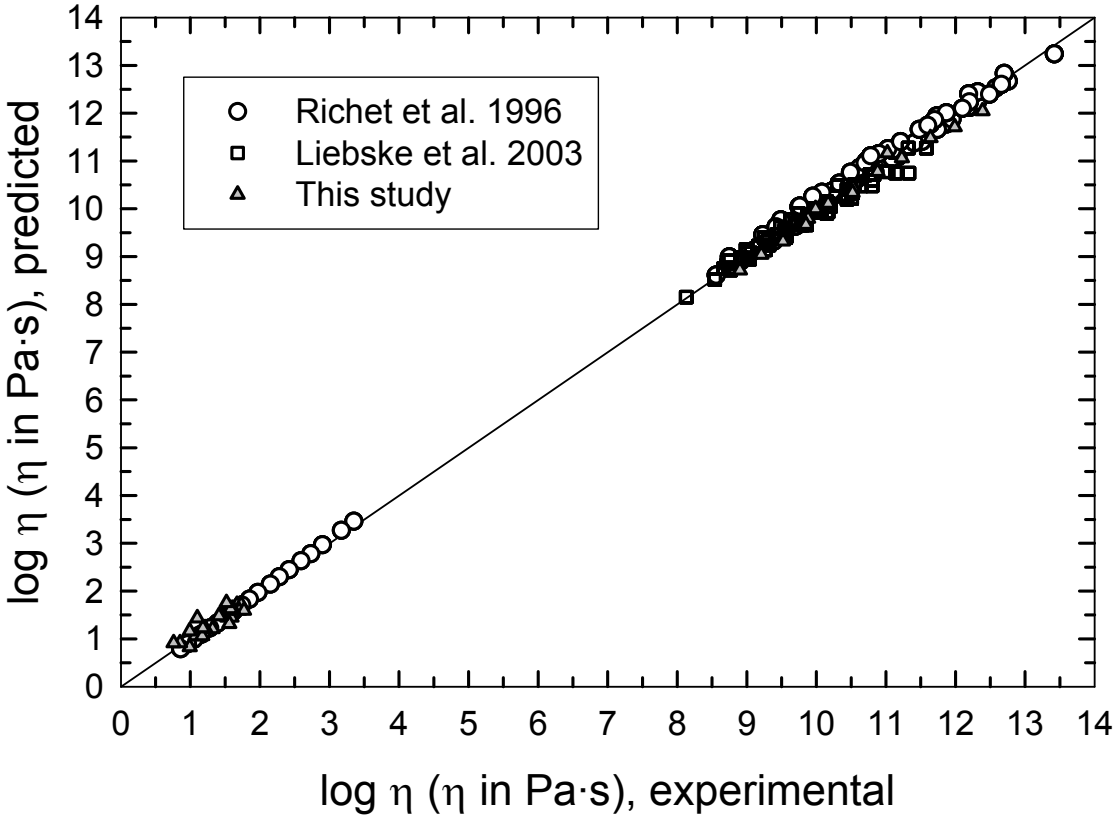

Fig. 4.8. Comparison between between experimental and calculated viscosities for andesitic melts.

Including temperature in the last term of Eqn. 4.7 was required to achieve a good fit of viscosity isotherms both at low and at high temperature (Fig. 4.6). However, this disadvantage in doing so is that this equation can not be extrapolated to low temperatures, as illustrated by dashed lines in Fig. 4.7. Therefore, application of Eqn. 4.7 for viscosities $>10^{12}$ Pa·s is not recommended for water contents >3wt%. At lower water contents the last term in Eqn. 4.7 becomes less important and the model may be applied to slightly higher viscosities, but due to lacking experimental data it is limited to $<10^{14}$ Pa·s.

5. Experiments (part II). Viscosity of natural andesite.

5.1. Application of the iron-free model to natural andesite.

Simplified iron-free compositions were used in the viscosity experiments (see Chapter 4) and the question remains whether the results can be transferred to natural andesites which contain ferrous and ferric iron in various ratios, depending on redox conditions. In the high viscosity range, viscosity data for nominally dry melts cover a range of 2.5 orders of magnitude at constant temperature (Fig. 5.1a). Results *of Richet et al. (1996)* for a Montagne Pelee andesite are in good agreement with the prediction of the model, but all other studies yield considerably lower viscosities. One explanation for the spread of the data may be a difference in melt composition and/or differences in redox state of iron. *Liebske et al. (2003)* found a decrease in viscosity by 1.7 log units in average when Fe^{3+}/Fe_{total} decreases from 0.58 to 0.21.

Difference in the experimental techniques may also contribute to minor extent to the variation in viscosity data for dry andesite. However, a more severe problem in the low temperature studies is fast crystallization of iron oxides, in particular in oxidized melts (*Neuville et al., 1991; Richet et al., 1996; Liebske et al., 2003*). Hence, experimental data are often difficult to interpret in terms of viscosity of a supercooled andesitic melt. Data for hydrous iron-bearing melts are scarce in the high viscosity range. Viscosity of an andesitic melt containing 1.88 wt% H_2O at 860 K is about 0.7 log units lower than predicted by the new model (*Liebske et al., 2003*) implying that Eqn. 4.7 is suitable at least as a first approach to estimate the viscosity of natural water-bearing andesites in the high-viscosity range.

Fig 5.1a

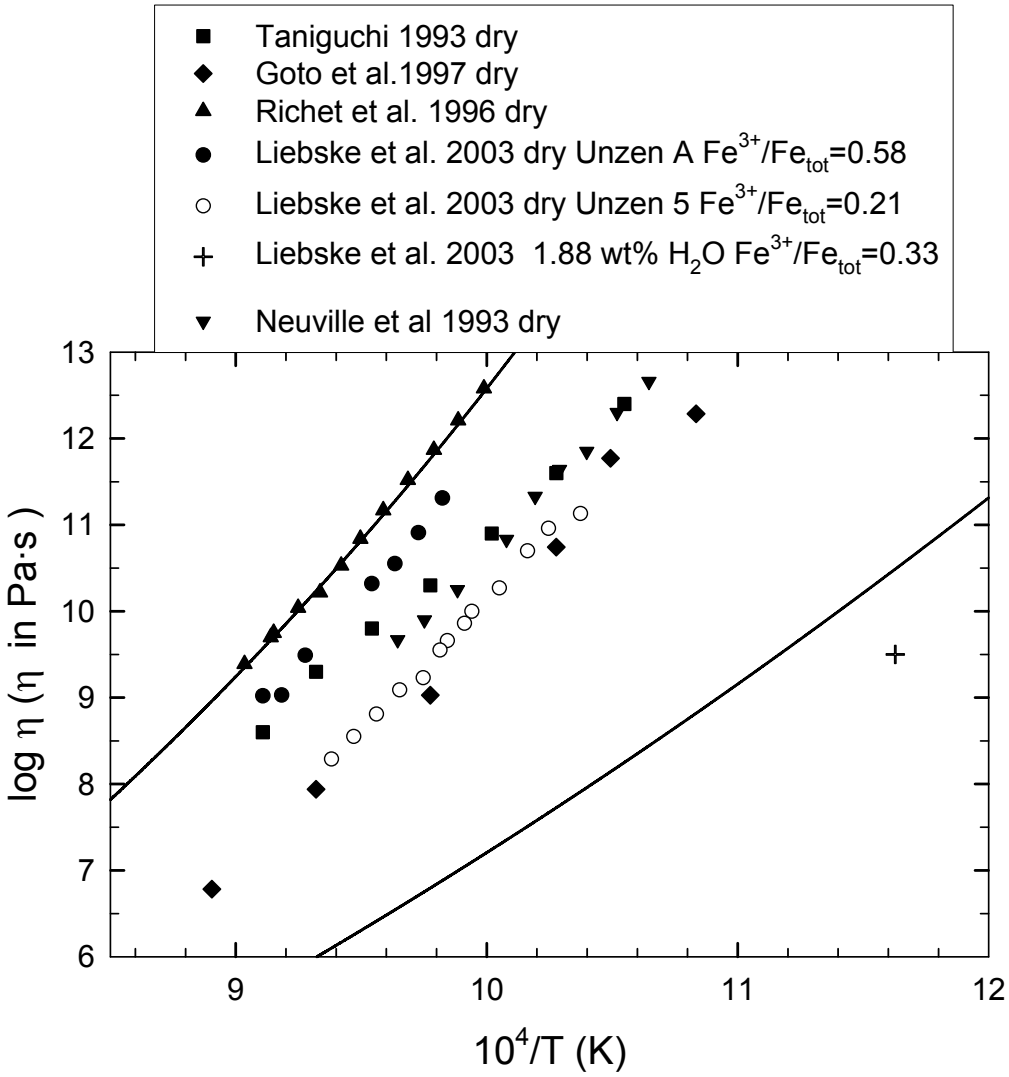
Taniguchi 1993 dry
Goto et al.1997 dry
Richet et al. 1996 dry
Liebske et al. 2003 dry Unzen A Fe3+/Fetot=0.58
Liebske et al. 2003 dry Unzen 5 Fe3+/Fetot=0.21
Liebske et al. 2003 1.88 wt% H2O Fe3+/Fetot=0.33
Neuville et al 1993 dry
log η (η in Pa·s)
10^4/T (K)
13
12
11
10
9
8
7
6
9
10
11
12

Fig 5.1b

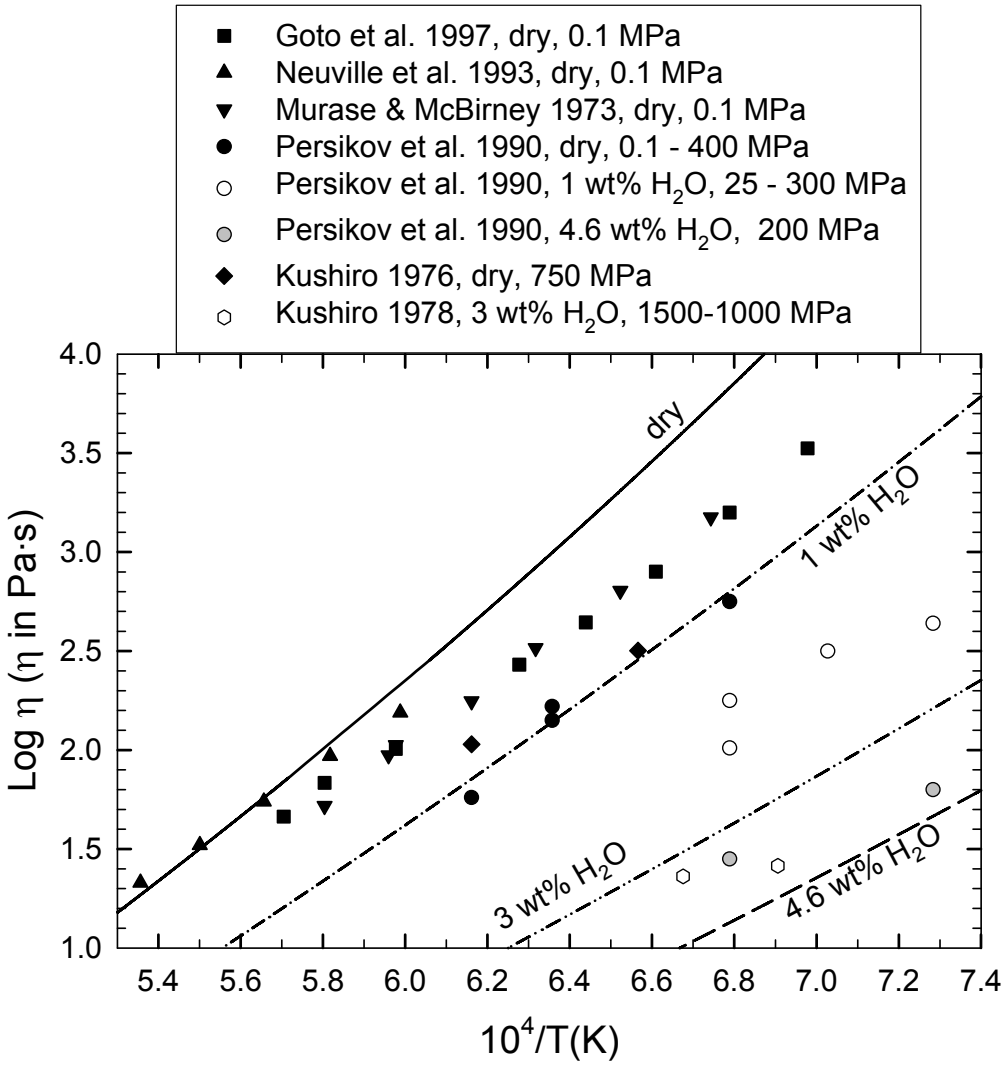

Fig. 5.1. Compilation of experimental data for natural (iron-bearing) andesite in the high (**a**) and low (**b**) viscosity range. The full and dashed lines represent the model given in eqn. 4.7. The Fe^{2+}/Fe_{tot} in the melts and glasses has only been determined in the study *Liebske et al. (2003)*.

In the low-viscosity range the model agrees well with data for nominally dry iron-bearing andesite from *Neuville et al. (1993)*, but other studies (*Murase and McBirney, 1973; Goto et al., 1997; Persikov et al., 1990; Kushiro et al., 1976*) yield viscosities up to 0.8 log units lower than the prediction (Fig. 5.1b). Measurements of *Persikov et al. (1990)* on andesites containing about 1 wt% H_2O are also about 0.8 log units lower than calculations by the model whereas data for more hydrous melts (3 – 4.6 wt%) are in better agreement. The major problem for the interpretation of the experimental data is

that the redox state of iron and the water content of the melt are unknown or poorly constrained. Moreover, differences in bulk composition (e.g., NBO/T), pressure and experimental techniques may affect the viscosity data.

In conclusion, the model given by eqn. 4.7 (Chapter 4) is probably well suited to predict relative viscosity variations as a function of melt water content and temperature in andesitic melts. However, is not possible to evaluate in detail the potential of this new model for predicting the absolute viscosity of natural iron-bearing andesite because the effect of Fe^{2+}/Fe_{tot} can not be quantified at present for hydrous melts. Viscosities predicted by eqn. 4.7 are close to those determined for iron-bearing melts at oxidizing conditions by *Liebske et al. (2003)*, at least in the high viscosity range (Fig. 5.1a). Lower viscosities are expected for more reduced melts. Differences of almost one order of magnitude, which may be due to changing Fe^{2+}/Fe_{tot} ratios, are also observed in the low viscosity range (Fig. 4.9b). Thus additional experiments on natural compositions and in particular with a control of the redox state of iron are the aim of this chapter to solve the possible role of Fe coordination on viscosities of andesitic melts.

5.2 Unzen andesite.

The occurrence of enclaves in lava dome and flow are interpreted as mingling processes between magmas of different composition and their formation mechanism include:

- Injection of mafic magma into a silicic one;
- Separation and floating of enclaves from a layer of mafic magma into a more evolved due to coupled crystallization and vesiculation.
- Vesiculation of a mafic magma within a densely stratified reservoir
- Breaking of a solid magma layer by injection of new magma and condition

The condition under which such magma will mingle rather than mix may provide a fundamental control on the development of hybrid magmas (*William and Tobisch, 1994*).

During the 1991-1995 eruption at Unzen, enclaves hosted in the erupted rocks have (see figure 2.6, SiO_2 vs K_2O diagram of the Unzen volcanic rocks) silica content in the range of 53 to 62 wt %. The composition of the starting material is given in table 5.1.

5.3 Starting materials

The starting composition is based on an andesite from Unzen Volcano (Pre Unzen 500 kyr; *Chen et al., 1993*). Anhydrous glass was synthesized by melting a mixture of oxides and carbonates at 1873 K for 4 h in a Pt crucible in air. More details on the synthesis conditions are given in chapter 4 and *Liebske et al. (2003)*. Compositions of glasses are given in Table 5.1 (two dry glass batches were synthesized labelled as compositions MDIB 1 and MDIB 2). To equilibrate for the conditions of viscosity experiments, anhydrous glass powder was filled in AuPd capsule and re-melted for 20 h at 1523 K, 500 MPa in an internally heated gas pressure vessel, IHPV (sample MDIB 12, Table 5.2).

To produce strongly reduced glass, glass powder was mixed with an appropriate portion of carbon, filled into a graphite crucible, and melted for 1 h at 1523 K and at ambient pressure in an oven flushed with a gas mixture composed by 93% Ar and 7% H_2. Thus glasses with Fe^{2+}/Fe_{tot} ratio as high as 0.91 could be produced (see Table 5.2 sample R 13). To improve homogeneity, the crushed reduced glass was filled in a large AuPd

Table 5.1. Electron microprobe analysis and water content of the starting material (wt%).

	MDIB1 (dry)	MDIB2 (dry)	MDIB24	MDIB25	MDIB30	Liebske et al. (2003)	Neuville et al. (1993)
SiO_2	55.11 (0.44)	54.18 (0.60)	57.60 (0.40)	59.56 (0.50)	56.86 (0.50)	56.65 (0.41)	61.17
TiO_2	1.09 (0.05)	1.09 (0.07)	0.92 (0.05)	0.93 (0.05)	1.04 (0.04)	1.01 (0.04)	0.84
Al_2O_3	18.39 (0.36)	18.41 (0.19)	14.98 (0.21)	15.45 (0.25)	16.90 (0.17)	17.41 (0.15)	17.29
FeO [a])	9.16 (0.32)	9.52 (0.33)	7.56 (0.39)	7.14 (0.35)	7.55 (0.38)	8.16 (0.21)	5.39
MnO	0.08 (0.06)	0.09 (0.06)	0.00 (0.08)	0.06 (0.04)	0.04 (0.04)	0.13 (0.04)	-
MgO	2.88(0.17)	2.93 (0.09)	2.77 (0.10)	2.79 (0.11)	3.14 (0.12)	4.30 (0.07)	3.35
CaO	8.44 (0.25)	8.69 (0.32)	6.37 (0.20)	6.46 (0.24)	7.13 (0.18)	7.38 (0.11)	5.83
Na_2O	3.38 (0.25)	3.41 (0.29)	3.06 (0.21)	3.26 (0.22)	3.31 (0.13)	3.23 (0.15)	3.85
K_2O	1.41 (0.08)	1.42 (0.08)	1.57 (0.08)	1.61 (0.07)	1.56 (0.06)	1.56 (0.07)	1.39
Fe^{2+}/Fe_{tot}	0.41	0.44	[b]	[b]	[b]	-	-
H_2O (IR)	0.015	0.016			2.88	0.015	
H_2O (KFT)			4.80	3.32	2.95-2.91		
Total	99.98	100.02	99.63	100.56	100.43	99.85	99.11

Notes. Numbers in parenthesis correspond to 1 σ standard deviation. Analysis of andesites studied by *Neuville et al. (1993)* and *Liebske et al. (2003)* are shown for comparison. H_2O contents were measured by IR spectroscopy using the peak height of the absorption band at 3550 cm^{-1} and the calibration of Mandeville et al. (2002) and/or by Karl-Fischer titration.

[a]) Total iron is given as FeO; [b]) Fe^{2+}/Fe_{tot} before and after experiments is given in table 5.2.

[b]) Numbers in parenthesis correspond to 1 σ standard deviation

capsule (diameter of 8mm) and re-melted for 30 min at 1573 K, 500 MPa in the IHPV. Annealing time was very short in these rums in order to avoid loss of iron which is expected to be crucial in particular at high Fe^{2+}/Fe_{tot} ratio.

The procedure to synthesize water-bearing glasses is described in detail in the previous chapter. Distilled water was added stepwise to a dry glass powder in AuPd capsules (diameter of 5-6 mm, length of 30-40 mm). The synthesis of relatively oxidized glasses was performed in an IHPV at 300-500 MPa and 1523 K for 24 h under intrinsic conditions. Hydrogen fugacity in the vessel is typically ~1 bar at these conditions, resulting in an oxygen fugacity close to that buffered by the $MnO\text{-}Mn_3O_4$ (MMO) assemblage if pure H_2O fluid is present in the capsule (*Berndt et al., 2002*). To produce the reduced hydrous glasses, the syntheses were performed for 20 to 70 h at 1050°C and 200 MPa in an IHPV equipped with a Shaw membrane (for details on the experimental apparatus, see *Berndt et al., 2002*). For these runs the amount of H_2O (10 wt% relative to the loaded glass powder) in the capsule was in excess to the expected water solubility and Au capsules were used which are more efficient than AuPd capsules to depress iron loss. Hydrogen was filled in the IHPV so that a hydrogen fugacity of ~20 bar was adjusted during experiment

Samples were quenched either by the rapid quench method (see *Berndt et al., 2002*) or by normal quench (by switching off the power; initial cooling rate is about 200 K / min).

Using the rapid quench method avoids the formation of quench crystals, but the glass cylinders accumulate stress and often brake. In such a case, the cylinders can not be used

for a second viscosity determination. On the other hand, the normal quench method allows multiple experiments with the same glass, but quench crystals are formed. To check whether quench crystals could influence the viscosity measurements, annealing experiments were performed. Quench crystals-bearing sample was heated up and quenched (using the rapid quench technique) immediately after reaching the target temperature. After such treatments at 1423 K and at 1473 K the quench crystals dissolved completely. Hence, influence of quench crystals on the viscosity experiments is not expected.

For the viscosity experiments a cylinder (diameter: 4 or 5 mm; length: 10 – 15 mm) was cored out of the synthesized glasses. The residual glass was crushed to fine grained powder except for some fragments to be used for determination of the water content and the Fe^{2+}/Fe_{tot} ratio. Loading procedure of capsules for viscosity experiments is described in detail in the previous chapter.

5.3.1 Electron microprobe analyses

The chemical composition of the glasses was determined by electron microprobe Cameca SX100. Measurement conditions were the same used for the iron free andesite: defocused beam of 15 µm diameter, accelerating voltage of 15 kV and a beam current of 4 nA. The nominally dry andesitic glasses MDIB 1 and MBIB 2 are more mafic than those used by *Liebske et al. (2003) and Neuville et al. (1993)* (see Table 5.1). Silica content was slightly higher in hydrous viscosity samples than in the dry starting glass. The glass powder used for preparation of hydrous glasses was separated from the dry glass batch after the second

melting, whereas the analysis of the dry glass was performed after an additional melting at 1873 K. Probably the andesite glass was not completely homogenized after the second melting. However, consistency of the overall dataset implies that slight variations in compositions (except for water content and Fe^{2+}/Fe_{tot}) have minor influence on viscosity.

5.3.2 Water determination

The water content of the glasses was determined by Karl- Fischer Titration (KFT) and infrared spectroscopy (IR). To account for unextracted water (*Behrens and Stuke, 2003*), water contents measured by KFT were corrected by adding 0.13 wt% H_2O. The accuracy of the KFT analysis is estimated to be 0.10 wt%, including the uncertainty in the amount of unextracted water and the error in the titration rate (for details of the analytical technique and error estimation see *Behrens and Stuke, 2003 and Leschik et al., 2004*). To test the homogeneity of H_2O concentrations in selected samples, wafers from different part of the samples were analyzed by KFT. Data are labelled with the superscript *t* (top), *b* (bottom) and *c* (center) in Table 5.2. Variation of water content was always within the analytical error.

Mid-infrared (MIR) absorption spectroscopy was used to characterize the water content in particular for water-poor glasses. Absorption spectra of doubly polished glass slabs with thickness of 0.05-0.30 mm were recorded using an IR microscope Bruker IRscopeII connected to an FTIR spectrometer Bruker IFS88. Water contents were derived from the

peak height of the OH stretching vibration band at 3550 cm^{-1} after subtraction of a linear baseline. The absorption coefficient of 62.3 L $mol^{-1}cm^{-1}$ determined by *Mandeville et al. (2002)* was used in the evaluation of the MIR spectra.

Water distribution in some water-rich post-experimental glasses was measured using near-infrared (NIR) spectroscopy. Simple linear baselines were fitted to the OH combination band at 4500 cm^{-1} and the molecular H_2O band at 5200 cm^{-1} (TT baseline according to *Ohlhorst et al., 2001*). This baseline correction is reliable to quantify the total water content but may have systematic errors in the determination of hydrous species concentrations (cf *Ohlhorst et al., 2001*). However, water speciation measured in glasses at room temperature does not reflect the equilibrium speciation in the melt during viscosity experiments (*Dingwell and Webb, 1990*), and, hence, it is not important for the interpretation of the viscosity data.

5.3.3. Colorimetric determination of ferrous iron in silicate glasses

A 6 mg to 9 mg portion (glass chips) of each sample was used for determination of ferrous-ferric ratios using a colorimetric method modified after *Wilson (1960)*. Samples were dissolved with concentrated HF to which a solution of ammonium vanadate in 5M sulfuric acid was added. At these acid conditions the released ferrous iron reacts with V^{5+} forming V^{4+} and ferric iron (reaction $Fe^{2+} + V^{5+} = Fe^{3+} + V^{4+}$). The reaction products are more stable with respect to oxidation in air than ferrous iron so that the initial redox state of the glass is preserved in the solution. After complete sample dissolution at room temperature saturated hot boric acid (353 K) was added instead of beryllium sulphate as

proposed by *Wilson (1960)* to neutralize excess HF and to bring eventually formed fluorides back into solution. Fe^{2+} is regenerated by adjusting a pH value of ~5 using an ammonium acetate buffer. For the colorimetric analysis 2:2'bipyridyl was added which forms a stable complex with Fe^{2+}. To quantify the concentration of this complex the characteristic absorption band at 523 nm was used. Measurements of concentrations of ferrous Fe and total Fe were made on the same solution before and after adding solid hydroxylamine hydrochloride. This reducing agent converts all ferric Fe into the ferrous state. Since both Fe^{2+} and total Fe determination was done on the same solution, uncertainties in the Fe^{2+}/Fe_{tot} ratios arise mainly from the absorbance measurements for which a 1 cm transmission cell in an UV/VIS spectrometer *Zeiss Specord S10* was used. Calibration of the spectrometric technique was made by measuring ferrous ammonium sulfate solutions with different known Fe^{2+} concentrations.

In each analytical session several internal standards were processed to assess the accuracy and reproducibility of the method. These standards included the glassy USGS standard RGM-1 rhyolite, and two synthetic glass in-house standards, PU-3 andesite and CT-1 basalt (synthesized from oxides and carbonates at 1873 K in air). The mean values of Fe^{2+}/Fe_{tot} (all $\pm 2\sigma$ error) determined by the colorimetric method are 0.75 ± 0.04 for RGM-1 (n=8), 0.40 ± 0.03 (n=12) for PU-3, and 0.41 ± 0.02 (n=8) for CT-1. For RGM-1 the determined values of ferrous Fe (FeO = 1.29 ± 0.08 wt%) and total Fe (FeO_{total} = 1.71 ± 0.06 wt%) are equivalent within 1σ with the certified values (FeO = 1.27 ± 0.05 wt%; FeO_{total} = 1.67 ± 0.03 wt%; Fe^{2+}/Fe_{tot} = 0.76 ± 0.03). The total Fe concentrations of the synthetic glass standards determined with the colorimetric method (PU-3 FeO_{total} = 7.21 ± 0.06 wt%; CT-1 FeO_{total} = 12.93 ± 0.70 wt%) are in good agreement with FeO_{total}

analyses by electron microprobe (PU-3 FeO_{total} = 7.74 ± 0.42 wt%; CT-1 FeO_{total} = 13.17 ± 0.47 wt%). From the results of the replicate analyses of different standards, the precision assigned to the reported Fe^{2+}/Fe_{tot} ratios is ± 0.03 (2σ).

The Fe^{2+}/Fe_{tot} ratios of glasses before viscosity experiments and after viscosity experiments are given in Tables 1 and 2. No significant change in redox state is observed during the viscosity determination (Figure 5.2).

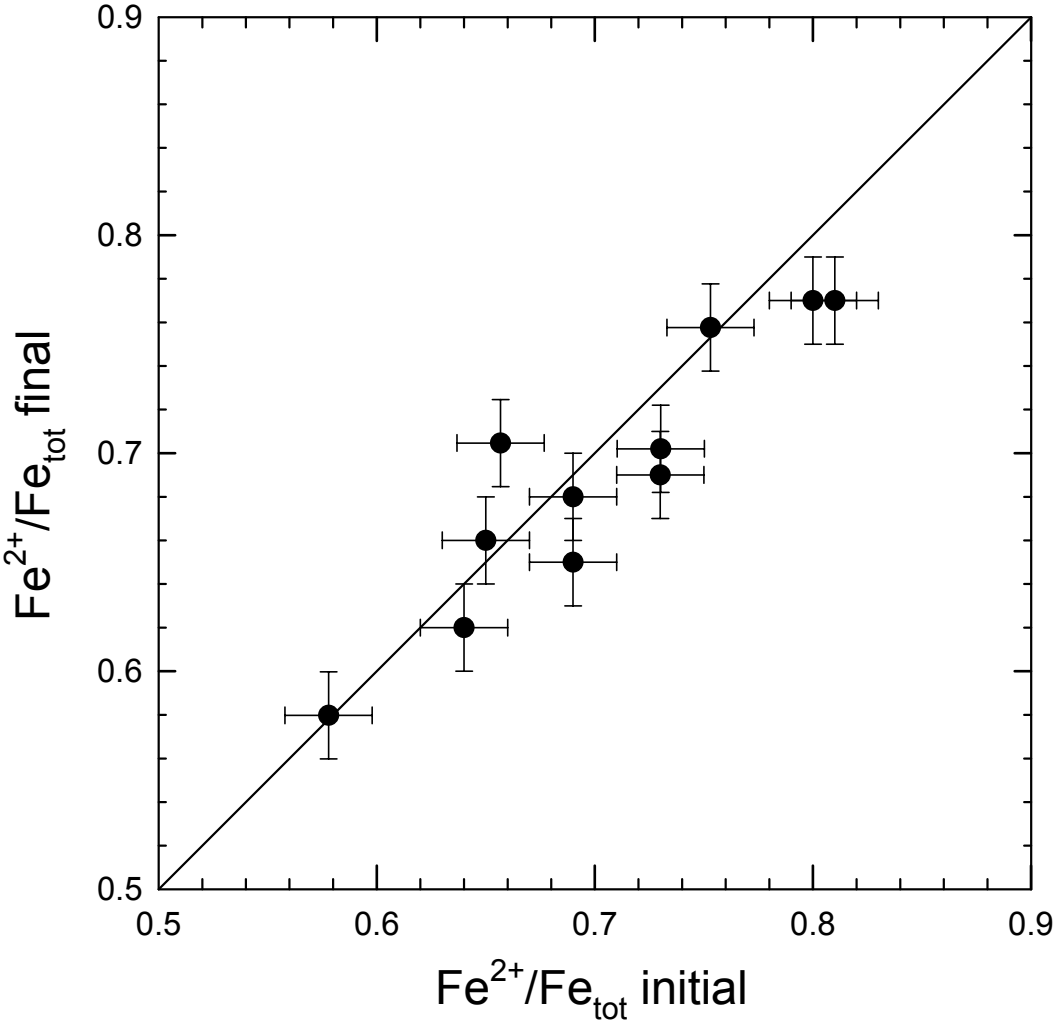

Fig.5.2. Comparison of the Fe^{2+}/Fe_{tot} ratio in glasses before and after experiments.

Comparison of the Fe^{2+}/Fe_{tot} ratio of the air-melted starting material (Table 1) with those of the viscosity samples (Table 2) emphasize the importance of pre-equilibration of samples at similar conditions as used in the viscosity experiments. Fe^{2+}/Fe_{tot} ratio of air-melted glasses are in the range of 0.41 – 0.44 whereas samples processed in the IHPV have redox ratios above 0.58.

5.4. Viscosity experiments

5.4.1. Falling sphere method.

Determination of viscosity required the measurement of the exact position of the sphere in the glass cylinder before and after experiment. Because the glasses are not transparent in the visible, X-ray images were used to monitor sphere positions (*SIEMENS HELIODENT DS X-rays camera, KODAK INSIGHT IP-21 films*, and exposure time of 0.16 s). Some run products were cracked and could not be completely expelled from the capsule without destruction. In this case only part of the capsule was removed to enable recording X-ray images. To calibrate the images, a transparent glass piece with copper wires in well defined intervals was used (Fig. 5.3). The distance between the wires was measured on a microscope stage equipped with a micrometer scale. In some experiments, more than one sphere was used (Pt and Pd spheres) that allows us multiple determination of viscosity. After welding shut the capsule, a pre-experiment was performed in an IHPV for a few minutes to establish well-defined starting positions of the spheres (condition: 1523 K and 300-500 MPa for AuPd capsules; 1323 K and 200 MPa for Au capsules)

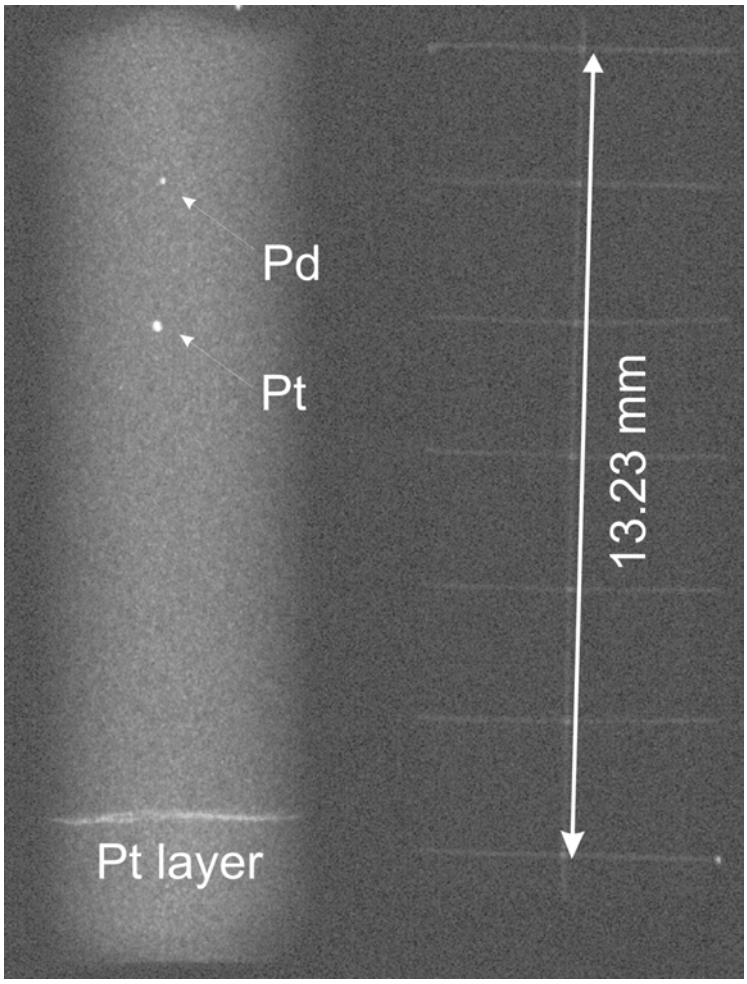

Fig. 5.3. X-ray images showing platinum and palladium spheres in an andesitic glass (left). Distance is measured relative to the platinum powder. A glass slide with copper wires in defined distance is used to calibrate the positions on the image (right).

Table 5.2. Experimental conditions and results of viscosity experiments using the falling sphere method.

No.	H_2O initial (wt%)	H_2O final (wt%)	Pressure (MPa)	T (K)	Sphere radius (μm)	C_f	Dwell time (s)	Effective time (s)	Falling distance (cm)	η (Pa·s)	Fe^{2+}/Fe_{tot} before experiments	Fe^{2+}/Fe_{tot} after experiments
MDIB32a	6.10^{t}		500	1473	61.5 ± 1 (Pd)	0.98	300	346	0.517	4.9 ± 0.7	0.58	
	6.31^{b}				54± 1 (Pd)				0.219	9.3 ± 1.1		
MDIB32b				1423	61.5 ± 1 (Pd)		900	943	0.818	9.0 ± 0.9		
					54± 1 (Pd)				0.432	12.8 ± 1.2		
MDIB32c				1373	61.5 ± 1 (Pd)		900	940	0.649	11.1 ± 1.0		
					54± 1 (Pd)				0.316	18.1 ± 1.7		
MDIB32d		6.20^{t}		1323	54± 1 (Pd)	0.98	2700	2735	0.603	53.4 ± 5.0		0.61
MDIB24	$5.17^{t}/4.78^{b}$	4.80^{c}	1000*	1473	48± 1 (Pd)	0.98	900	923	0.303	14.5 ± 1.4	0.66	0.70
MDIB 4	$3.67^{t}/3.64^{b}$		500	1523	56 ± 1 (Pd)	0.98	360	409	0.291	8.9 ± 1.0	0.73	
					50 ± 1 (Pt)				0.403	10.2 ± 1.1		0.69
MDIB31a	$3.50^{t}/3.44^{IR}$			1473	62 ± 1 (Pd)	0.98	600	646	0.292	17.2 ± 1.7	0.73	
		3.30^{b}			55 ± 1 (Pd)				0.125	31.6 ± 3.1		0.70
MDIB10a	3.46^{b}			1473	52 ± 1 (Pt)	0.98	393	439	0.135	34.9 ± 3.7	-	
					62.5 ± 1 (Pd)	0.98			0.097	32.3 ± 3.4		
MDIB10b		3.38^{t}		1523	52 ± 1 (Pt)	0.90	420	469	0.309	15.2 ± 1.6		0.70
MDIB25	$3.36^{t}/3.30^{b}$	3.32^{c}	1000*	1523	72.5 ± 2.5 (Pt)	0.95	300	325	0.436	16.2 ± 1.8	0.68	
					57.5 ± 1 (Pt)	0.98			0.278	16.7 ± 1.9		0.68
MDIB30a	2.91^{b}		500	1473	82.5 ± 2.5 (Pt)	0.98	600	646	0.619	28.6 ± 2.7	0.65	
	2.88^{t-IR}				52 ± 1 (Pt)	0.98			0.245	28.7 ± 2.9		
MDIB30b				1423	82.5 ± 2.5 (Pt)	0.98	1020	1063	0.510	56.5 ± 5.2		
					52 ± 1 (Pt)	0.98			0.201	55.3± 5.3		
MDIB30c				1523	52 ± 1 (Pt)	0.98	300	349	0.105	36.3 ± 4.1		
MDIB30d		2.95^{t-IR}		1373	82.5 ± 2.5 (Pt)	0.98	3000	3040	0.867	96.3 ± 8.5		
					52 ± 1 (Pt)	0.98			0.397	83.5 ± 7.8		0.66
MDIB29	2.47^{t}			1473	60 ± 2.5 (Pt)	0.98	600	646	0.379	24.7 ± 2.4	0.75	
	2.52^{b}	2.47^{t}			47± 1 (Pt)	0.98			0.263	21.9 ± 2.2		0.76
MDIB12a		0.06^{t-IR}	500	1523	200 ± 5 (Pt)	0.93	2700	2749	1.231	342 ± 34		
MDIB12b		0.08^{b-IR}	2000*	1473	200 ± 5 (Pt)	0.93	2700	2746	0.525	802 ± 80		0.61
R13	-	0.02^{IR}	300	1573	90 ± 2.5Pt	0.96	1200	1251	0.596	67.2 ± 7.4	0.91	0.83
R6	5.23^{t}	5.11^{t}	200	1323	65 ± 2 Pt	0.98	900	921	0.742	21.1 ± 2.2	0.64	0.62
R7	5.15^{t}	5.22^{c}	200	1323	95 ± 2.5 Pt	0.96	300	321	0.365	31.3 ± 3.7	0.69	0.65
R9	4.83^{t} /4.81^{b}	4.82^{b}	200	1323	92.5 ± 2.5 Pt	0.96	420	441	1.0123	14.7 ± 1.6	0.80	0.77
R10	4.84^{t} /4.80^{b}	4.83^{t}	200	1323	60 ± 1 Pd	0.98	1200	1221	0.335	26.5 ± 2.7	0.81	0.77

Notes Fig.5.2. Experiments with the same sample are presented in the order in which they were performed. Sphere radii were determined before incorporation in the glass. C_F refers to the Faxen correction. Supscripts *t, b* and *c* at water contents refer to measurements of slabs from the top, the bottom and the center of the cylinder, respectively. An additional supscript *IR* is used to distinguish infrared spectroscopy from KFT analyses.
* Experiments performed in a piston cylinder apparatus, all others were carried out in IHPVs.
R6, R7, R9, R10 were performed in Au capsules at controlled oxygen fuga

Most of the viscosity experiments were performed under intrinsic conditions in IHPV as described in the previous chapter. Run duration was always short (300 – 3000 s) so that only minor changes in iron content or redox state of iron were expected. Some additional experiments at elevated pressures of 1000 – 2000 MPa were performed in an end-load ¾ inch piston cylinder apparatus, PCA, (*Voggenreiter company*) at INGV in Rome. A NaCl-crushable alumina-pyrex assemblage was used for the nominally dry sample MDIB12 and a crushable alumina-pyrophyllite-pyrex assemblage for the hydrous samples MDIB24 and MDIB25 (see *Freda et al., 2001*) for the effect of assemblage on water budget of capsules processed in PCA). Experiments were first pressurized and then heated at a rate of 200 K/min up to 20 K below the target temperature. A smaller rate of 40 K/min was applied within the last 20 K of heating to avoid overshooting. Temperature was controlled within ±3 K using one $W_{95}Re_5$-$W_{74}Re_{26}$ (type C) thermocouple located on top of the sample. The experiment was terminated by switching off the heating power while maintaining pressure constant. The initial quench rate was about 2000 K/min.

The viscosity η is calculated by Stokes law (see equation 4.2). To account for movement of spheres during heating and cooling, the effective run duration for each experiment as described in Chapter 4 was calculated (equation 4.4). The density of hydrous andesitic

glasses as a function of the total water content, $C_{H_2O_t}$ (in wt %) was calculated with the equation

$$\rho = 2661(\pm 7) - 18.4(\pm 2.0) \cdot C_{H_2O_t} \quad (5.1)$$

reported by *Ohlhorst et al. (2001)*. When using the melt density in Eqn. 5.1 at experimental conditions instead of glass density results in higher viscosity by at most 3% (Chapter 4). This difference is small compared to the experimental error of viscosity and no correction was applied for it.

The settling distance was measured with Corel Draw 12 software after scanning the X-ray images with a resolution between 600 and 1200 dpi. The estimated error of distance measurement is about ± 10 µm, mainly determined by the resolution of the micrometer scale on the microscope stage. This error, together with the uncertainty in run duration, in radius of spheres and in temperature (estimated to be ± 30s, 1-5 µm and ± 10 K, respectively; see chapter 4) accumulate to an overall error in viscosity determination of 9 - 14 % (Table 2).

5.4.2 Creep method

Creep experiments under pressure were performed to measure melt viscosity above the glass transition temperature. Experimental procedures follow those described by *Schulze et al. (1999)*. The rate of deformation of cylindrical glass samples is measured when

applying a constant uniaxial stress (*Neuville and Richet, 1991*). The viscosity is calculated as described in chapter 4 (equation 4.5).

The reproducibility of viscosity measurements with the high pressure parallel plate viscometer is within ± 0.15 log unit (*Schulze et al., 1999*). To check for possible water loss during creep experiments, polished sections along the cylindrical axis were prepared and analyzed by IR microspectroscopy.

In previous studies, rapid crystallization of iron oxide was a major problem in measurement of the viscosity of andesitic melts near the glass transition (*Neuville et al., 1993; Richet et al., 1996; Liebske et al., 2003*). In order to minimize the influence of crystallization, the samples were heated as fast as possible to the temperature of the first viscosity measurement. Hence, the viscosity data have higher uncertainty than in previous studies because the apparatus was not completely relaxed, but the overall error of the viscosity data obtained from experiments is estimated to be within ± 0.2 log unit.

5.5. Results

5.5.1. Falling sphere experiments.

The falling sphere data cover a range of water content from nominally dry to 6.2 wt%, a Fe^{2+}/Fe_{tot} from 0.58 to 0.83 (considering data after experiments) established from quenched glass and temperature from 1323 to1573 K (Table 5.2). The minimum viscosity measured with the falling sphere method is 4.9 Pa·s using a Pd sphere with a radius of 61 μm and 5 min run time at 1473 K (Table 5.2, sample MDIB 32a). Viscosity values

measured using spheres with different radii inserted in the same sample are identical within uncertainty (Tab. 5.2 e.g. MDIB 4, MDIB 10a, MDIB 29, MDIB 30a and 30b). Runs at same temperature and pressure using samples with similar water content and redox state of iron agree within 0.17 log units (R6, R7) and 0.33 log units (R9, R10), respectively. The relatively large deviation in the second case is probably due to the uncertainty in run duration for the short experiment R9 (dwell time of only 420 s).

Although it is not easy to directly extract the role of changing Fe^{2+}/Fe_{tot} at a given water content and temperature from the available datasets in Table 5.2 (no experiments could be performed with exactly the same amount of water), the data indicate that the effect of redox state is very low for water-rich samples (2.5 to 6.2 wt% H_2O) in the Fe^{2+}/Fe_{tot} range of 0.61- 0.76. At 1323 K, the viscosity of samples R6 to R10 (Table 5.2) containing 4.8 to 5.2 wt% H_2O varies only between 14 and 31 Pa·s for Fe^{2+}/Fe_{tot} ratios increasing from 0.62 to 0.77 and no clear tendency (increasing or decreasing viscosity with changing Fe^{2+}/Fe_{tot}) is observed in the dataset. By contrast, in melts with low water contents, the viscosity decreases noticeably with increasing Fe^{2+}/Fe_{tot} ratio. The comparison of data obtained for "nominally dry" samples (e.g. R13 and J And1; Table 5.2) in the high temperature range indicate that changing Fe^{2+}/Fe_{tot} from 0.83 to 0.60 may cause a variation of up to 1 log unit. Although there is a difference of 50 K between experiment R13 and J And1, it is obvious that the viscosity is higher in the melt with the lower Fe^{2+}/Fe_{tot} ratio, when extrapolated to the one temperature.

5.5.2. Creep experiments

Creep experiments were successful for only one sample, which contained 3.3 wt% H_2O (MDIB 7, Table 5.3). An attempt with a sample containing 5.1 wt% H_2O failed because of rapid loss of water during viscosity measurement. The viscosity datum obtained for this glass at 792 K was about 1 log unit higher than predicted by the new Fe-bearing model (see below) and by the variation of viscosity with water content observed for iron-free analogue compositions (*Richet et al., 1996*; see also chapter 4). The sample shows a dehydrated rim after experiment which probably strongly strengthened the sample.

With the sample MDIB 7 three measurements at the same temperature (747 K) were performed during the experimental sequence (Fig. 5.4). The obtained viscosity data agree within ± 0.15 log units. However, the viscosity-time record shows an increase of viscosity with time already for the second measurement, indicating that iron-oxides started to crystallize from the glass (*Richet et al., 1996; Liebske et al., 2003*). The change in viscosity, however, is small and the data presented in Table 5.3 are most likely still representative for the andesitic melts. Water determination by KFT after the experiments agree within the value measured for the starting glass, indicating that water loss was not severe during the experimental sequence with MDIB 7.

Table 5.3. Results of parallel plate viscometry at 300 MPa.

Sample	Temperature (K)	log η exp.(Pa·s)	Fe^{2+}/Fe_{tot}	H_2O (wt%)
MDIB7	747	10.33	0.70	3.30
	757	10.07		
	747	10.36		
	768	9.77		
	747	10.47		

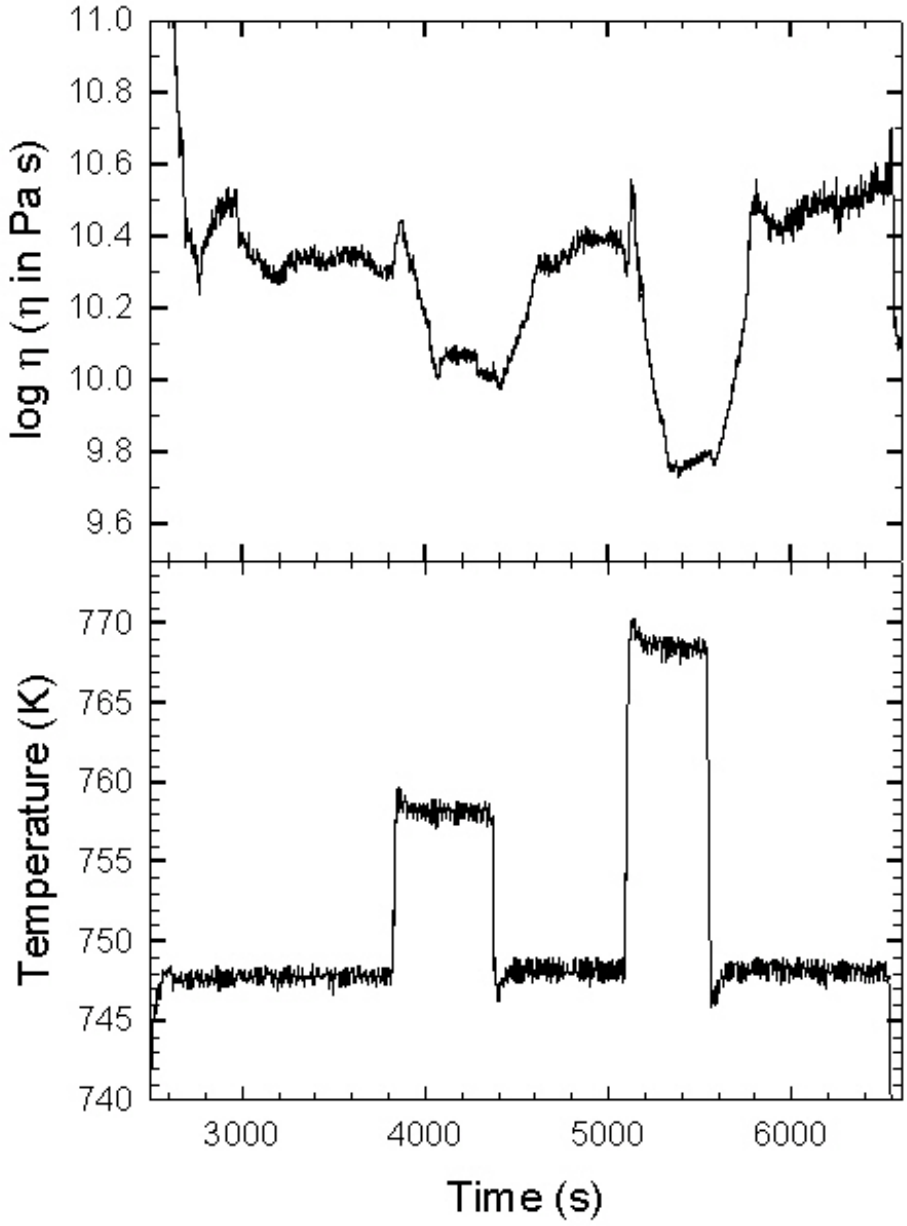

Fig 5.4.Creep experiment on sample MDIB 7 containing 3.30 wt% H_2O. Note that the viscosity started to increase with time at constant temperature from the third temperature step.

5.6. Discussion

5.6.1 Loss of iron during experiments and implication for viscosity determination

One problem with high pressure experiments using Fe-bearing samples at high temperature is the loss of iron from the melt to the capsule material, in particular at low water content of the melt and high hydrogen fugacity in the vessel (e.g., *Sisson and Grove, 1993; Berndt et al., 2005*). The average iron loss was quantified using the colorimetric method and/or electron microprobe. For the centre of the glass cylinders electron microprobe analysis yielded similar iron content when compared with bulk measurements using colorimetry (Table 5.4). Near the capsule walls the melts were more depleted in iron content, but this may not have affected the viscosity data because the spheres are located in the centre of the cylinder and move along the cylindrical axis.

Table 5.4. Total iron contents in run products using AuPd capsules.

Sample	Temperature (K)	Microprobe FeO_{tot} (wt%)	Colorimetry FeO_{tot} (wt %)
MDIB25	1523	7.34	7.07
MDIB30		7.74	7.39
MDIB31	1473	7.71	7.39
MDIB32		7.66	7.73

Samples obtained from experiments performed in Au capsule (Table 5.2) show only little changes in iron when compared to the starting material despite of high hydrogen fugacity in the IHPV, in agreement with studies on basaltic system using the same IHPV (*Berndt et al., 2005*). The iron loss for samples R6 to R10, with starting material MDIB 2 (table

5.1) is 0.5 ± 0.3wt% FeO_{tot}. The iron loss is more significant when using Au-Pd capsules, even at low hydrogen fugacity (intrinsic conditions of IHPV). Among the samples analyzed for iron loss, two glasses (MDIB 30, MDIB 25) are products from experiments conducted at the highest temperature (1523 K). One of these samples (MDIB 30) was even used in a series of experiments at different temperatures. Thus, the iron loss is expected to be particularly strong for this sample. However, the loss of 1.7 wt% FeO_{tot} detected for MDIB 30 is similar to the value found for MDIB 25 (2 wt% FeO_{tot}). Glasses from experiments performed at 1473 K show similar or slightly lower iron loss (MDIB 31 and MDIB 32). Thus, iron loss is low but not negligible in the experiments performed in AuPd capsules. The problems related to iron loss may explain some differences in viscosity obtained at similar conditions (water content and temperature). For example, the viscosity determined in experiment MDIB 32d (1323 K, 6.2 wt% H_2O), in which 2 wt% FeO_{tot} loss was observed, is higher than the viscosity determined in experiment R6 (1323 K, 5.2 wt% H_2O) with less than 0.7 wt% FeO_{tot} loss (compare Table 5.2). Since the water content in MDIB 32d is higher than in R6, a lower viscosity is expected from the experiment MDIB 32d.

5.6.2. Viscosity model for Fe-bearing andesite melt as a function of Fe^{2+}/Fe_{tot}

The originality of the dataset is that it allows to improve the viscosity model for andesite melt established for a Fe-free composition by *Richet et al. (1996)* and the model presented in chapter 4. The two models showed that the effect of dissolved water on andesitic melts is more pronounced at low than at high water content, as expected from

other compositions investigated in the past (e.g., *Hess and Dingwell, 1996; Richet et al., 1996; Scaillet et al., 1996; Schulze et al., 1996, 1999; Romano et al., 2001, 2003; Whittington et al., 2000, 2001; Liebske et al., 2003; Zhang et al., 2003; Giordano et al., 2004*). Several studies (*Mysen and Virgo 1989, Dingwell and Virgo 1988, Dingwell 1991, Liebske et al., 2003*) have shown that oxidation state of iron is a parameter which needs to be taken into account to model the viscosity of silicate melts with high Fe contents. In the system Na-Si-Fe-O (composition NS4F40) and at 1473 K, *Dingwell and Virgo (1988)* observed a decrease in viscosity by 0.81 log units when decreasing the Fe^{2+}/Fe_{tot} ratio from 0 to 0.77. Moreover a decrease in log viscosity of 0.34 log units was found for $NaFeSi_2O_6$ melt when increasing the Fe^{2+}/Fe_{tot} ratio from 0.08 to 0.82 at 1703 K. As shown in *Liebske et al. (2003)*, when the Fe^{2+}/Fe_{tot} ratio increases from 0.42 to 0.79 in an andesite melt, the viscosity decreases by ~ 1.7 log units at 1061 K. This indicates that previous determinations made at ambient conditions (no control of fO_2) may not be geologically relevant.

A major problem in setting up a general viscosity model for andesite melts is due to inconsistencies within and between the data sets and lack of information on the redox state of iron in most of previous studies. In the high viscosity range (just above the glass transition) published data for nominally dry andesitic melts cover a range of more than two orders of magnitude at constant temperature (see data compilation in *Liebske et al., 2003*, Fig. 10). In part these variations in viscosity may be due to variations in melt composition and/or differences in redox state of iron. *Liebske et al. (2003)* found a decrease in viscosity by 1.7 log units in average when Fe^{2+}/Fe_{tot} increases from 0.42 to

0.79. Additionally, differences in the applied experimental techniques (*Goto et al., 1997 and Taniguchi, 1993* – fiber elongation; *Neuville et al., 1993* and *Richet et al., 1996* – creep experiments at 1 atm; *Liebske et al., 2003* - high pressure parallel plate viscometry) may contribute to the variation in viscosity data for dry andesite. However, a more severe problem in the low temperature studies is rapid crystallization of iron oxides, especially in oxidized melts (*Neuville et al., 1991, Richet et al., 1996, Liebske et al., 2003*). Hence, actual experimental data are often difficult to interpret in terms of the viscosity of a supercooled crystal-free andesitic melt.

In the modelling were considered only data from *Liebske et al., (2003)*, for water-poor melts in the high viscosity range, because of the unknown redox state of iron (and possible affect of crystallization of iron oxides) in the other studies (*Taniguchi, 1993; Goto et al., 1997; Neuville et al., 1993; Richet et al., 1996*). Data for the viscosity of hydrous melts near the glass transition are limited to one measurement on a sample containing 1.88 wt% H_2O studied by *Liebske et al. (2003)* and five measurements on a sample containing 3.30 wt% H_2O measured in this study. Redox state of iron is similar in both melts and, hence, variation of viscosity with Fe^{3+}/Fe_{tot} can not be constrained for hydrous melts in the high viscosity range. However, minor variation of η with Fe^{2+}/Fe_{tot} were found for dry melts with similar Fe^{2+}/Fe_{tot} (0.30) at high viscosity and the viscosity of water-rich melts above the liquidus is not sensitive to Fe^{2+}/Fe_{tot}. Thus, data for hydrous samples just above the glass transition can be applied in a wider range of Fe^{2+}/Fe_{tot} without significant error (between 0.65 and 0.75).

Although several data sets are available for the viscosity of andesitic melts above the glass transition, most of them (*Murase and McBirney, 1973; Kushiro et al., 1976, 1978; Persikov et al., 1990; Neuville et al., 1993; Goto et al., 1997*) suffer from the unknown redox state of iron. Beside the data from this study I have used in the modeling the measurements of *Neuville et al. (1993)* on water-poor melts measured with the concentric cylinder technique. The redox state of iron was not reported in that study. A basic assumption which I made in using the data is that the melts were in equilibrium with air at all temperatures. With this assumption Fe^{2+}/Fe_{tot} was calculated with the model of *Moretti (2006)*.

The data base for modelling the viscosity as a function of temperature, water content and Fe^{2+}/Fe_{tot} ratio consists of 46 measurements from *Liebske et al. (2003)*, 5 measurements from *Neuville et al. (1993)* 36 measurements from this new study. An empirical viscosity model based on the VFT approach was chosen to account for the non-Arrhenian temperature dependence of viscosity. Data were fitted using a non-linear least-square regression. After various attempts of trial and error the following equation was found best to reproduce best the experimental data and the observed viscosity trends

$$\log\eta = -5.72 + \frac{8530.8}{(T - 59.8)} + \frac{1845.1}{(T - 650.6)} * \exp\left[\frac{196.1}{\left(\frac{Fe^{2+}}{Fe_{tot}} * T\right)}\right] * \exp\left(-452.5 * \frac{w}{T}\right) \qquad (5.2)$$

where η is the viscosity in Pa·s, T the temperature in K, w is the water content in wt% and Fe^{2+}/Fe_{tot} is the relative proportion of ferrous iron. This equation reproduces the experimental data with a 1σ standard deviation of 0.20 log units (Fig. 5.5). The maximum

deviation from the model (about 0.8 log units) is observed for the viscosity of dry melts at 1670 K reported by *Neuville et al. (1993)*. Clearly the data for the dry melt at ambient pressure show systematic deviation from the prediction of the model. At high temperature (1867 K) the viscosity is underestimated by the model, at low temperature (1670 K) it is overestimated. This may indicate that either the assumption of redox equilibrium of the melts with air is not correct for these experiments or that the model is not well constrained at these conditions.

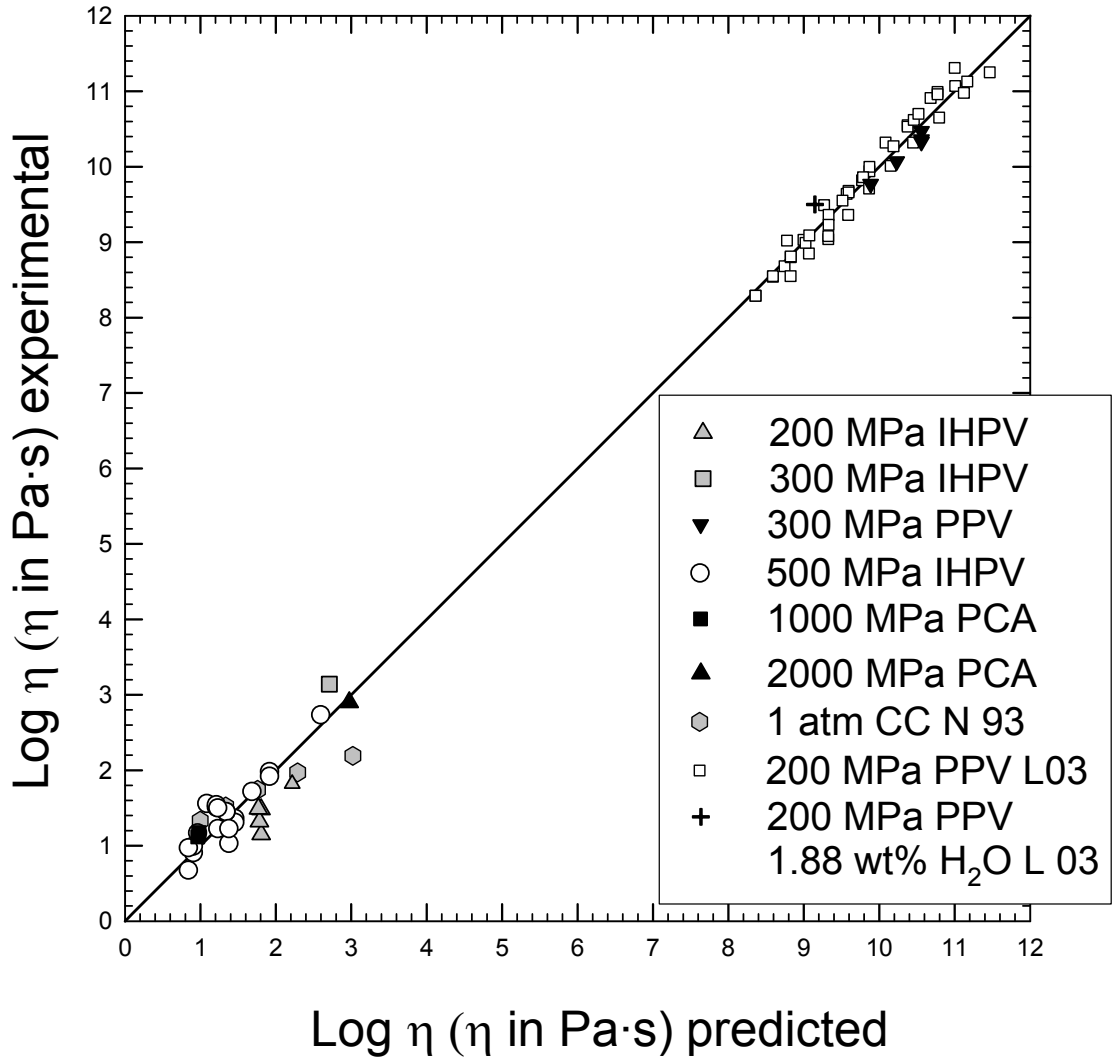

Fig 5.5. Comparison of experimental viscosity data for iron-bearing andesitic melts with predictions of the new model (Eqn. 5.2). IHPV, PPV, PCA and CC in the legend refer to internally heated pressure vessel, parallel plate viscometer, piston cylinder apparatus and concentric cylinder, respectively. Data from *Liebske et al. (2003)*, LO3, and *Neuville et al. (1993)*, N93; are used in the construction of the models in addition to the new data.

To improve the model, more data are required for the water-poor melt in particular at reduced condition. Data for hydrous melts in the low viscosity range covering a wide range of pressure are very well reproduced by the new model (Fig. 5.6).

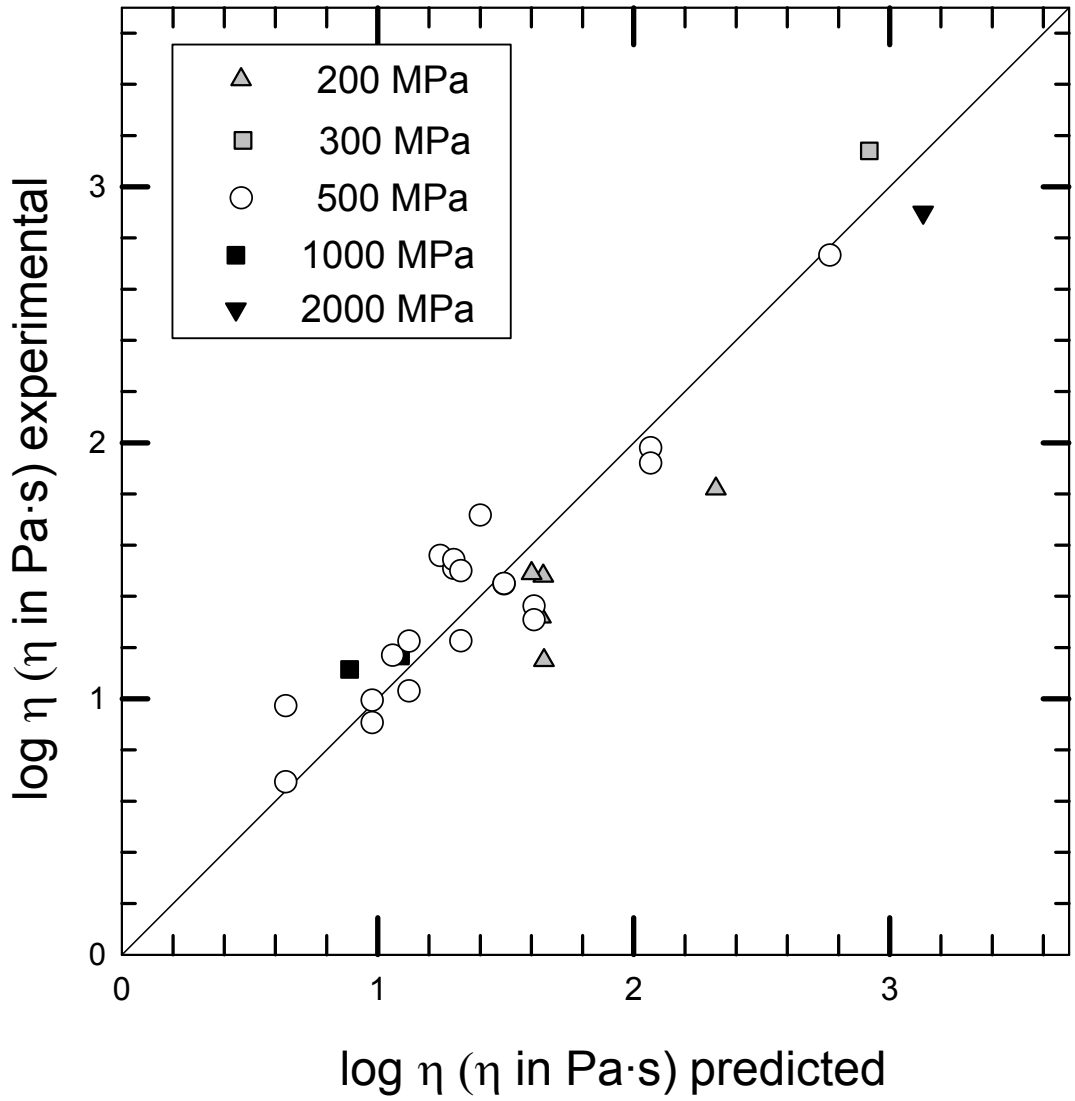

Fig. 5.6. Falling sphere viscosity data for Fe-bearing andesitic melts in comparison with the prediction of the new model. The IHPV and PCA abbreviations are referred to internally heated pressure vessel and to piston cylinder apparatus used to perform falling sphere experiments.

The predicted trends for different redox ratios of iron are plotted in Fig. 5.7. For water-rich melts difference due to Fe^{2+}/Fe_{tot} can not be resolved by the experimental data. It has to be emphasized that the dependence on redox ratio of iron is constrained mainly by the

data for dry melts at low temperature (*Liebske et al., 2003*) and the high temperature data from this study (samples MDIB12, R13).

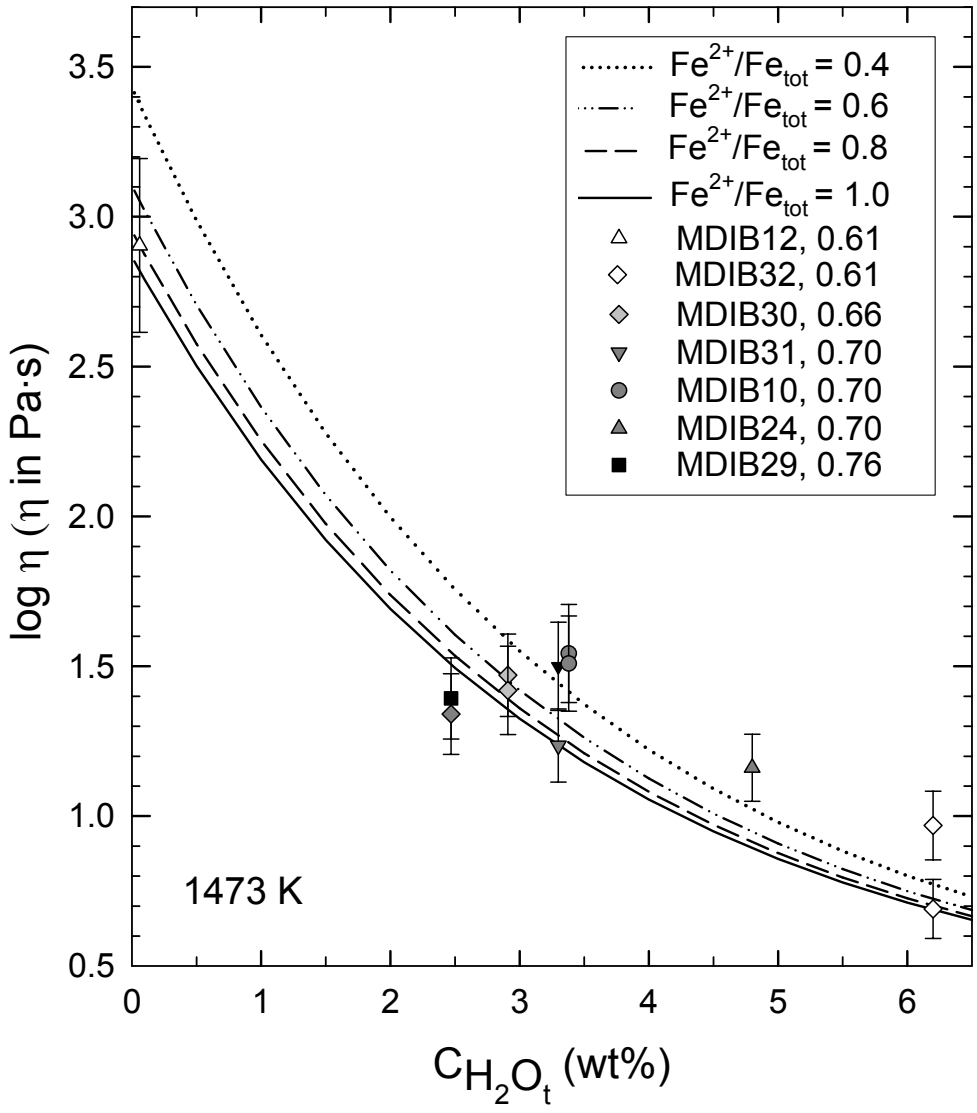

Fig. 5.7. Effect of redox state on iron and water content on the viscosity of andesitic melts at 1473 K.

The viscosity model presented in chapter 4 and determined for a Fe-free andesite is compared with the model given by equation (5.2) to check the applicability of viscosity

models elaborated for Fe-free melts. Figure 5.8 shows the effect of water on viscosity of Fe-free and Fe-bearing andesitic melts with Fe^{2+}/Fe_{tot} of 0.7 at 1273 and 1473 K. Fe^{2+}/Fe_{tot} ratio of 0.7 is representative for a f_{O2} corresponding approximately to the QFM buffer at high temperature, which is relevant for geological conditions in magma chambers. Significant differences (up to approximately 1 order of magnitude) between the two models are observed at low water contents. The differences become negligible at water contents higher than 4 wt% H2O. Differences are higher at low temperature but melts with an andesitic composition are not anymore in equilibrium at 1273 K and water contents below 4 wt% because crystallization should occur (e.g., *Botchanikov et al.,* under review).

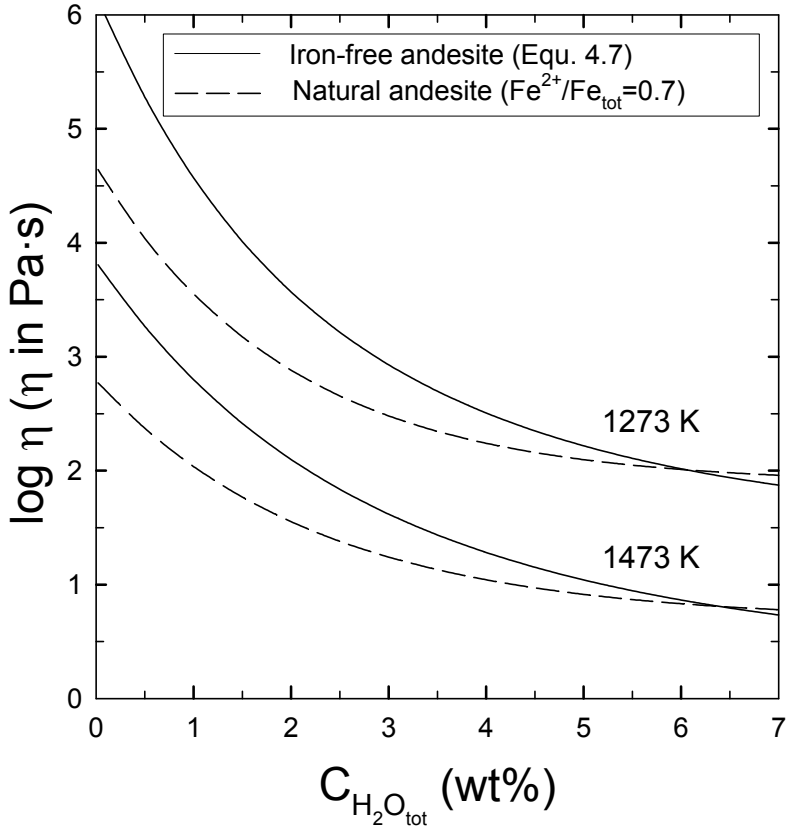

Fig. 5.8. Effect of redox state on iron and water content on the viscosity of andesitic melts at 1473 K.

5.6.3. Pressure effect on viscosity of andesitic melts.

Scarfe et al. (1987) found that in the low viscosity range, the viscosity in some silicate melts with NBO/T>1, like $CaMgSi_2O_6$, increases with pressure, whereas most silicate and aluminosilicate melts with NBO/T<1 $NaAlSi_3O_8$, $NaAlSi_2O_6$, K_2O-MgO-5 SiO_2, andesite, tholeitic basalt, are characterized by a negative pressure effect (decrease in viscosity with increasing pressure). An "anomalous" negative pressure effect on viscosity was also found in the high viscosity range for polymerized melts such as albite melts or tonalite melts (*Schulze et al., 1999; Behrens and Schulze, 2003*). In the system albite-diopside a crossover between positive and negative pressure dependence of viscosity was found between an NBO/T of 0.1 to 0.3 (composition close to $Ab_{74}Di_{26}$), depending on temperature (*Behrens and Schulze, 2003*). From these studies a minor effect of pressure on melt viscosity is expected for andesitic melts. Results from *Liebske et al. (2003)* confirm this suggestion in the high viscosity range (10^8-$10^{11.5}$ Pa s) for Fe-free andesitic analogue composition with water contents from 0 to 2 wt%. In the pressure range from 0.1 to 300 MPa the variation of viscosity was found to be less than 0.3 orders of magnitude. In the low viscosity range, for the Fe-free andesite was found no significant dependence of viscosity on pressure in the range 0.1 to 500 MPa for a melt with similar composition. Thus, in Fe-free andesites, the effect of pressure is minor and can be neglected for geologically relevant conditions.

Results of falling sphere experiments with Fe-bearing andesite melts in the pressure range from 200 to 2000 MPa suggest that pressure is of minor influence for andesitic melts at geological relevant conditions. The consistency of overall data and agreement between modelling and experimental data (Fig. 5.5) supports this conclusion, although experimental pairs in which only pressure is changing are not available (identical water content, Fe^{2+}/Fe_{tot} and temperature),

5.7. Implication for mixing-mingling processes at Unzen volcano

It has been emphasized in previous studies (e.g., *Nakada and Motomura, 1999; Venezky and Rutherford, 1999; Holtz et al., 2005*) that the Unzen dacite of the 1991-1995 eruption was probably generated from a mixing process between a phenocryst-rich low-temperature (rhyolitic) and a nearly aphiric high-temperaure magma (basalt-andesitic). This is based on petrographic observations with plagioclase and hornblende phenocrysts showing compositional zoning and reverse zoning at the rims (*Nakamura, 1995; Nakada and Motomura, 1999*) and on experimental phase equilibria investigations (*Venezky and Rutherford, 1999; Holtz et al., 2005; Sato et al., 2005*). It has been demonstrated that mixing of an almost aphyric andesitic magma with a phenocryst-rich rhyolitic magma has initiated the 1991 eruption of the Unzen volcano (*Nakada and Motomura, 1999*). The temperature of the injected andesitic magma is estimated to be near 1050°C with a water content of 4 wt%. (*Holtz et al., 2005; Sato et al., 2005*). The temperature of the partially crystallized magma in the chamber before mixing is estimated to be 760-780°C and the

water content of the residual rhyolitic melt is inferred to be about 8 wt% (*Holtz et al., 2005*).

Among the parameters governing the efficiency of mixing processes, viscosity is a crucial factor. Using viscosity models elaborated for hydrous rhyolitic melts (*Hess and Dingwell, 1996*) and for Fe-bearing andesitic melt (this study) the melt viscosities prior to eruption, the evolution of viscosities of mixed silicate melts and the efficiency of magma mixing can be estimated. Figure 5.9a shows the viscosity of the two end-member melts as a function of water content. Assuming a water content of 4 and 8 wt% H_2O for the andesitic and the rhyolitic melt, respectively, the melt viscosity is 1.9 and 4.1 log units (Pa·s), respectively, prior to eruption. Thus, directly after injection, the viscosity of the hot andesitic melt is about two orders of magnitude lower than that of the cold rhyolitic melt (Fig. 5.9a) and mingling processes, rather than mixing, between the two magmas should occur.

The average temperature of the magma after mixing is estimated to be 900 to 930°C (*Venezky and Rutherford, 1999; Holtz et al., 2005*) Assuming that equilibrium temperature is reached within a short period (mingling enhances equilibrium temperature distribution), the viscosity of the two end-member melts will change. At 930°C (T after mixing), the andesitic melt with 4 wt% H_2O and Fe^{2+}/Fe_{tot} ratio of 0.65, would have a similar viscosity as the rhyolitic melt with 8 wt% (Fig. 5.9b). Assuming equilibrium conditions, the andesitic melt containing 4 wt% H_2O should crystallize at 930°C and mixing processes will involve residual melts from a partially crystallized andesitic system and rhyolitic melts. However, at 930 °C, the viscosity of mixed melts (with a

composition corresponding to the rhyodacitic groundmass) with water contents in between the two end-members (4 to 8 wt% H_2O) is not expected to differ strongly from that of the two end-members (increasing silica content is compensated by the increasing water content). In conclusion, the nearly identical viscosity of the end members (independently on mixing ratios) and the low viscosity of the melts (10^3 Pas) favour chemical mixing processes. This is probably an important factor explaining the chemically homogeneous composition of the groundmass of Unzen dacite erupted over a period of 4 years.

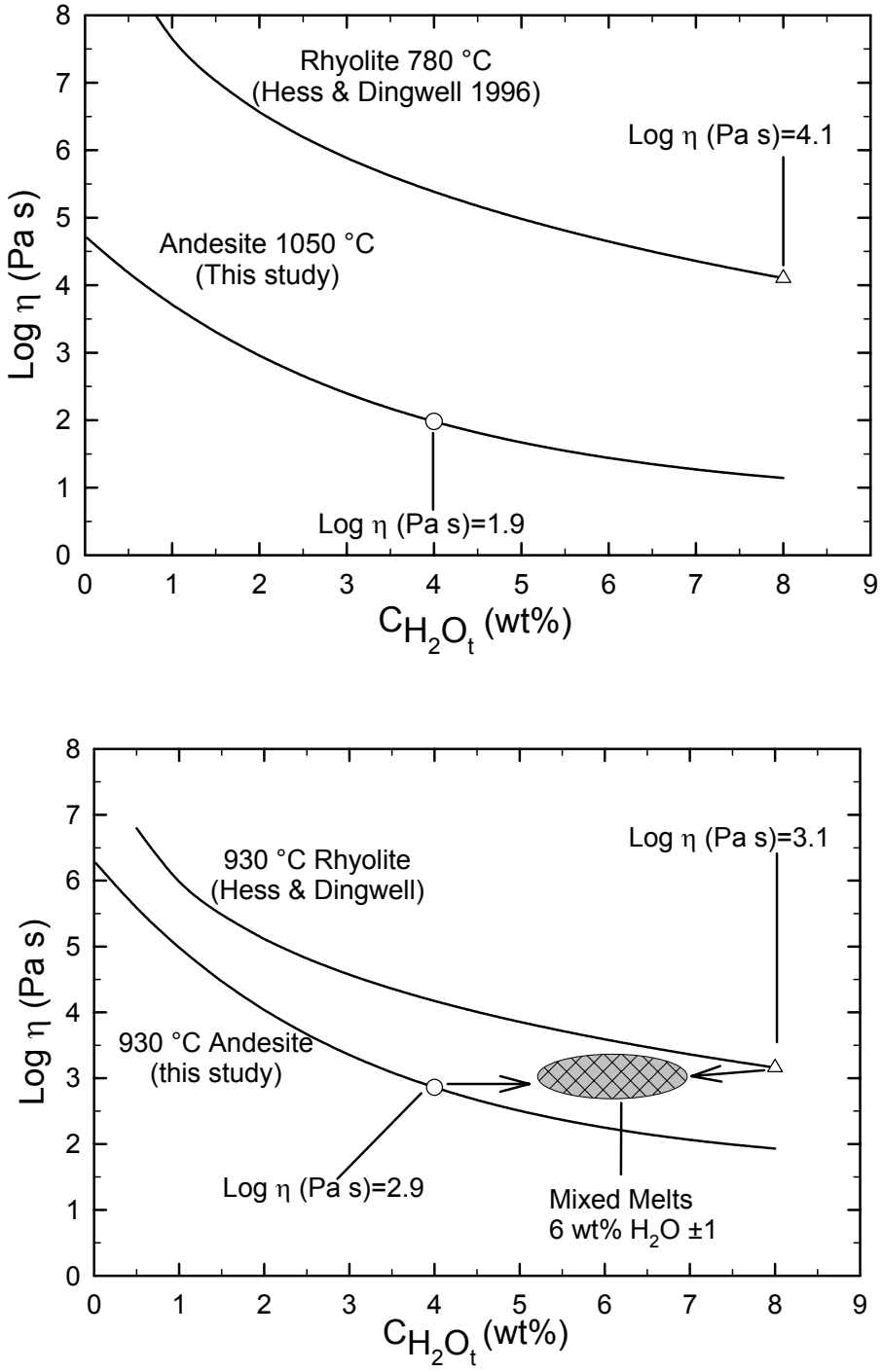

Fig 5.9. Viscosity of rhyolitic and andesitic melts at conditions prior to eruption of the Unzen volcano. The figure on top **(a)** shows the initial viscosity of the melt in the magma chamber (rhyolite) and in the ascending melt (andesite). This situation favors mingling of the magmas. The figure on bottom **(b)** illustrates the situation after thermal equilibrium. Similarity of viscosity observed in this case favors magma mixing.

6. Experiments (part III). Viscosity of partially crystallized andesite.

6.1 Basic knowledge

Rheological properties like viscosity will change with the volume fraction of crystals in melts. The melt fraction (Φ) is required to specify weather the system is controlled by liquid or solid properties. In nature, such variation of Φ can have a strong effect on the behavior of volcanoes and their products: convection in magma chambers ascent of magma through the conduit, flow of lava on the Earth's surface. Magma viscosity can increase by a factor of 10^{13} over a temperature interval of about 200°C; hence, the rates at which magmatic processes can proceed are more strongly influenced by this than by any other physico-chemical property (*Pinkerton and Stevenson 1992*). In literature *(Petford, 2003; Renner et al., 2000; Lejeune & Richet, 1995)* it is common to specify ranges in which the viscosity abruptly increases due to the diminution of Φ. Usually, this limit is termed as RCMP or "*rheological critical melt percentage"* and is defined as melt content at the *"breakdown of the solid and interlocked crystalline skeleton"* (*Arzi, 1978*). In his work on the viscosity of partially melted granite, *Arzi (1978)* observed a dramatic decreases of viscosity with melt fraction above Φ = 0.1 (Fig. 6.1(a)). However, the suggestion that a viscosity threshold exits at Φ = 0.1 is based on only three samples and without data at high Φ. In the same paper experiments were carried out using a maximum melt fraction of Φ = 0.18. Thus, the relation of *Roscoe (1952)* was used to predict viscosity of granite magma with higher Φ (see Fig. 6.1b). Using this

relationship (considering a melt viscosity $\eta = 10^4$ Pa·s) the data of Arzi (1978) are fitted to a curve (Fig. 6.1a) describing the viscosity of granite in a range of melt fraction between solidus and liquidus.

Fig. 6.1 (b) (melt fraction vs. log strength) shows basically three delimited regions: the first with $0 < \Phi > 0.2$ (solid behavior), the second $0.6 < \Phi > 1$ (liquid behavior) and a third region with $0.6 < \Phi > 0.2$ (RCMP). The last region shows three different areas with different colors. The dashed line delimits the RCMP constrained by the data of *Lejeune and Richet (1995)* whereas the light grey area is made from the data of *van der Molen & Paterson (1979)*. In dark grey is represented the Critical Melt Fraction (CMF or the area where the decrease in strength with increasing melt fraction reaches a maximum) of *van der Molen and Paterson (1979)*. *Rosenberg and Handy*, *(2005)* pointed out that all data in fig 6.1 were obtained using an apparatus that could not measure sample strength less than 1 MPa. Hence, the sample strengths at $\Phi = 0.2$ in *der Molen and Paterson (1979)* and $\Phi = 0.4$ in *Rutter and Newman, (1995)* are unknown and < 1MPa. This limitation may have masked potential deviation from a linear trend of strength vs. Φ. In fact, *Bagdassarov and Dorfman (1998)*, indicate that the strength of a granite sample containing 50 vol% crystals is much lower than 1 MPa (black circle in fig. 6.1(b)).

Lejeune and Richet, (1995), studied the viscosity of partially crystallized $Mg_3Al_2Si_3O_{12}$ melts under uniaxial compression. The solids particles in the melts were well-rounded spherulite of aluminous enstatite having the same composition as the melts. They note that the rheology changes abruptly at volume fraction of crystals close to 40vol% and the viscosity becomes non-Newtonian. As long as the crystal fraction does not exceed 70 vol% the deformation is irregular and becomes again regular with low melt fraction. They suggest that the influence of solid suspension on the rheology of magmas is

determined by the volume fraction of crystals. Their data are in good agreement with Roscoe's prediction, but they found a transition between solid like to liquid like behavior at a melt fraction much higher than that suggested by *Arzi (1978)* and *van der Molen & Paterson (1979).*

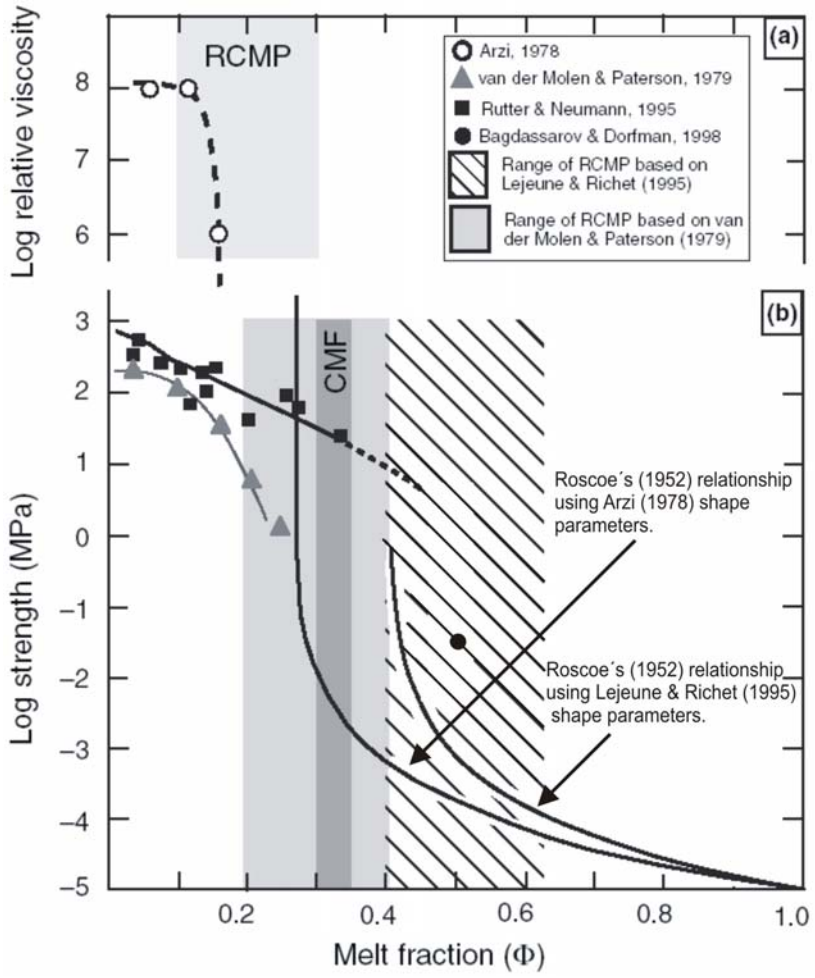

Fig. 6.1. RCMP (rheological critical melt percentage) areas (from *Rosenberg & Handy 2005*).

a) Relative viscosity (sample viscosity/melt viscosity) for Westerly granite *(Arzi 1978).* The range of melt fraction corresponding to RCMP as proposed by Arzi (1978) are reported in light grey.

b) Aggregate strength v. melt fraction for Westerly granite (*Ruter and Neumann, 1995*) and Delegate Aplite (*van der Molen and Paterson, 1979*). Roscoe's relationship is plotted (left curve on the diagram) with the shape parameters used in the formulation of *Arzi (1978)* and with those suggested by *Lejeune and Richet (1995)* (right curve on the diagram). In both cases, a melt viscosity of 10^4 Pa·s was used. The range of melt fractions corresponding to the RCMP as constrained by the data of *van der Molen and Paterson, (1979)* and *Lejeune and Richet (1995)* are shown in light grey and with dashed line, respectively. The Critical Melt Fraction CMP of *van der Molen and Paterson, (1979)*, i.e. the area where the decrease in strength with increasing melt fraction reaches a maximum, is shown in dark grey. Open square are

Rosenberg and Handy, *(2005)* in their review of the previous experimental data on the deformation of partially melted crustals rocks, infer that the relationship of aggregate strength to melt fraction is non-linear. At melt fractions, $\Phi < 0.07$, the dependence of aggregate strength on Φ is higher than at $\Phi > 0.07$ and they suggest that it is the increase of melt-interconnectivity that causes the dramatic drop in strength between the solidus and a melt fraction of 0.07. *Rosenberg and Handy*, *(2005)* term this drops the "*melt connectivity transition"* (MCT) (see Fig. 6.2).

A second, less-pronounced strength drop occurs at higher melt fractions and corresponds to the breakdown of the solid (crystal) framework. They named this drop as the *"solid-to-liquid transition"* (SLT), corresponding to the well known *"rheologically critical melt percentage"*. As conclusion, *Rosenberg and Handy (2005)* argue that change in the melt fraction across the SLT may be important for the dynamics of magma chambers, where flow is expected to be confined in part of the chamber where the volume fraction of crystals locally increase above, or decrease below 50%.

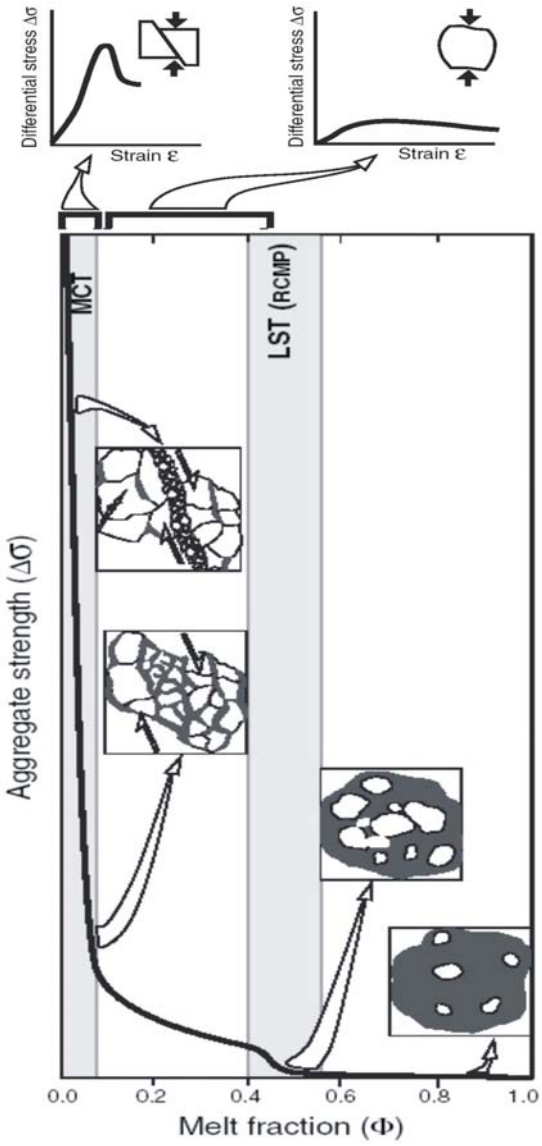

Fig.6.2. Schematic plot of aggregate strength vs. melt fraction. The two drops occur at higher melt fractions *"solid-to-liquid transition"* (LST) ($0.4< \Phi >0.6$) and corresponds to the breakdown of the solid (crystal) framework and at $\Phi = 0.07$ "*melt connectivity transition"* (MCT). (from *Rosenberg & Handy 2005*).

This final chapter focuses on measurements on crystal-bearing melts and the intention is to improve the knowledge on the viscosity behavior in magmas. Using creep apparatus together with falling sphere method viscosity was measured in a Φ range between 0.79 and 0.62 varying the water content in the melt.

6.2 Effect of crystal content.

It has long been recognized (*Einstein, 1911*) that the most important factors governing the viscosity of dilute suspensions are the viscosity of the liquid phase and the particle concentrations. It is clear that viscosity increases with increasing crystal content, but it is not clear how much and in which way. It depends mainly of the amount and shape of crystals but the size also probably plays an important role. Of course, the amount of volatiles dissolved in the melts (e.g. water) contributes to changes in melt viscosity as shown before. Magmas have a temperature below their liquidus, with a certain amount of crystals in suspension. Viscosity measurements above the liquidus are the starting point to understand natural phenomena. Usually the effective viscosity of magma has been estimate from the *Einstein-Roscoe* equation

$$\eta = \eta_m (1 - \phi/\omega)^{-2.5} \qquad (6.1)$$

where η is the effective viscosity of a liquid with a volume fraction ϕ of crystals and η_m is the viscosity of the melt; ω is a constant . In 1981, *Marsh* has concluded that ω can reach a value of 0.6, suggesting that a volume fraction of crystals equal to 0.6 correspond to the rigid state of crystal-melt system. Thus, the following equation is often used to estimate the effect of crystals on the relative viscosity in the simulation of natural magma:

$$\eta = \eta_0 (1 - \phi/0.6)^{-2.5} \qquad (6.1.1)$$

Simha (1940) derived a theoretical equation taking into account the non-spherical shape of crystals in suspension on the relative viscosity [$\eta_{R=}\eta_{system}/\ \eta_{melt}$]. For thin disks the relative viscosity was expressed by $\eta_r = 16f / 15\tan^{-1}f$ (f = axial ratio).

In 1968, the effect on viscosity of a wide range of crystal contents was studied by *Sherman*. He proposed that the relative viscosity increases with the mean diameter and the concentration of suspended solids according to the relation

$$\ln \eta_R = \ln(\eta / \eta_0) = \frac{\alpha D_m}{\left(\frac{\theta_{\max}}{\theta}\right)^{1/3} - 1} - 0.15 \qquad (6.2)$$

where η_0 is the viscosity of crystals-free liquid, D_m is the mean diameter, α is a constant that depends on D_m, $\theta_{\max}$ is the content of solids at maximum packing and θ is the content of suspended particles. In natural systems θ changes progressively during crystallization, thus the composition of residual liquid (hence η_0) changes, too. By keeping in mind this last concept it is possible to use equation 6.1 and 6.2, only considering constant melt composition

More recently *Sato (2005)* studied the interaction of crystals in melts. In this paper the viscosity of high-Al basalt from Fuji volcano was studied in the temperature range 1230-1130 °C. Results show an increase in viscosity from ca. 52 Pa·s at 1230°C (above the liquidus) to ca. 1950 Pa·s at 1130°C with a crystal content of 23 vol%. The relative viscosity is larger by a factor of 4-5 compared with the predictions of the *Einstein Roscoe* equation using the parameter of *Marsh (1981)*. In this crystallization experiment the observed increase in viscosity is affected not only by the increase in volume fraction of crystals but also by the change in melt composition as result of the crystallization processes.

In the next section, the experimental procedure used for carry out viscosity measurements on partially crystallized samples will be introduced.

6.3 Viscosity of partially crystallized andesite

The conditions for experiments on partially crystallized andesites were based on phase equilibria for Unzen relevant systems (*Nakada and Motomura, 1999; Holtz et al., 2005; Sato et al., 2005*):

(I) the fraction of crystals should be at most 30 vol% so that the rheological properties are dominated by the melt viscosity.

(II) the water content in the melt should be low (less than 4 wt%) to prevent significant loss of water during creep experiments at ambient pressure.

Crystallization experiments were performed at 500 MPa in the T-range 1100-1120°C in an IHPV. Phases formed at these conditions in Unzen andesite are mainly Fe-rich iron-titanium oxides, plagioclase, ortho-clinopyroxene. The synthesis conditions for samples MDIB 6, PC7 and PC15_1 are reported in table 6.1. Electron microprobe analyses of residual melt and crystals in sample MDIB 6 are reported in table 6.2 and are similar in composition (dacitic) to the PC_7 and PC15_1 samples. The anorthite content in the plagioclase averages about An_{57}. Crystallization usually is not homogeneous within the whole sample (see Fig.6.3). It appears that former surfaces of the glass powder used in the synthesis are preferred sites for crystallization, probably due to the presence of secondary phases.

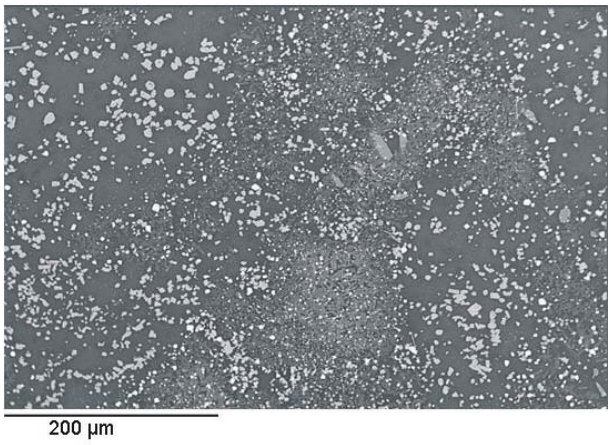

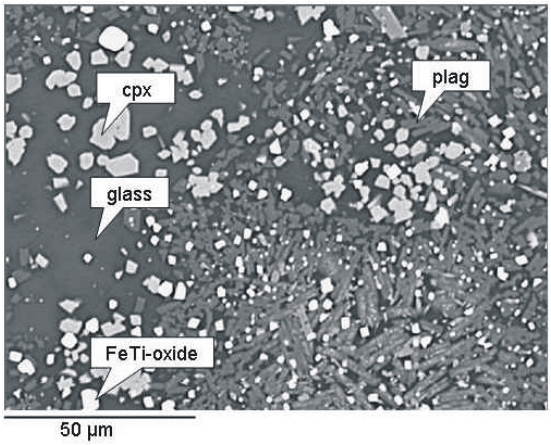

Fig 6.3a Fig 6.3b

Fig.6.3 . Backscattered electron image of partially crystallized andesite MDIB6 containing 2 wt% H_2O on two different scales (synthesis at 1100°C /500 MPa). a) overview b) details

However, because the falling distance for spheres is much larger than the scale of the heterogeneities and in creep experiments the average property of the whole cylinder is measured, it is assumed that inhomogeneity in crystal distribution has minor importance.

Tab 6.1. Syntheses conditions for partially crystallized andesites.

No.	T (°C)	P (MPa)	t (h)	wt% H_2O added	phases observed	Estimated volume fraction of crystals %*
MDIB6	1100	500	72	1.98	plag, cpx, opx, FeTi-oxide, glass	≈ 30
PC7	1120	500	45	3.81	Plag FeTi-oxide, glass	≈ 21
PC15_1	1120	500	59	0.82	plag, cpx, FeTi-oxide, glass	≈ 38

*The volume fraction was estimated using the analySIS software able to separate the different phases present in the system and to calculate the respective areas.

To calculate the amount of crystals present in the system, the software analySIS was applied. Using a backscattered electron image (e.g. Fig. 6.3), this software is able to distinguish between different phases present which can be separated and for each one it is possible to calculate the respective areas.

Tab. 6.2 Electron microprobe data (wt%) for the partially crystallized sample MDIB 6 in comparison to the starting material MDIB2.

	Starting material MDIB2	Residual glass after partial crystallization	n = 3 Cpx	n = 4 Opx	n = 4 Plag	n = 2 Ox
SiO_2	55.11	66.10 (0.56)	49.45 (0.58)	52.98 (0.36)	55.45 (2.40)	0.41 (0.11)
TiO_2	1.09	0.73 (0.07)	0.69 (0.08)	0.26 (0.02)	0.18 (0.04)	5.35 (1.47)
Al_2O_3	18.33	14.50 (0.47)	4.79 (0.43)	3.21 (0.14)	25.92 (2.01)	4.43 (0.20)
FeO	9.16	3.89 (0.37)	10.14 (0.06)	15.22 (1.48)	2.25 (1.02)	80.73 (0.87)
MnO	0.08	0.02 (0.04)	0.00 (0.00)	0.00 (0.01)	0.00 (0.01)	0.00 (0.00)
MgO	2.88	1.16 (0.18)	14.73 (0.35)	27.16 (1.07)	0.62 (0.57)	3.33 (0.54)
CaO	8.44	3.48 (0.24)	19.67 (0.42)	1.53 (0.14)	11.12 (0.71)	0.24 (0.02)
Na_2O	3.38	3.41 (0.15)	0.49 (0.02)	0.05 (0.04)	4.27 (0.29)	0.02 (0.00)
K_2O	1.42	2.29 (0.17)	0.05 (0.01)	0.02 (0.01)	0.41 (0.11)	0.04 (0.01)
Total	99.89	95.58	100.02	100.44	100.22	94.55

Note: 1 σ standard deviation is reported in parenthesis. Cpx, Opx, Plag and Ox refer respectively to Clinopyroxene, orthopyroxene, Plagioclase and iron-titanium oxide. n is the number of crystals analyzed

6.3.1 Results of creep experiments in comparison with previous models.

Results of a creep experiment with a sample synthesized at 1100°C/500 MPa (MDIB6) are shown in Figure 6.4. A continuous increase in viscosity with time is evident even at constant conditions (e.g. 550 °C and 2200 g). Crystallization of iron oxides during annealing near the glass transition can be a serious problem, as observed for pure andesitic melts (see *Liebske et al. 2003*). Hence, only the initial period of the creep experiment can be interpreted in terms of a viscosity representative for a supercooled andesite. Another interesting point is the apparent decrease in viscosity with increasing load (compare the last data of the first set of measurements at constant temperature with the first measurement after changing the load in Fig. 6.4). This might indicate a non-Newtonian behavior of the magma. In other words, increasing the stress on the magma makes the magma more fluid. However, this hypothesis needs to be verified by additional experiments.

After the experiment, the force on the sample was removed by accident before the temperature fell below the Tg of the glass. As a consequence, the sample foamed, making the determination of the volatile content of the glass phase impossible. However, strong foaming indicates that the major part of water was still dissolved at the end of the experiment. BSE images of the run product indicate that the crystalline phases are basically unchanged. In particular, no growth of rims around the crystals were observed. This observation is consistent with a low crystal growth rate at these temperatures consistent with small diffusion rates in the melt.

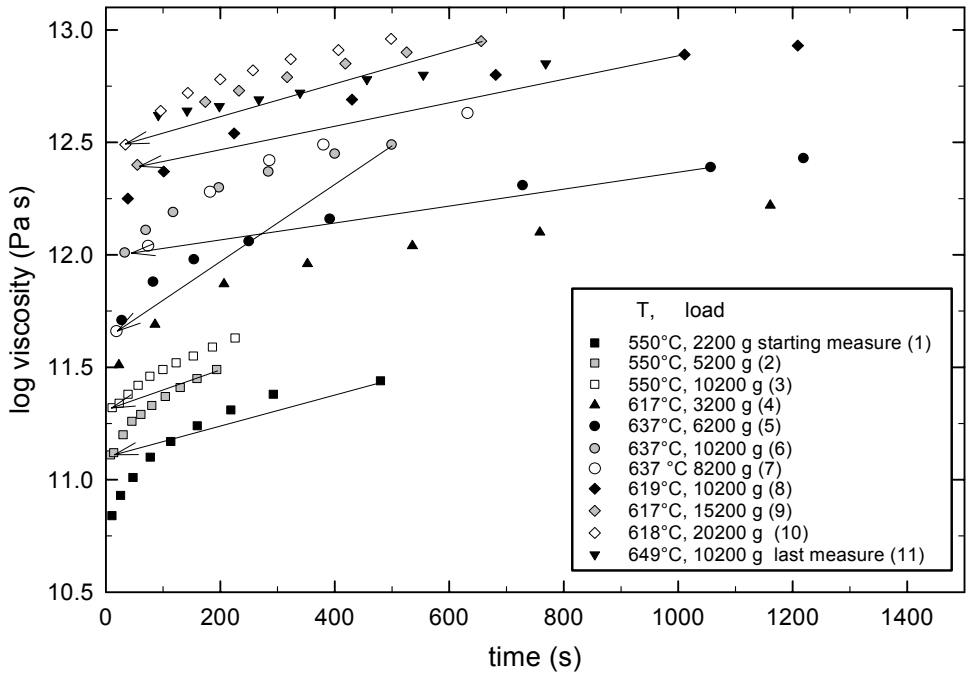

Fig. 6.4 - Creep experiment with sample MDIB6 at ambient pressure. Numbers in parenthesis refer to the suite of isothermal experiments. The load is proportional to the force on the sample.

The trends shown for sample MDIB 6 are the same of the other experiments done with the creep apparatus. The sample PC7 after experiments presented only a light brown coat on the surface. As indicate by KFT analyses after the creep experiment, about 1 wt% of water was loss (H_2O after creep experiment was 2.51 wt%). This also explains the increase in viscosity while BSE image did not show a change in the crystal phases. No changes were observed in the PC15_1 sample after experiment. Water content was identical compared with the initial and no change in crystals or residual melt was observed by microprobe analysis. For viscosity data of MDIB 6, PC7 and PC15_1 see the appendix.

In figures 6.5 and 6.6 viscosity vs. time is plotted respectively for the sample PC7, PC15_1 (for synthesis condition see Table 6.1). Viscosity always increases with experimental time.

For the sample PC7 (Fig 6.6), which already had a high initial water content of 3.81 wt% before crystallization, a final water content of the melt of about 5 wt % is expected (taking into account a crystals content by about 20 vol%).

Considering that andesite melt containing 4.8 wt% at 779 K and a Fe^{2+}/Fe_{tot} of 0.7, has a viscosity of $10^{7.5}$ Pa·s (prediction calculated using equation 5.2) and a rhyolitic melts at the same condition has a viscosity of $10^{8.8}$ Pa·s (calculated with the model of *Hess and Dingwell, 1996*) it is possible to estimate that the viscosity of the dacite melt produced after crystallization has a viscosity of $10^{8.1}$ Pa·s.

As expected the viscosity of the magma is higher than that of the melt, as can be see in Fig. 6.5. For comparison I have calculated the predicted effect of dispersed crystals on melt viscosity by:

$$\eta/\eta_m = (1- \phi/0.6)^{-2.5} \qquad (6.3)$$

and by the empirical equation of *Sato, (2005):*

$$\eta/\eta_m = 0.32 \cdot exp(13.06 \cdot \phi) \qquad (6.\ 4)$$

where η is the magma viscosity, η_m is the viscosity of the melt and ϕ is crystallinity. However, it has been noted that the equation of *Sato (2005)* was derived for a basaltic magma near the liquidus and may be not directly transferable to an andesitic magma near the glass transition of the interstitial melt.

Calculations are listed in Table 6.3 and can be directly compared with the first viscosity result show in figures 6.4, 6.5 and 6.6

All creep experiments had shown the same viscosity trend: using Einstein-Roscoe equation with Marsh's parameter the calculate viscosity is lower respect the prediction of Sato 2005. Both *Einstein-Roscoe* and *Sato (2005)* models reveal a viscosity lower than that measured in creep experiments (values reported in table 6.3).

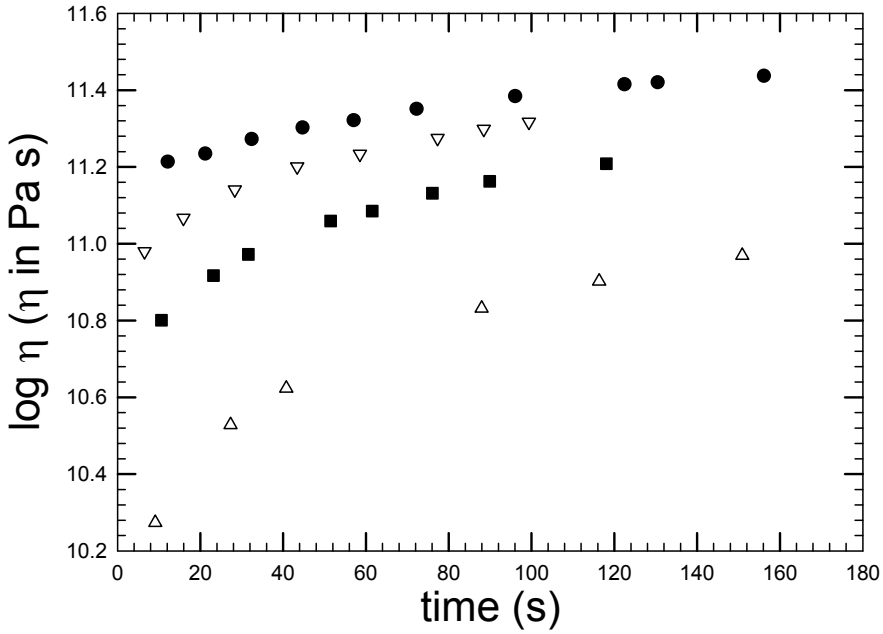

Fig 6.5. Creep experiment with sample PC7 at ambient pressure. The load is proportional to the force on the sample and the temperature is constant (779K). Load was stepwise increased during experiment.

Tab. 6.3. Viscosity of partially crystallized Andesite. Calculations are performed considering the increasing of water and silica content in the residual melts.

Sample	Cryst.cont (vol%) [a)]	Temp (K)	H_2O(wt%) after Creep experiment	log vis (Pa·s) andesite melt	Estimated melt log vis (Pa·s) [b)]	log vis (Pa·s) by *Einstein-Roscoe* [c)]	log vis (Pa·s) by *Sato, (2005)*	log vis (Pa·s) exp.
MDIB 6	0.30	823	3.00	8.34	8.77	9.52	9.97	10.80
PC7	0.21	779	4.81	7.40	8.11	8.57	8.80	10.20
PC20_1	0.38	1028	1.20	6.86	7.28	8.37	8.94	9.50

Note: [a)] to calculate the amount of crystals present in the system, the software analySIS was employed (see text);
[b)]The estimated melt viscosity was obtained from extrapolation of the melt viscosity calculated with the model shown in equation 5.2 for natural andesite considering an $Fe^{2+}/Fe_{tot} = 0.7$ and the *Hess and Dingwell (1996)* model for rhyolite melt.
[c)]Einstein Roscoe equation is used with Marsh's parameter;

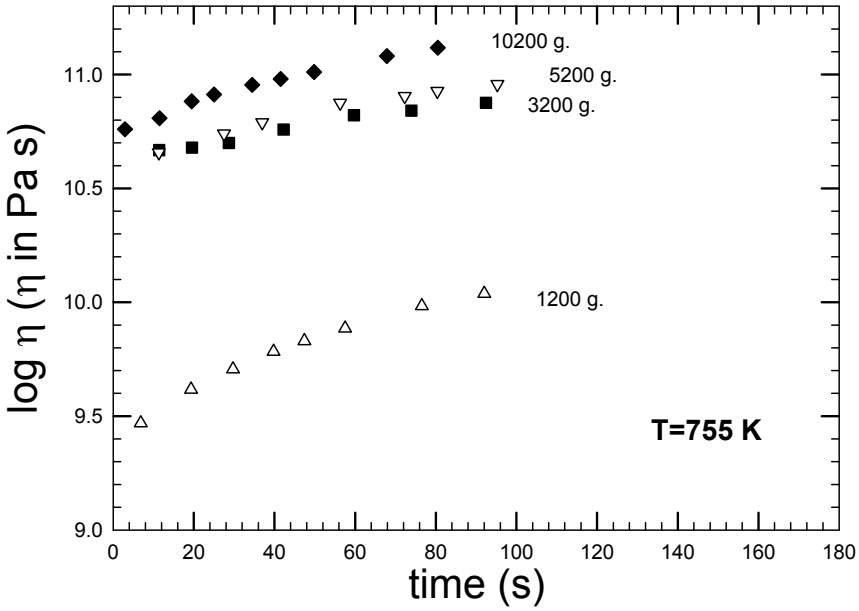

Fig 6.6. Creep experiment with sample PC15_1 at ambient pressure. The load is proportional to the force on the sample and the temperature is constant (755K).

6.3.2 Falling sphere experiments with partially crystallized andesite.

Falling sphere experiments were performed to study the viscosity of partially crystallized andesite in the low range. A pre-requisite to prove the effective viscosity representative for the partially crystallized melt is that the diameter of the sphere is much larger than both the crystals and the distance between the crystals. First attempt was made on samples MDIB 13 and MDIB 14. Both sample were synthesized at 1393 K and 500 MPa (Table 6.4). The water content added before the synthesis was 2 wt% for MDIB 13 and 1wt% for MDIB 14. After synthesis sample were analyzed with microprobe to check glass and crystals composition. MDIB 14 showed unexpected high degree of crystallization covering about

60 vol% of the sample probably due to loss in water; microprobe results for MDIB 13 are shown in Table 6.5.

Tab. 6.4. Crystallization experiments performed in IHPV at 500 MPa.

No.	T (K)	t (h)	wt% H_2O added	phases observed	Estimated volume fraction of crystals
MDIB13	1393	72	2.00	plag, FeTi-oxide, glass	≈10 %
MDIB14	1393	72	1.00	plag, cpx, opx, FeTi-oxide, glass	≈60 %

The estimated volume of crystals in MDIB 13 was in the order of 10% and the sample was used for falling sphere experiments. A Pt-sphere diameter of about 1 mm was used to probe the effective viscosity of the medium. After the pre-experiments, to define the sphere position, an experiment was performed at the same synthesis conditions (Table 6.4).

Tab. 6.5. Electron microprobe data for MDIB 13

	MDIB 13 after synthesis	MDIB 13 after falling sphere experiment
SiO_2	58.52(0.32)	63.12 (0.45)
TiO_2	0.98 (0.04)	0.82 (0.08)
Al_2O_3	15.02 (0.22)	14.66 (0.31)
FeO	7.27 (0.33)	5.58 (0.25)
MnO	0.10 (0.09)	0.06 (0.07)
MgO	2.79 (0.13)	1.99 (0.15)
CaO	6.54 (0.26)	5.01 (0.22)
Na_2O	3.30 (0.09)	3.36 (0.09)
K_2O	1.67 (0.13)	1.98 (0.11)
Tot	96.18	95.90

Note the increase in SiO2 content after falling sphere experiment. (1 σ standard deviation is reported in parenthesis).

Unfortunately, the spheres do not moved after the estimated time. A second experiment with a larger run time gave the same result. A microprobe check for this sample showed

that the amount of crystals increase amount of crystals and the SiO_2 content of the melts had incresed (Tab.6.5).

From this data it turned out that crystals content and composition of partially crystallized andesites may strongly change during the viscosity measurements because it is practically impossible to establish exactly the same condition as in the crystallization experiments. Small variations in temperature and water content (initiated for instance by loading the sample into a new capsule with an input of air) may produce a large change in volume fraction of crystals and melt composition (i.e., the water content of the melt). Thus, conditions during the experiments can not be reliably controlled. A modification of the experimental strategy is required.

6.4 New strategy for falling sphere experiments with crystal-bearing melts.

An alternative, which can be used to study the viscosity behavior in systems containing crystals at high temperature, is to add insoluble minerals to the melt to establish a defined melt/crystal ratio. The first idea was to add plagioclase in a pre-hydrated glass powder and run short experiments to avoid the dissolution of plagioclase at high temperature. Unfortunately these experiments failed because plagioclase started rapidly to dissolve when the experimental temperature was reached.

Watson and Harrison, (1983) have experimentally defined the saturation behavior of zircon in crustal anatectic melts (granitic to andesitic melt) as a function of both temperature and composition. The results provide a model of zircon solubility given by:

$$\ln D_{Zr}\,zircon/melt = -3.80 - \left[0.85 \cdot (M-1)\right] + \frac{12900}{T} \qquad (6.5)$$

where D_{Zr} *zircon/melt* is the concentration ratio of Zr in the stoichiometric zircon to that in the melt, T is the absolute temperature, and M is the cation ratio (Na + K + 2Ca)/(Al · Si). This solubility model is based principally upon experiments at 1133, 1203, and 1293 K, but has also been confirmed at temperatures up to 1773 K for M = 1.3. The lowest temperature experiments (1023 and 1073 K) yielded relatively imprecise, low solubilities, but the measured values are nevertheless in agreement with the predictions of the model.

For M = 1.3 (a normal peraluminous granite), these results predict zircon solubilities ranging from ~100 ppm dissolved Zr at 1023 K to 1330 ppm at 1293 K.

Because the relatively low solubility of zircon in crustal anatectit melt derived from *Watson and Harrison, (1983)* model (equation 6.5), zircon crystals have been selected to prepare crystals bearing melts as magma analogues.

Zircon crystals were purchased from the company *Dr. F. Krantz, Rheinisches Mineralien-Kontor GmbH & Co. Bonn, Germany*. The selected crystals (size of 1 mm to 1 cm in diameter) were crushed and sieved using mesh of 100 µm in diameter. The obtained zircon powder was directly poured in a glass beaker filled with deionized water. This allows us to separate most of the fine powder from the hand picked crystals. Part of the water was poured away and the rest was removed with a syringe. The final product was then dried at one atmosphere oven at 383 K for 24 h. However a small amount of fine powder (about 10 µm in diameter) was still present in the final product (see Fig. 6.9 and 6.10). The dried crushed zircons were manually mixed with a pre-synthesized hydrous andesitic powder (grain size fractions between 100 and 250 µm).

A first test on how zircon behaves at high temperatures, was performed for 210 minutes at 1473 K, 300 MPa using a glass with 3.52 wt% H_2O. Two zircon crystals were analyzed using microprobe to check the initial composition (Table 6.5). A decrease of about 12 wt % of ZrO_2 and a slight increase in SiO_2 was observed from the core to the rim (probably contaminated by glass, see Table 6.5) and may be explained by a starting interaction between crystals and melt. However, the shape of the crystals show no dissolution features, i.e. edges are still very sharp and not smoothed (fig 6.9 and 6.10) and probably the fine grained ZrO_2 was mainly dissolved to saturate the melt with respect to ZrO_2.

In the same microprobe session, the quenched hydrous andesitic glass with about 9 vol% of added zircon crystals was analyzed and 1.67 wt% of ZrO_2 was detected (see table 6.7).

Tab.6.5. Microprobe analysis of two zircons crystals (wt%)

	core1	rim1	core2	rim2
SiO_2	32.11	35.14	31.56	34.41
TiO_2	0.01	0.18	0.01	0.17
Al_2O_3	0.00	4.04	0.00	3.82
FeO	0.00	2.23	0.00	1.99
MnO	0.09	0.04	0.08	0.05
MgO	0.00	0.82	0.00	0.90
CaO	0.01	1.89	0.01	1.75
Na_2O	0.00	0.00	0.00	0.00
K_2O	0.02	0.33	0.02	0.39
ZrO_2	63.43	50.92	64.17	52.92
H_2Otot	3.52	3.52	3.52	3.52
Tot.	99.18	99.11	99.37	99.92

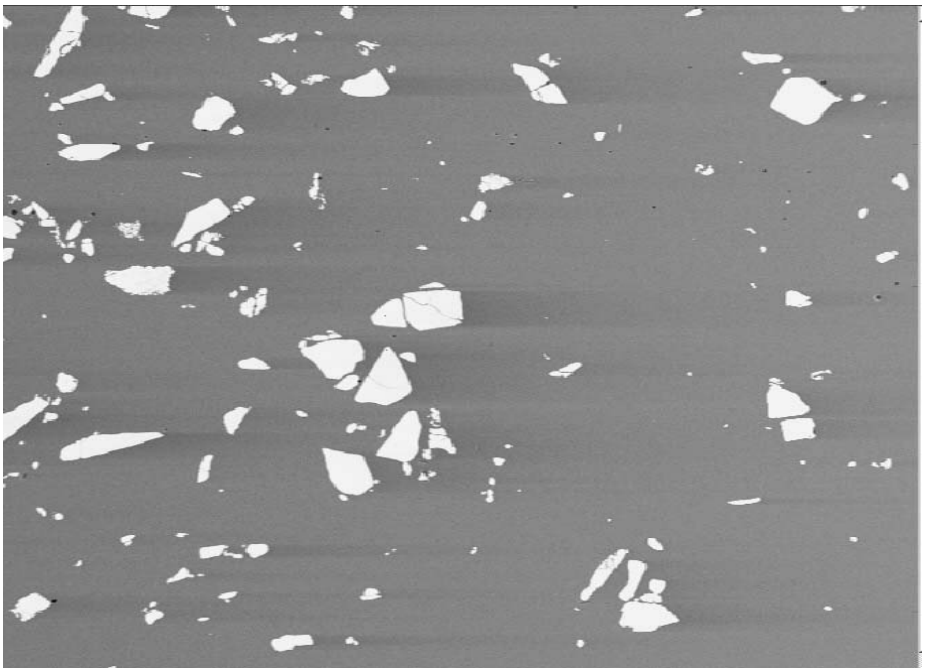

Fig. 6.9. Backscattered electron image of Zr1 sample after 30 min. synthesis performed at 1523 K, 300 MPa.

A pre-run 180 min. at 1473 K and 300 MPa was used for Zr2, Zr4 and Zr7 samples. It seems that solubility of Zr in andesitic melt is up to two-three times higher than that predicted by the model of *Watson and Harrison, (1983)* for crustal anatectit melt (granitic to andesitic melts) (e.g. the model at 1473 K predict about 4800 ppm Zr (= 0.62 wt% ZrO_2) while the studied andesitic melts contained 10000 ppm Zr; see ZrO_2 content in sample Zr1, Table 6.4). However, it is important to note that the difference between the model of *Watson and Harrison (1983)* and the new data shown in Table 6.4, is probably due to the higher temperature (see Tab. 6.6) used in these experiments.

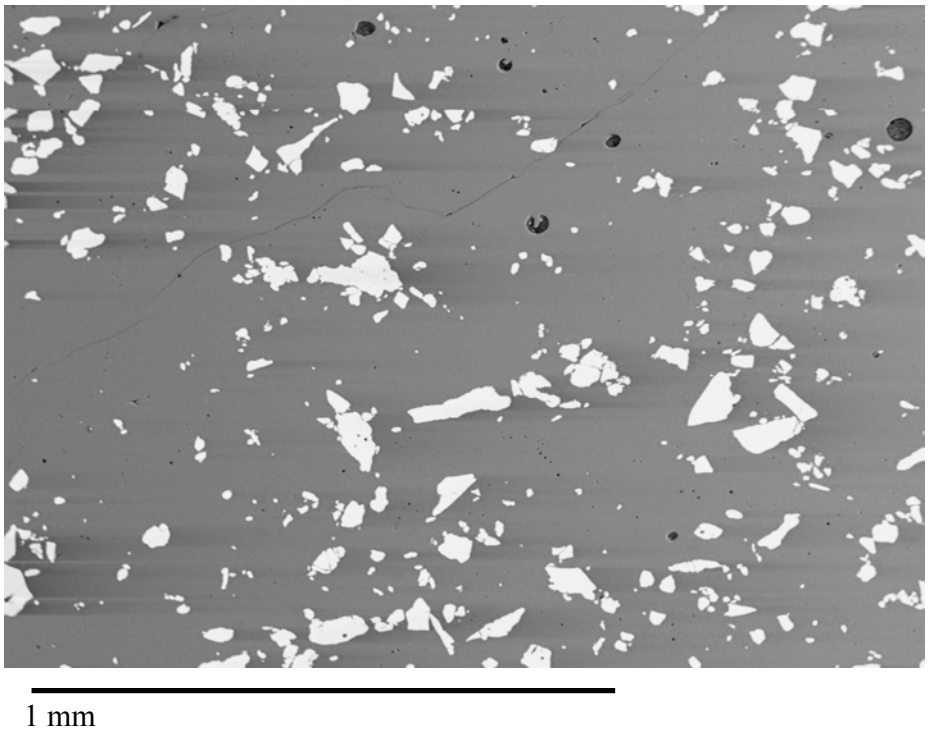

Fig. 6.10. Backscattered electron image of Zr2 sample after falling sphere experiment at 1373 K, 300 MPa for 10 min.

Falling sphere experiments were performed by varying the amount of dissolved water and keeping the crystals content (added before experiments) constant at 20 vol% (Table 6.6). Platinum spheres were utilized in these experiments with a diameter varying between 840 and 930 μm. Two experiments with sample Zr7 (a and b Table 6.6) were performed with durations of 1849 and 3649 s, respectively. The viscosities derived from these experiments are in good agreement (0.12 log units in difference) and demonstrates that constant velocity is achieved for a Pt sphere with a radius of 465 μm.

Table 6.6. Falling sphere experiments with partially crystallized andesite. 20 vol% of zircon crystals were added to the glass in all samples. All experiments were performed in an IHPV at 300 MPa

No.	H_2O_t (wt%)	T (K)	Sphere radius (μm)	C_F	Dwell time (s)	Corrected time (s)	Falling distance (cm)	Log η (Pa·s)
Zr 7a	0.52	1523	465 ± 5	0.83	1800	1849	0.721	3.28
Zr 7b	0.52	1523	465 ± 5	0.83	3600	3649	1.072	3.40
Zr 4	2.98	1423	420 ± 5	0.85	600	643	0.388	3.01
Zr 2	4.02	1373	420 ± 5	0.85	600	640	0.248	3.20

Table 6.7. Microprobe analysis of glasses in Zr1, Zr2, Zr4 and Zr7 samples after experiments compared with starting material MDIB 2. Values are reported as wt% and 1 σ standard deviation is ginen in parenthesis.

	MDIB 2	Zr 1	Zr 2	Zr 4	Zr 7
SiO_2	54.18 (0.60)	50.35 (0.40)	51.12 (0.54)	53.26 (0.47)	53.13 (0.41)
TiO_2	1.09 (0.07)	1.11 (0.05)	1.01 (0.05)	1.07 (0.06)	1.08 (0.07)
Al_2O_3	18.41 (0.19)	18.38 (0.31)	17.70 (0.20)	18.01 (0.30)	18.21 (0.27)
FeO	9.52 (0.33)	8.89 (0.37)	8.33 (0.38)	8.42 (0.44)	8.36 (0.58)
MnO	0.09 (0.06)	0.03 (0.07)	0.02 (0.07)	0.01 (0.07)	0.01 (0.07)
MgO	2.93 (0.09)	3.56 (0.12)	3.27 (0.13)	3.29 (0.12)	3.37 (0.11)
CaO	8.69 (0.32)	7.94 (0.14)	7.68 (0.24)	7.71 (0.22)	7.91 (0.21)
Na_2O	3.41 (0.29)	3.35 (0.19)	3.09 (0.19)	3.13 (0.18)	3.20 (0.19)
K_2O	1.42 (0.08)	1.48 (0.07)	1.46 (0.08)	1.48 (0.08)	1.57 (0.09)
ZrO_2	-	1.67 (0.08)	0.91 (0.18)	1.46 (0.17)	1.46 (0.20)
H_2Otot	-	3.52	4.02	2.98	0.52
Tot.	99.74	100.28	98.61	100.82	98.82
Zircon content added (vol%)	-	9	20	20	20

Comparison with data predicted from the *Einstein-Roscoe* equation with *Marsh* parameter and from the equation proposed by *Sato (2005)* is shown in Table 6.8 and Fig. 6.10. Moreover, a comparison with viscosity of melts calculated with the equation 5.2, is given. Conditions for the calculated melt viscosity values were the same reported in Table 6.6. For the Fe^{2+}/Fe_{tot} ratio, a value of 0.7 was used in agreement with the previous viscosity data (see chapter 5) showing a value between 0.65 and 0.75 for most of the viscosity data

obtained using IHPV apparatus. This value is also relevant for geological conditions in magma chambers. However changing the Fe^{2+}/Fe_{tot} ratio to more oxidized values (e.g. $Fe^{2+}/Fe_{tot} = 0.4$) will change the melt viscosity by about 0.3 log units at these condition (see model of Fe-bearing andesite, Equ. 5.2).

Table 6.8. Falling sphere experiments with zircon-bearing melt in comparison with literature models.

No.	Log η andesite melt (Pa·s) [a)]	Log η *Einstein-Roscoe* (Pa·s)	Log η *Sato, (2005)* (Pa·s)	Log η experiments (Pa·s)
Zr 7a	2.28	2.72	2.92	3.28
Zr 7b	2.28	2.72	2.92	3.40
Zr 4	1.65	2.09	2.29	3.01
Zr 2	1.61	2.05	2.25	3.20

Note: [a)]values calculated using equation (5.2) with an $Fe^{2+}/Fe_{tot} = 0.7$.
For experimental condition see Table 6.5

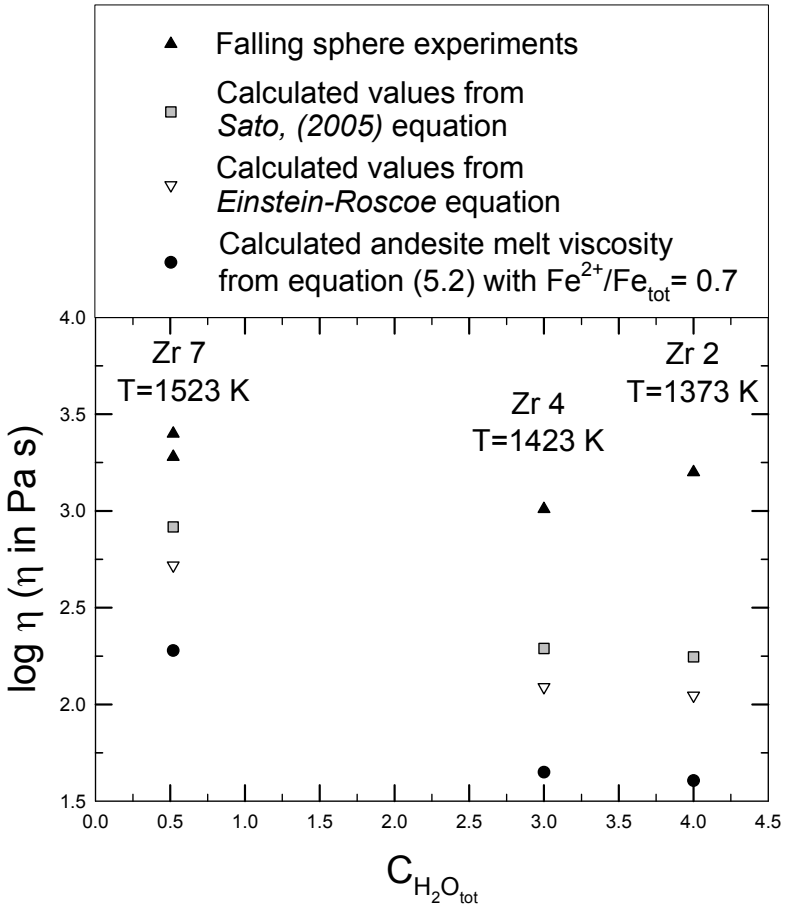

Fig. 6.10. Falling sphere data compared with *Einstein-Roscoe and Sato (2005)* equations. Zr 2,4 and 7 have 20 vol% of crystals added before experiments

6.5. Results and discussion

Falling sphere data show values higher than those calculated from the models of *Einstein(1911) and Roscoe (1952)* and *Sato (2005)* as well as from the viscosity data measured at room pressure with the creep apparatus. However, the samples used for creep experiments are very different than those used in the falling sphere experiments (e.g. melt composition, crystals composition, content and shape) and it is not possible to compare directly the results.

Creep data may have a large uncertainty due to the possible changes in the system during the run, e.g. loss of water at the sample surface and formation of iron oxides.

An interesting point is the apparent decrease in viscosity with increasing load (MDIB 6 in Fig. 6.4: compare the last datum of the first set of measurements at constant temperature with the first measurement after changing the load). This might indicate a non-Newtonian behavior of the magma. In other words, increasing the stress on the magma makes the magma more fluid but this hypothesis needs more experiments to be confirmed.

In the falling sphere experiments measured viscosity shows a deviation from literature models at low water content of about 0.5 log units. At higher water content a difference of about 1 log units is observed. It seems that the departure from the two models is higher at higher water content. Change in composition using zircon crystals is not high (only 1.6 wt% ZrO_2 was incorporate in the andesitic glass after experiments) and should not have big influence on viscosity. However, more experiments are needed for proof this hypothesis. Falling sphere is probably the best method to investigate partially crystallized systems. It is possible to use this method only in a relatively high temperature range that may not reproduce all natural temperature systems. However, combined with creep measurement,

falling sphere experiments performed on melts doped with zircon crystals, can give a good possibility to investigate how magma behaves at different crystals content.

7. Conclusions and outlook.

Viscosity of andesitic melts and magmas was investigated over a wide range of temperature (743-1573 K) and pressure (200-2000 MPa). A creep apparatus at 1 atm and parallel plate viscometer were used in the pressure range 0.1 - 400 MPa in the high viscosity range (10^8-10^{12} Pa·s) and temperature between 743 and 834 K. For the low viscosity determination, falling sphere experiments were performed at a pressure range of 200 to 2000 MPa and temperature range of 1323 to 1573 K.

The initial goal of this work was to determinate the viscosity of an analogue andesite. Results show a strong dependence of viscosity melts from temperature and water content (the main parameters governing viscosity of silicate melts). Thus, using the combined data set for Fe-free andesitic melts from literature *(Richet et al., 1996* and *Liebske et al., 2003)* and the new data an equation (4.7) to predict viscosity was obtained. However with the simplified Fe-free model it was not possible to estimate the effect of redox of iron on viscosity (e.g. Liebske et al., 2003). Thus, a natural andesite, with composition similar to the 1991-1995 eruption at Unzen volcano, Japan, was used as starting material for the viscosity determination.

In this second step, the Fe^{2+}/Fe_{tot} ratio was measured for all samples using a modified Wilson method. The new iron-bearing andesite viscosity data were combined with the available literature data on iron-bearing andesite (with defined Fe^{2+}/Fe_{tot} content). Thus, a new equation was obtained fitting the data with a non linear least-square

regression able to predict viscosity of Fe-bearing andesitic melt as a function of temperature (K), water (wt %) and Fe^{2+}/Fe_{tot} content. The model was then used to test the efficiency of magma mixing processes occurring prior the 1991-1995 eruption at Unzen volcano.

In the third step the viscosity of partially crystallized andesite was investigated utilizing creep and falling sphere methods. Creep results indicate continous increase in viscosity during the experiments performed in a temperature range between 779 and 1028 K. This may be explained with the crystallization processes that can occur as also demonstrated from literature data *(Liebske et al., 2003*) and loss of water especially from the surface of the samples. It is possible to extrapolate from these experiments at least one viscosity value from the beginning of the measurements.

To measure low viscosities of partially crystallised andesite sample, falling sphere experiments were performed using Pt sphere with diameter exceeding of about 1 order of magnitude the diameter of the crystals. This procedure is required to measure the effective viscosity. Unfortunately with crystallized sample falling sphere experiments were unsuccessful probably due to recrystallization processes even if the experiments were carried out at the identical condition of the previous synthesized magma. Thus, a new strategy was developed for measuring partially crystallized andesite. Zircon crystals were added in the previously synthesized glass powder. After remelting at 1473 K for more than 3 hours, ZrO_2 present in the melts was measured using microprobe analysis. The result (about 1.6 wt% of ZrO in the MDIB 2 andesite melts) allows one for estimation of the viscosity of partially crystallized silicate.

Both creep and the falling sphere data show a viscosity higher than that calculated with the *Einstein-Roscoe* and *Sato, (2005)* equations. It seems that the deviation is

larger with increasing water content in the "residual" melts. However, it is not possible to make a direct comparison between the two data sets because creep experiments were performed on sample containing a residual melt almost dacitic in composition and different crystals content, shape and type. On the other hand, falling sphere experiments were performed using sample with a constant andesitic melts composition (except the ZrO_2 dissolved to saturate the melt) and with a previously defined size of zircon crystals.

To continue to study the interaction between melt and crystals using both creep and falling sphere experiments is a future goal. Experiments should be performed varying crystallinity, water content, temperature and Fe^{2+}/Fe_{tot} ratio in the melt. The new "zircon" strategy gives the opportunity to choose and keep the desired melt composition. Thus, is possible to investigate different magmatic systems and develop a new model able to predict the viscosity of magma relevant for volcanic scenarios.

References

Adam, G., and Gibbs, J.H., 1965. On the temperature dependence of cooperative relaxation properties in glass forming liquids. Journal of Chemical Physics, 43: 139-146.

Angell, C.A., 1985. Strong and fragile liquids. In: Ngai KL, Wright GB (eds) Relaxation in complex systems. Nat Technical Information Service Springfield, Va. USA, 3-15.

Aoki, K., Ishiwaka, K., Kanisawa, S., 1981. Fluorine in rock from continental and oceanic regions and petrogenetic application, Contributions to Mineralogy and Petrology, 76, Issue 1: 53-59.

Arzi, A., 1978. Critical phenomena in the rheology of partially melted rocks. Tectonophysics, 44: 173–184.

Avramov, I., and Milchev, A., 1988. effect of disorder on diffusion and viscosity in condensed systems. Journal of non-Crystalline Solids, 104: 253-260.

Avramov, I., 1994. Viscosity of undercooled melts. Journal of Material Science Letters, 13: 1367-1369.

Avramov, I., 1998a. Viscosity of glass forming melts. Preceeding 6th International Otto Shott Colloquium. Jena (Germany): 198-203.

Avramov, I., 1998b. Viscosity of glass forming melts. Journal of non-Crystalline Solids, 238: 6-10.

Bagdassarov, N., and Dorfman, A.M., 1998. Viscoelastic behaviourof partially molten granites. Tectonophysics, 290: 27–45.

Baker, L.L., and M.J. Rutherford, (1996). "Sulfur diffusion in rhyolite melts." Contributions to Mineralogy and Petrology 123: 335-344.

Behrens, H. and Jantos, N., 2001. The effect of anhydrous composition on water solubility in granitic melts. American Mineralogist 86, 14-20.

Behrens, H., and Schulze, F., 2003. Pressure dependence of melt viscosity in the system $NaAlSi_3O_8$-$CaMgSi_2O_6$. American Mineralogist, 88(8-9): 1351-1363.

Behrens, H. and Stuke, A., 2003. Quantification of H_2O contents in silicate glasses using IR spectroscopy - a calibration based on hydrous glasses analyzed by Karl-Fischer titration. Glass Science and Technology, 76(4): 176-189.

Berndt, J., Liebske, C., Holtz, F., Freise,M., Nowak, M., Ziegenbein, D., Hurkuck, W., Koepke, J., 2002. A combined rapid-quench and H_2-membrane setup for internally heated pressure vessels: Description and application for water solubility in basaltic melts, American Mineralogist, 87, 1717-1726.

Berndt, J., Koepke, J., Holtz, F., 2005. An experimental investigation of the influence of water and oxygen fugacity on the differentiation of MORB at 200 MPa. Journal of Petrology 46: 135-167.

Botcharnikov, R.E., Koepke, J., Holtz, F., McCammon, C., and Wilke, M. (2005) The effect of water activity on the oxidation and structural state of Fe in a ferrobasaltic melt. Geochimica et Cosmochimica Acta (in press).

Bottinga, Y. and Weill, D.F., 1972. Viscosity of Magmatic Silicate Liquids - Model for Calculation. American Journal of Science, 272(5): 438-475.

Bottinga, Y., and Richet, P., 1995. Silicate melts: the “anomalous” pressare dependance of the viscosity. Geochimica et Cosmochimica Acta, 59: 2725-2731.

Bouhifd, M.A., Richet, P., Besson, P., Roskosz, M., and Ingrin, J., 2004. Redox state, microstructure and viscosity of a partially crystallized basalt melt. Earth and Planetary Science Letters, 218 (1-2): 31-44.

Bourgue, E., and Richet, P., 2001. The effect of dissolved CO_2 on the density and viscosity of silicate melts: a preliminary study. Earth and Planetary Science Letter, 193: 57-68.

Bourgue, E., 2003. Effets des volatils CO2 et H2O sur les Proprété rhéologiques de magmas. Ph.D. Thesis.

Brearley, M., Dickinson, J.E.Jr., and Scarfe C.M., 1986. Pressure dependence of melt viscosity on the joint diopside-albite. Geochim. Cosmoch. Acta 50: 2563-2570.

Brearley, M., and Montana, A., 1989. The effect of CO_2 on the viscosity of silicate liquids at high pressure. Geochimica et Cosmochimica Acta, 50: 2563-2570.

Bryce, J.G., Spera, F.J., and Stein, D.J., 1999. Pressure dependence of self-diffusion in the $NaAlO_2$-SiO_2 system: Compositional effects and mechanisms. American Mineralogist, 84: 345-356.

Brooker, R.A., Kohn, S.C., Holloway, J.R., McMillan P.F., and Carrol, M.R., 1999. solubility, speciation and dissolution mechanism for CO_2 in melts on the $NaAlO_2$-SiO_2 join. Geochimica Cosmochimica Acta, 63(21): 3549-3565.

Brooker, R.A., Kohn, S.C., Holloway, J.R., McMillan P.F., 2001a. Structural controls on the solubility of CO_2 I silicate melts. Part 1: Bulk solubility data. Chemical Geology, 174(1-3): 225-239.

Brooker, R.A., Kohn, S.C., Holloway, J.R., McMillan P.F., 2001b. Structural controls on the solubility of CO_2 I silicate melts. Part 2: IR characteristics of carbonate groups in silicate glasses. Chemical Geology, 174(1-3): 241-254.

Brown, G.E.Jr., Farges, F., Calas, G., 1995. X-ray scattering and X-ray spectroscopy studies of silicate melts. Reviews in Mineralogy, 32: 318-410..

Browne, B.L., Eichelberger, J.C., Patino, L.C., Vogel, T.A., Dehn, J., Uto, K., Hoshizumi, H., 2005. Generation of porphiric and equigranular mafic enclave during magma recharge events at Unzen volcano, Japan. Journal of Petrology doi: 10.1093/petrology/egi076.

Carroll, M.R., and Webster, J.D., 1995. Solubility of sulfur, noble gases, nitrogen, chlorine and fluorine in magmas. Reviews in Mineralogy, 30: 231-279.

Chakraborty, S., 1995. Diffusion in silicate melts Structure, Dynamics and Properties of Silicate Melts. Reviews in Mineralogy, 32: 411-503.

Chen, H.C., De Paolo, D.J., Nakada, S. and Shieh, Y.M., 1993. Relationship between eruption volume and neodymic isotopic composition at Unzen volcano. Nature, 362: 831-834.

Cormier, L., Gaskell, P.H., Calas, G., Soper, A.K., 1998. Medium-range order around titanium in a silicate glass studied by neutron diffraction with isotopic substitution. Phisical review B vol.58 n 17: 11322-11330.

Dingwell, D.B., Mysen B.O., 1985. Effect of water and fluorine on the viscosity of albite melt at high pressure: a preliminary investigation. Earth and Planetary Science Letters, 74: 266-274.

Dingwell, D.B., Scarfe C.M., Cronin D.J., 1985. The effect of fluorine on viscosity in the system Na_2O-Al_2O_3-SiO_2: implication for phonolites, trachytes and rhyolites. American Mineralogist, 70: 80-87.

Dingwell, D.B., Virgo, D., 1988. Viscosity oxidation state relationship for hedenbergitic melt. Canegie Institute Washington. Yearbook, 87: 48-53.

Dingwell, D.B., 1989. Effect of fluorine on the viscosity of diopside liquid. American Mineralogist, 74: 333-338.

Dingwell, D.B., Webb S.L. 1989. Structural relaxation in silicate melt and non-Newtonian melt rheology in igneus processes. Physics and Chemistry of Minerals, 116: 508-516.

Dingwell, D.B., Webb S.L., 1990. Relaxation in silicate melts. European Journal of. Mineralogy, 12: 427-449.

Dingwell, D.B., 1995. Relaxation in silicate melts: some application. Reviews in Mineralogy, 32: 21-66.

Dingwell, D.B., 1999. Rheology of granitic melts. In: Understanding Granites: Modern and Classical Approaches. Geological Society of London Special Publication 168: 27-38.

Dixon, J.E., Stopler, E.M., Holloway, J.R., 1995. An experimental study of water and carbon dioxide solubilities in mid-ocean ridge basaltic liquids. Part I: calibration and solubility models. Journal of Petrology 36: 1607-1631.

Douchas, M. P., and Gerlach, T. M., 1995, Sulfur dioxide scrubbing during the 1992 eruption of Crater Peak, Mount Spurr, Alaska in Keith, T., ed., The 1992 eruptions of Crater Peak Vent, Mount Spurr volcano, Alaska: U.S. Geological Survey Bulletin B-2139: 47-57.

Einstein, A., 1911. Eine neue Bestimmung der molekuldimensionen. Annals of Physics, 19: 289-306.

Farges, F., Brown G. E. Jr., Navrotsky, A., Gan H., Rehr, J.J., 1996. Coordination chemistry of titanium (IV) in silicate glasses and melts: II. Glasses at ambient temperature and pressure. Geochimica et Cosmochimica Acta, 60: 3039-3053.

Farges, F., Brown G. E. Jr., 1997. Coordination chemistry of titanium (IV) in silicate glasses and melts: IV. XANES studies of synthetic and natural volcanic glasses and tektites at ambient temperature and pressure. Geochimica et Cosmochimica Acta, 61 N.9: 1863-1870.

Farges, F., Munoz, M., Siewert, R., Malavergne, V., Brown, G.E., Jr., Behrens, H., Nowak, M., Petit, P., 2001. Transition elements in water-bearing silicate glasses/melts. Part II. Ni in water-bearing glasses. Geochimica et Cosmochimica Acta, 65: 1679-1693.

Faxen, H., 1923. Die Bewegung einer starren Kugel längs der Achse eines nit zäher Flüssigkeit gefüllten Rohres. Arkiv för Mathematik, Astronomi och Fysik, 17(27): 1-28.

Freda, C., Baker, D.R., Ottolini, L., 2001. Reduction of water loss from gold-palladium capsules during piston-cylinder experiments by use of pyrophyllite powder. American Mineralogist 86: 234-237.

Giordano, D. and Dingwell, D.B., 2003a. The kinetic fragility of natural silicate melts. Journal of Phisics: Condensed Matter, 15: 945-954.

Giordano, D. and Dingwell, D.B., 2003b. Non-Arrhenian multicomponent melt viscosity: a model. Earth and Planetary Science Letters, 208(3-4): 337-349.

Giordano, D., Romano, C., Dingwell, D.B., Poe, B. and Behrens, H., 2004. The combined effects of water and fluorine on the viscosity of silicic magmas. Geochimica et Cosmochimica Acta, (in press).

Glasstone, E., Laidler, K.J., and Eyring, H., 1941. The theory of rate processes. McGraw-Hill Book Company. Inc., The United state of America.

Godovikov, A., A., 1979. *Khimicheskie osnovy sistematiki mineralov* (Chemical Principles of Mineral Classification), Moskov: Nedra.

Goto, A., Maedea, I., Nishida, Y. and Oshima, H., 1997. Viscosity equation for magmatic silicate melts over a wide temperature range. Proceedings of Unzen international Workshop: decade volcano and scientific drilling. Shimabara, Japan. 100-105.

Grove, T.L., Elkins-Tanton, L.T., Parman, S.W., Chatterjee, N. Müntener, O. and Gaetani, G.A., 2003. Fractional crystallization and mantle-melting controls on

cal-alcaline differentiation trends. Contributions to Mineralogy and Petrology, 145: 515-533.
Gupta, P.K., 1987. Negative pressure dependence of the viscosity. Journal of the Ceramic Society, 70, C152-C153.
Hess, K.U. and Dingwell, D.B., 1996. Viscosities of hydrous leucogranitic melts: A non-Arrhenian model. American Mineralogist, 81(9-10): 1297-1300.
Holtz F., Pichavant M., Barbey P., Johannes W., 1992. Effects of H_2O on liquidus phase relations in the haplogranitic system at 2 and 5 kbar. American Mineralogist, 77, 1223-1241.
Holtz F., Behrens H., Dingwell D.B., Johannes W., 1995. Water solubility in haplogranitic melts. Compositional, pressure and temperature dependence. Americam Mineralogist, 80, 94-108.
Holtz, F., Roux, J., Ohlhorst, S., Behrens, H., Schulze, F., 1999. The effects of silica and water on the viscosity of hydrous quartzofeldspathic melts. American Mineralogist 84(1-2): 27-36.
Holtz, F., Sato, H., Lewis, J., Behrens, H. and Nakada, S., 2005. Experimental petrology of the 1991-1995 Unzen dacite, Japan. Part I: phase relations, phase chemistry and pre-eruptive conditions. Journal of Petrology, 46 (2): 339-354.
Hoshizumi, H., Uto, K., Watanabe, K., 1999. Geology and eruptive history of Unzen volcano, Shimabara Peninsula, Kyushu, SW Japan. Journal of Volcanology and Geothermal Research, 89: 81-94.
Huang, D., and McKenna, G.B., 2001. New insights into fragility dilemma in liquids. Journal of Chemical Physics, 114 : 5621-5630.
Kahle, A., Winkler, B. and Hennion, B., 2003. Is Faxen's correction function applicable to viscosity measurements of silicate melts with the falling sphere method? Journal of Non-Newtonian Fluid Mechanics, 112(2-3): 203-215.
Kauzmann, W., 1948. The nature of the glassy state and the behaviour of liquids at low temperature. Chemical Reviews, 43, 219-256.
Koepke, J. and Behrens, H., 2001. Trace element diffusion in andesitic melts: An application of synchrotron X-ray fluorescence analysis. Geochimica et Cosmochimica Acta, 65(9): 1481-1498.
Kuryaeva, R.,G., 2004. Degree of polymerization of aluminosilicate glasses and melts. Glass Physics and Chemistry, vol. 30, No. 2 p., 157-166.
Kushiro, I., Yoder, H.S. and Mysen, B.O., 1976. Viscosities of Basalt and Andesite Melts at High-Pressures. Journal of Geophysical Research, 81(35): 6351-6356.
Kushiro, I., 1978. Viscosity and structural changes of albite (NaAlSi3O8) melt at high pressure. Earth and planetary Science Letter, 41: 87-90.
Ishihara, K., 1993. Continuous magma supply inferred from discharge rate of magma and ground-deformation rate at Mt. Unzen, Japan. Ann. Disas. Prev.Res. Inst., Kyoto Univ. 36 (B1), 219-230.
Lange, R.A., 1995. The effect of H_2O, CO_2 and F on the density and viscosity of silicate melts. Reviews Mineralogy, 30: 331-369.
Lejeune, A.M., Bottinga, Y., Trull, T.W. and Richet, P., 1999. Rheology of bubble-bearing magmas. Earth and Planetary Science Letters, 166(1-2): 71-84.
Lejeune, A.M. and Richet, P., 1995. Rheology of Crystal-Bearing Silicate Melts - an Experimental-Study at High Viscosities. Journal of Geophysical Research-Solid Earth, 100(B3): 4215-4229.
Liebske, C., Behrens, H., Holtz, F. and Lange, R.A., 2003. The influence of pressure and composition on the viscosity of andesitic melts. Geochimica et Cosmochimica Acta, 67(3): 473-485.

Mandeville, C.W., Webster, J.D., Rutherford, M.J., Taylor, B.E., Timbal, A., Faure K., 2002. Determination of molar absorptivities for infrared absorption bands of H_2O in andesitic glasses. American Mineralogist, 87(7): 813-821.
McBirney, R., and Murase, T., (1984). Rheological properties of magma. Ann. Rev. Earth and Planetary Science Letters, 12: 337-357.
McMillan, P.F., 1994. Water solubility and speciation model. Review in Mineralogy, 30: 131-156.
Marsh, B.D., 1981. On the crystallinity, probably occurrence, and rheology of lava and magma. Contributions to Mineralogy and Petrology, 78: 85-98.
Martinez, L.M., and Angell, C.A., 2001. A thermodynamic connection to the fragility of glass-forming liquids. Nature, 410: 663-667.
Miyabuchi, Y., 1999. Deposits Associated with the 1990-1995 eruption of Unzen volcano, Japan. Journal of Volcanology and Geothermal Research 89: 139-158.
van der Molen, I., and Paterson, M.S., 1979. Experimental deformation of partially-melted granite. Contributions to Mineralogy and Petrology, 70: 299-318.
Mori, S.,Ojami, E., and Suzuki, A., 2000. Viscosity of albite melt to 7 GPa at 2000 K. Earth and Planetary Science Letters, 175, 87-92.
Moynihan, C.T., 1995. Structural relaxation and the glass trasnsition. Reviews in mineralogy, 32: 1-19.
Murase, T. and McBirney, R., 1973. Properties of some common igneous rocks and their melts at high temperatures. Geological Society of America Bulletin 84, 3563-3592.
Mysen, B.O., Arculus R.J., and Eggler, D.H., 1975. Solubility of carbon dioxide in melts of andesite, tholeiite, and olivine nephelinite composition to 30 Kbar pressure. Contributions to Mineralogy and Petrology, 33: 227-239.
Mysen, B.O., 1976. The role of volatile in silicate melts: solubility of carbon dioxide and water in feldspar, pyroxene, and feldspathoid melts to 30 Kb and 1625°C. American Journal of Scince, 276: 969-996.
Mysen, B.O., Rjerson, F.J., Virgo, D., 1980. The influence of TiO_2 on the structure and derivative properties of silicate melts. American Mineralogist, 65: 1150-1165.
Mysen, B.O., Virgo, D. and seifert, F.A. 1985. Relationship between properties and structure of aluminosilicate melts. American Mineralogist, 70: 88-105.
Mysen, B.O., 1988. Structure and properties of silicate melts. Elsevier Science Publisher B.V., Amsterdam. p 354.
Nakamura, M., 1995. Continuous mixing of crystals mush and replenished magma in the ongoing Unzen eruption. Geology, 23: 807-810.
Nakada, S. & Motomura, Y., 1999. Petrology of the 1991-1995 eruption at Unzen: effusion pulsation and groundmass crystallization. Journal of Volcanology and Geothermal Research, 89: 173-196.
Nakada, S., Shimizu, H., Ohta, K., 1999. Overview of the 1990-1995 eruption at Unzen volcano. Journal of Volcanology and Geothermal Research, 89: 1-22.
Nakada, S., Uto, K., Sakuma, S., Eichelberger, J.C., Shimizu, H., 2005. Scientific results of conduit drilling in the Unzen Scientific Drilling Project (USDP). Scientific drilling N.1, doi:10.2204/iodp.sd.1.03.2005.
Neuville, D.R. and Richet, P., 1991. Viscosity and Mixing in Molten (Ca, Mg) Pyroxenes and Garnets. Geochimica et Cosmochimica Acta, 55(4): 1011-1019.
Neuville, D.R., Courtial, P., Dingwell, D.B. and Richet, P., 1993. Thermodynamic and rheological properties of rhyolite and andesite melts. Contributions to Mineralogy and Petrology, 113: 572-581.

Nishi, K., Ono, H., Mori, H., 1999. GPS measurements of ground deformation caused by magma intrusion and lava discharge: the 1990-1995 eruption at Unzendake volcano, Kyushu, Japan. Journal of Volcanology and Geothermal Research, 89: 23-34.

Nowak, M. and Behrens, H., 1995. The speciation of water in haplogranitic glasses and melts determined by in situ near-infrared spectroscopy. Geochimica and Cosmochimica Acta, 59: 3455-3450.

Nowak, M. and Keppler, H., 1998. The influence of water on the environment of transition metals in silicate glasses. American Mineralogist, 83: 43-50.

Nowak, M. and Behrens, H., 2001. Water in rhyolitic magmas: getting a grip on a slippery problem. Earth and Planetary science Letters, 184: 515-522.

Ochs, F.A., and Lange, R.A., 1999. The density of hydrous magmatic liquids. Science, 283(5406): 1314.

Ohlhorst, S., Behrens, H. and Holtz, F., 2001. Compositional dependence of molar absorptivities of near-infrared OH- and H_2O bands in rhyolitic to basaltic glasses. Chemical Geology, 174(1-3): 5-20.

Persikov, E.S., Zharikov, V.A. Bukhtiyarov, P.G. and Polskoy, S.F., 1990. The effect of volatiles on the properties of magmatic melts. European Journal of Mineralogy, 2: 621-642.

Persikov, E.S., 1991. The viscosity of magmatic liquids: Experiment, generalized patterns. A model for calculation and prediction. Applications. Advances in Physical Chemistry, 9: 1-41.

Persikov, E.S., and Bukhtiyarov, P.G., 1999. Influence of temperature and pressure effect on the viscosity of model and magmatic melts of acid-ultrabasic composition. Geochemistry International, 37, 1130-1140.

Petford, N., 2003. Rheology of granitic magmas during ascent and emplacement. Annual Reviews Earth Planetary Science, 31: 399-427.

Philpott, A.R., 1990. Principles of igneous and metamorphic petrology. Prentice Hall, NJ; 498 pages.

Pinkerton, H., and Stevenson, R.J., 1992. Methods of determining the rheological properties of magmas at suliquidus temperature. Journal of Volcanology and Geothermal Research, 53: 47-66.

Ponader, C.W., Boek, H., Dickinson,J.E., Jr., 1996. X-ray absorption study of the coordination of titanium in sodium-titaium-silicate glasses. Journal of Non Crystalline Solids, 201: 81-94.

Rao, B.V.J., 1963. Influence of TiO_2 on properties of glasses in the system K2O-PBO-SiO2-TiO2 ans its relation to structure. Journal of the Ceramic Society, 46 (3): 107-114 1963.

Reid, J.E., Suzuki, A., Funakoshi, K.I., Terasaki, H., Poe, B.T., Rubie, D.C., Ohtani, E., 2003. The viscosity of $CaMgSi_2O_6$ liquid at pressures up to 13 GPa. Physics of the Earth and Planetary Interiors, 139 (1-2): 45-54.

Renner, J., Evans, B., Hirth, G., 2000. On the rheologically melt fraction. Earth and Plenetary Science Letter, 181: 585-594.

Richet, P., Bottinga, Y., Tequi, C., 1984. Heat capacity of sodium silicate liquid. Journal of the Ceramic Society, 67: C6-C8.

Richet, P. and Neuville D.R., 1992. Thermodinamics of silicate melts: configurational properties. In: Advances in Physical Geochemistry v. 11: 132-161.

Richet, P., and Bottinga, Y., 1995. Rheology and configurational entropy of silicate melts. Reviews in Mineralogy vol. 32: 67-93.

Richet, P., Lejeune, A.M., Holtz, F. and Roux, J., 1996. Water and the viscosity of andesite melts. Chemical Geology, 128(1-4): 185-197.

Romano, C., Dingwell D.B., and Behrens H., 1995. The temperature dependence of the speciation of water in $NaAlSi_3O_8$-$KAlSi_3O_8$ melts:an application for fictive temperature derived from synthetic fluid inclusion. Contributions to Mineralogy and Petrology, 122: 1-10.

Romano, C., Poe, B., Mincione, V., Hess, K.U. and Dingwell, D.B., 2001. The viscosities of dry and hydrous $XAlSi_3O_8$ (X = Li, Na, K, $Ca_{0.5}$, $Mg_{0.5}$) melts. Chemical Geology, 174(1-3): 115-132.

Romano, C., Giordano D., Papale P., Mincione V., Dingwell D.B., Rosi, M., 2003. The dry and hydrous viscosities of alkaline melts from Vesuvius and Phlegrean Fields. Chemical Geology, 202 (1-2): 23-38.

Rosenberg, C.L., and Handy, M.R., 2005. Experimental deformation of partially melted granite revisited: implication for continental crust. Journal of Metamorphic Geology, 23, 19-28.

Roscoe, R., 1952. The viscosity of suspensions of rigid spheres. British Journal of Applied Physics, 3, 267–269.

Russell, J.K., Girdano, D. and Dingwell D.B. 2003. High-temperature limits on viscosity of non-Arrhenian silicate melts. American Mineralogist, 88: 1390-1394.

Rutter, E. & Neumann, D.H.K., 1995. Experimental deformation of partially molten Westerly granite under fluid-absent conditions, with implications for the extraction ofgranitic magmas. Journal of Geophysical Research, 100: 15697–15715.

Seno, T., 1977. The instantaneous rotation vector of the Philippine Sea plate relative to the Eurasian plate. Tectonophysics 42, 209-226.

Sato, H., Holtz, F.,Behrens, H., Botcharnikov, R., Nakada, S., 2005. Experimental petrology of the 1991-1995 Unzen dacite. Part II: Cl/OH partitioning between horneblende an melt and its implications for the origin of oscillatory zoning of horneblende phenocrysts. Journal of Petrology, Vol. 46 N. 2: 339-354.

Sato, H., 2005. Viscosity measurements of subliquidus magmas:1707 basalt of Fuji volcano. Journal of Mineralogical and Petrological Science, 100: 133-142.

Scaillet, B., Holtz, F., Pichavant, M. and Schmidt, M., 1996. Viscosity of Himalayan leucogranites: Implications for mechanisms of granitic magma ascent. Journal of Geophysical Research-Solid Earth, 101(B12): 27691-27699.

Scarfe, C. M., Mysen, B.O., and Virgo, D., 1979. changes in viscosityand density of melts of sodium disilicate, sodium metasilicate, and diopside composition with pressure. Carnegie Institution Washington Yersbook, 78, 547-551.

Scarfe, C. M., 1986. Viscosity and density of silicate melts. In: Short Course in Silicate Melts (Ed. C.M. Scarfe). Mineralogical Association Canada, 12: 36-56.

Scarfe, C.M., Mysen, B.O. and Virgo, D., 1987. Pressure dependence of the viscosity of silicate melts. In Magmatic processes: physicochemical principles, Vol. Special Publication No. 1 (ed. B. O. Mysen). The Geochemical Society: 504-511.

Scholze, H. (1991) Glass: nature, structure, and properties. Springer, New York, pp 454.

Schulze, F., Behrens, H., Holtz, F., Roux, J. and Johannes, W., 1996. The influence of H_2O on the viscosity of a haplogranitic melt. American Mineralogist, 81(9-10): 1155-1165.

Schulze, F., Behrens, H. and Hurkuck, W., 1999. Determination of the influence of pressure and dissolved water on the viscosity of highly viscous melts:

Application of a new parallel-plate viscometer. American Mineralogist, 84(10): 1512-1520.

Schulze, F., 2000. Untersuchung zum Einfluß von druck und gelöstem Wasser auf die Viskosität silikatischer Schmelzen – Anwendung eines "parallel-plate"-viscosimeter unter hohen Drücken, (2000). PhD thesis.

Sharma, S.K., Virgo, D., and Kushiro, I., 1979. Relationship between density, viscosity and structure of GeO_2 melts at low and at high pressure. Journal of Non-Crystalline Solids, 33, 235-248.

Shaw, H.R., 1963. Obsidian-H_2O viscosities at 100 and 200 bars in temperature range 700 degrees to 900 degrees C. Journal of Geophysical Research, 68(23): 6337-6343.

Shaw, H.R., 1972. Viscosities of magmatic silicate liquids - empirical method of prediction. American Journal of Science, 272(9): 870-893.

Shen, A., Keppler, H., 1995. Infrared spectroscopy of hydrous silicate melts to 1000°C and 10 Kbar: direct observation of H2O speciation in a diamond anvil cell. American Mineralogist, 80: 1335-1338.

Sherman, P., 1968. Emulsion science. Academic press, Orlando, Fla., 351 pp.

Silver L. A. and Stolper E. M., 1989. Water in albitic glasses. J. Petrol. 30: 667-709.

Silver L. A., Ihinger P. D., and Stolper E. M., 1990. The influence of bulk composition on the speciation of water in silicate glasses. Contributions to Mineralogy and Petrology, 104: 142-162.

Spera, F.,1999. A slippery problem with explosive consequences. Science, Vol 283, Issue 5406: 1275-1276.

Stebbins, J. F., 1995. Dynamic and structure of silicate and oxide melts: nuclear magnetic resonance studies. Reviews in Mineralogy, 32: 191-246.

Stolper, E.M. (1982). Water in silicate glasses: an infrared spectroscopic study, Contributions to Mineralogy and Petrology, 81: 1-17.

Stolper, E.M., 1989. the temperature dependence of the speciation of water in rhyolitic melts and glasses. American Mineralogist, 74: 1247-1257.

Suzuki, A., Ohtani, E., Funakoshi, K., and Terasaki, H., 2002. Viscosity of albite melt at high pressure and high temperature. Physics and Chemistry of Minerals, 29: 159-165.

Symonds, R.B., Rose, W.I., Bluth, G., and Gerlach, T.M., 1994. Volcanic gas studies: methods, results, and applications. Reviews in Mineralogy, 30: 1-66.

Tada, T., 1985. Spreading of the Okinawa Trough and its relation to the crustal deformation in the Kyushu (2). Journalv of Seismological Society of Japan, 38: 1-12, in Japanese with English abstract.

Tamic, N., Behrens, H., and Holtz, F., 2001. The solubility of H_2O and CO_2 in rhyolitic melts in equilibrium with a mixed CO_2-H_2O fluid phase. Chemical Geology, 174: 333-348.

Toplis, J.M., Dingwell, D.B., Hess, K.U., Lenci, T., 1997. Viscosity, fragility and configurational entropy of melts along the join SiO_2-$NaAlSiO_4$. American Mineralogist, 82: 979-990.

Tsukuda, E., 1993. Is the central Kyushu really rifting north to south? Mem. Geological Society of Japan, 41: 149-161, in Japanese.

Umakoshi, K., Shimizu, H., Matsuwo, N., 1994. Magma ascent path in the 1990-94 eruption of Fugendake, Unzen volcano, as inferred from precisely determined hypocentral distribution. Bullettin of Volcanology Society of Japan, 39: 223-235, in Japanese.

Venezky, D.Y. & Rutherford, M.J., 1999. Petrology and Fe-Ti oxide reequilibration of the 1991 Mount Unzen mixed magma. Journal of Volcanology and Geothermal Research, 89: 213-230.

Virgo, D., Mysen, B.O., Danckwerth, P., and Seifert, F., 1982. The anionic structure of 1 Atm. Melt in the system SiO2-NaFeO2, Carnegie Inst. Wash. Yearbook, 1982, vol.81, pp. 347-349.

Waff, H.S. (1975) Pressure induced coordination changes in magmatic liquids. Geophysical Research Letters, 2, 5, 193-196.

Watanabe, Kazunori, Hoshizumi, H., 1995. Unzen volcano. Geological map of volcano 8 (1:25.000). Geological Survey of Japan, in Japanese.

Watson, E.B., and Harrison, T.M., 1983. Zircon saturation revisited: temperature and composition effect in variety of crustal magma types. Earth and Planetary Science Letters, 64: 295-304.

William, Q., and Tobisch O.T., 1994. Microgranitic enclaves shapes and magmatic strain histories: constraints from drop deformation theory. Journal of Geophysical Research, vol. 99 NO B12: 24.359-24368.

Whittington, A., Richet, P. and Holtz, F., 2000. Water and the viscosity of depolymerized aluminosilicate melts. Geochimica et Cosmochimica Acta, 64(21): 3725-3736.

Whittington, A., Richet, P., Linard, Y. and Holtz, F., 2001. The viscosity of hydrous phonolites and trachytes. Chemical Geology, 174(1-3): 209-223.

Wood, M.J., and Hess, P.C., 1980. The structural role of Al_2O_3 and TiO_2 in immiscible silicate liquids in the system SiO_2-MgO-CaO-FeO-TiO_2- Al_2O_3. Contributions to Mineralogy and Petrology, 72: 319-328.

Woodcock, L.V., Angell, C.A., and Chessman, P., 1976. Molecular dynamics of the vitreous state: Simple ionic systems and silica. Journal of Chemistry and Physics, 65: 1565-1577.

Wong, J., Angell, C.A., 1976. Glass structure by spectroscopy. Dekker, New York, 864 pages.

Zhang, Y.X., Stopler, E.M., and Ihinger P.D., 1995. Kinetics of the reaction $H_2O + O = 2OH$ in felsic glasses: preliminary results. American Mineralogist, 80: 593-612.

Zhang, Y.X., Xu, Z.J. and Liu, Y., 2003. Viscosity of hydrous rhyolitic melts inferred from kinetic experiments, and a new viscosity model. American Mineralogist, 88(11-12): 1741-1752.

You, Y., 2002. Fibre drawing from diabase glass melts, technical report. Aalborg University. P. 62.

Appendix

Viscosity data for partially crystallized melt.
For synthesis condition, water content and crystals content see chapter 6.

Sample	Temperature (K)	Load (g)	Measure order	Sample length (mm)	Time (s)	Strain rate (S^{-1})*10^6	Log vis (Pa s)
MDIB6	823	2200	1	12.343			
				12.340	10.68	22.76	10.84
				12.343			
				12.337	25.86	18.80	10.93
				12.343			
				12.334	47.52	15.34	11.01
				12.343			
				12.331	77.55	12.54	11.10
				12.343			
				12.328	113.33	10.72	11.17
				12.343			
				12.325	159.74	9.13	11.24
				12.343			
				12.322	218.4	7.79	11.31
				12.343			
				12.319	292.55	6.65	11.38
				12.343			
				12.316	383.18	5.71	11.44
				12.343			
				12.313	479.74	5.07	11.49
		5200	2	12.293			
				12.290	8.17	525.57	11.11
				12.293			
				12.287	16.39	276.81	11.12
				12.293			
				12.284	29.99	159.39	11.20
				12.293			
				12.281	45.45	110.52	11.26
				12.293			
				12.278	61.05	86.26	11.29
				12.293			
				12.275	80.17	68.72	11.33
				12.293			

			12.272	103.95	55.34	11.37
			12.293			
			12.269	129.95	46.14	11.41
			12.293			
			12.266	159.20	39.19	11.45
			12.293			
			12.263	193.61	33.48	11.49
	10200	3	12.223			
			12.218	11.08	914.01	11.32
			12.223			
			12.213	23.46	448.95	11.34
			12.223			
			12.208	38.76	282.18	11.38
			12.223			
			12.203	56.39	201.14	11.42
			12.223			
			12.198	76.80	152.96	11.46
			12.223			
			12.193	99.77	121.81	11.49
			12.223			
			12.188	122.74	102.31	11.52
			12.223			
			12.183	152.77	84.85	11.55
			12.223			
			12.178	186.24	71.78	11.59
			12.223			
			12.173	225.83	60.99	11.63
890	3200	4	12.343			
			12.206	22.77	487.46	11.51
			12.208			
			12.203	85.92	132.01	11.69
			12.208			
			12.20	206.39	56.13	11.87
			12.208			
			12.197	352.20	33.58	11.96
			12.208			
			12.194	535.52	22.54	12.04
			12.208			
			12.191	758.17	16.24	12.10
			12.208			

			12.188	1160.86	10.82	12.22
910	6200	5	12.138			
			12.135	27.62	610.13	11.71
			12.138			
			12.132	82.37	207.54	11.88
			12.138			
			12.129	153.71	112.80	11.98
			12.138			
			12.126	249.62	70.43	12.06
			12.138			
			12.123	391.08	45.58	12.16
			12.138			
			12.118	728.05	25.04	12.31
			12.138			
			12.114	1056.43	17.56	12.39
			12.138			
			12.113	1218.68	15.29	12.43
	10200	6	12.090			
			12.087	33.09	626.79	12.01
			12.090			
			12.085	69.62	300.24	12.11
			12.090			
			12.083	117.31	179.56	12.19
			12.090			
			12.081	197.31	107.58	12.30
			12.090			
			12.079	283.77	75.37	12.37
			12.090			
			12.077	399.77	53.91	12.45
			12.090			
			12.075	499.09	43.50	12.49
	8200	7	12.093			
			12.09	18.61	1101.42	11.66
			12.093			
			12.088	73.83	279.83	12.04
			12.093			

			12.086	182.08	114.35	12.28
			12.093			
			12.085	285.55	73.20	12.42
			12.093			
			12.084	379.96	55.23	12.49
			12.093			
			12.082	631.80	33.47	12.63
892	10200	8	12.085			
			12.083	38.34	549.41	12.25
			12.085			
			12.081	101.30	209.54	12.37
			12.085			
			12.079	224.30	95.36	12.54
			12.085			
			12.077	430.05	50.11	12.69
			12.085			
			12.075	681.15	31.88	12.80
			12.085			
			12.073	1011.18	21.63	12.89
			12.085			
			12.072	1208.87	18.16	12.93
890	15200	9	12.058			
			12.055	54.99	424.31	12.40
			12.058			
			12.053	173.58	135.36	12.68
			12.058			
			12.052	232.65	101.34	12.73
			12.058			
			12.051	316.68	74.70	12.79
			12.058			
			12.050	418.43	56.73	12.85
			12.058			
			12.049	525.58	45.32	12.90
			12.058			
			12.048	655.80	36.44	12.95
	20200	10	12.035			

				12.033	34.21	734.16	12.49
				12.035			
				12.031	95.80	263.86	12.64
				12.035			
				12.030	143.30	176.96	12.72
				12.035			
				12.029	199.80	127.32	12.78
				12.035			
				12.028	256.99	99.31	12.82
				12.035			
				12.027	323.02	79.26	12.87
				12.035			
				12.026	406.40	63.20	12.91
				12.035			
				12.025	498.24	51.71	12.96
	922	10200	11	12.088			
				12.086	91.64	227.21	226.21
				12.088			
				12.085	141.86	147.35	146.35
				12.088			
				12.084	198.39	105.77	104.77
				12.088			
				12.083	267.27	78.81	77.81
				12.088			
				12.082	339.17	62.35	61.35
				12.088			
				12.081	456.17	46.53	45.53
				12.088			
				12.080	554.52	38.43	37.43
				12.088			
				12.078	768.49	27.94	26.94

Sample	Temperature (K)	Load (g)	Measure order	Sample length (mm)	Time (s)	Strain rate $(S^{-1})*10^6$	Log vis (Pa s)
MDIB 7	887	1200	1	4.870 4.867 4.870	9.11	67.62	10.27

		4.865	27.30	37.61	10.53
		4.870			
		4.864	40.77	30.22	10.62
		4.870			
		4.862	87.96	18.68	10.83
		4.870			
		4.861	116.33	15.89	10.90
		4.870			
		4.860	150.89	13.61	10.97
3200	2	4.851			
		4.848	10.64	58.12	10.80
		4.851			
		4.846	23.18	44.47	10.92
		4.851			
		4.845	31.61	39.13	10.97
		4.851			
		4.843	51.49	32.03	11.06
		4.851			
		4.842	61.49	30.17	11.09
		4.851			
		4.841	76.08	27.10	11.13
		4.851			
		4.840	89.89	25.23	11.16
		4.851			
		4.838	118.11	22.69	11.21
5200	3	4.832			
		4.830	6.52	63.48	10.98
		4.832			
		4.828	15.93	51.97	11.07
		4.832			
		4.826	28.34	43.82	11.14
		4.832			
		4.824	43.4	38.15	11.20
		4.832			
		4.822	58.56	35.34	11.23
		4.832			
		4.820	77.31	32.12	11.27
		4.832			
		4.819	88.46	30.41	11.30
		4.832			
		4.818	99.37	29.16	11.32
7200	4	4.809			
		4.806	12.12	51.47	11.21
		4.809			
		4.804	21.21	49.02	11.23
		4.809			
		4.802	32.40	44.93	11.27
		4.809			

				4.800	44.68	41.89	11.30
				4.809			
				4.798	57.05	40.09	11.32
				4.809			
				4.796	72.24	37.42	11.35
				4.809			
				4.793	96.02	34.65	11.38
				4.809			
				4.790	122.43	32.27	11.42
				4.809			
				4.789	130.46	31.88	11.42
				4.809			
				4.786	156.12	30.63	11.44

Sample	Temperature (K)	Load (g)	Measure order	Sample length (mm)	Time (s)	Strain rate (S-1)*10^6	Log vis (Pa s)
MDIB 15_1	961	1200	1	5.370			
				5.360	6.86	271.46	9.47
				5.370			
				5.350	19.33	192.67	9.62
				5.370			
				5.345	29.71	156.70	9.71
				5.370			
				5.342	39.77	131.11	9.78
				5.370			
				5.340	47.43	117.79	9.83
				5.370			
				5.338	57.52	103.60	9.89
				5.370			
				5.336	76.55	82.71	9.98
				5.370			

		5.334	92.02	72.85	10.04
3200	2	5.311			
		5.308	11.43	49.42	10.67
		5.311			
		5.306	19.55	48.16	10.68
		5.311			
		5.304	28.68	45.96	10.70
		5.311			
		5.302	42.27	40.09	10.76
		5.311			
		5.3	59.71	34.69	10.82
		5.311			
		5.298	73.96	33.10	10.84
		5.311			
		5.296	92.46	30.55	10.88
5200	3	5.285			
		5.280	11.33	83.50	10.66
		5.285			
		5.275	27.49	68.83	10.74
		5.285			
		5.273	36.96	61.43	10.79
		5.285			
		5.270	56.27	50.44	10.87
		5.285			
		5.267	72.3	47.11	10.90
		5.285			
		5.266	80.39	44.72	10.93
		5.285			
		5.264	95.27	41.71	10.96
10200	4	5.242			
		5.240	2.93	130.22	10.76
		5.242			
		5.235	11.49	116.22	10.81
		5.242			
		5.232	19.46	98.03	10.88
		5.242			
		5.230	25.02	91.49	10.91
		5.242			

		5.227	34.49	82.97	10.95
		5.242			
		5.225	41.55	78.05	10.98
		5.242			
		5.223	49.84	72.72	11.01
		5.242			
		5.220	67.87	61.84	11.08
		5.242			
		5.218	80.49	56.88	11.12
9200	5	5.215			
		5.214	12.15	15.78	11.63
		5.215			
		5.213	27.18	14.11	11.68
		5.215			
		5.212	43.52	13.22	11.71
		5.215			
		5.211	61.74	12.42	11.73
		5.215			
		5.210	82.87	11.57	11.76
		5.215			
		5.209	100.93	11.40	11.77
		5.215			
		5.208	119.96	11.19	11.78